AFRL-AFOSR-UK-TR-2016-0022

Mid-infrared photonic devices fabricated by ultrafast laser inscription

Ajoy Kar
HERIOT-WATT UNIVERSITY

07/01/2016
Final Report

Air Force Research Laboratory
AF Office Of Scientific Research (AFOSR)/ IOE
Arlington, Virginia 22203
Air Force Materiel Command

REPORT DOCUMENTATION PAGE

Form Approved
OMB No. 0704-0188

1. REPORT DATE *(DD-MM-YYYY)*	2. REPORT TYPE	3. DATES COVERED *(From - To)*
09-09-2016	Final	31 Dec 2012 to 28 Dec 2015

4. TITLE AND SUBTITLE
Mid-infrared photonic devices fabricated by ultrafast laser inscription

5a. CONTRACT NUMBER

5b. GRANT NUMBER
FA8655-13-1-3026

5c. PROGRAM ELEMENT NUMBER
61102F

6. AUTHOR(S)
Ajoy Kar

5d. PROJECT NUMBER

5e. TASK NUMBER

5f. WORK UNIT NUMBER

7. PERFORMING ORGANIZATION NAME(S) AND ADDRESS(ES)
HERIOT-WATT UNIVERSITY
RICCARTON
CURRIE, EDINBURGH, EH14 4AS GB

8. PERFORMING ORGANIZATION REPORT NUMBER

9. SPONSORING/MONITORING AGENCY NAME(S) AND ADDRESS(ES)
EOARD
Unit 4515
APO AE 09421-4515

10. SPONSOR/MONITOR'S ACRONYM(S)
AFRL/AFOSR IOE

11. SPONSOR/MONITOR'S REPORT NUMBER(S)
AFRL-AFOSR-UK-TR-2016-0022

12. DISTRIBUTION/AVAILABILITY STATEMENT
A DISTRIBUTION UNLIMITED: PB Public Release

13. SUPPLEMENTARY NOTES

14. ABSTRACT
This report details the work cared out at Heriot-Watt University over the last three years on the project titled Mid-infrared photonic devices fabricated by ultrafast laser inscription (grant award number FA8655-13-1-3026). This research was done in very close collaboration with the Novel Laser Technologies group at Sensors Directorate AFRL/RYDH at WPAFB in the USA. This project follows on from an initial grant that lead to the developed of the first ZnSe waveguides. In this report will detail our development of Cr:ZnSe waveguide laser in which we have demonstrated continuous wave, Modelocked and wavelength tuneable laser operation. Moving on from our work in Cr:ZnSe we started developing waveguides in Fe:ZnSe and have demonstrated the first Fe:ZnSe waveguide laser. Once the base laser sources had been developed the project moved on to the developed of waveguide component to facilitate the creation of a wavelength tuneable Mid-IR laser with no free space optical elements. To achieve this waveguides fabricated using ultrafast laser inscription in CaF2 and SBN have been developed at Heriot-Watt University.

15. SUBJECT TERMS
inscription bulk materials, photonic inscription, integrated waveguids in ZnSe, laser inscription, EOARD

16. SECURITY CLASSIFICATION OF:			17. LIMITATION OF ABSTRACT	18. NUMBER OF PAGES	19a. NAME OF RESPONSIBLE PERSON
a. REPORT	b. ABSTRACT	c. THIS PAGE			GONGLEWSKI, JOHN
Unclassified	Unclassified	Unclassified	SAR	74	19b. TELEPHONE NUMBER *(Include area code)* 011-44-1895-616007

Standard Form 298 (Rev. 8/98)
Prescribed by ANSI Std. Z39.18

Mid-IR waveguides fabricated by Ultra-fast laser inscription

Final Technical Report

31st of December 2012 to 28th of December 2015

Award no: FA8655-13-1-3026

A. K. Kar

Institute of Photonics and Quantum Sciences, Heriot-Watt University

Edinburgh EH14 4AS, Scotland

a.k.kar@hw.ac.uk

Contents

Introduction

This report details the work cared out at Heriot-Watt University over the last three years on the project titled Mid-infrared photonic devices fabricated by ultrafast laser inscription (grant award number FA8655-13-1-3026). This research was done in very close collaboration with the Novel Laser Technologies group at Sensors Directorate AFRL/RYDH at WPAFB in the USA. This project follows on from an initial grant that lead to the developed of the first ZnSe waveguides. In this report will detail our development of Cr:ZnSe waveguide laser in which we have demonstrated continuous wave, Modelocked and wavelength tuneable laser operation. Moving on from our work in Cr:ZnSe we started developing waveguides in Fe:ZnSe and have demonstrated the first Fe:ZnSe waveguide laser. Once the base laser sources had been developed the project moved on to the developed of waveguide component to facilitate the creation of a wavelength tuneable Mid-IR laser with no free space optical elements. To achieve this waveguides fabricated using ultrafast laser inscription in CaF_2 and SBN have been developed at Heriot-Watt University.

This project has been part of a long term collaboration between Heriot Watt University (HWU) and AFRL on the development of Mid-IR waveguides. As such there have been many different people contributing to this body of work. At HWU A. K. Kar is the research group leader with John R. Macdonald, G. Brown, S. J. Beecher and A. Lancaster also working on the project at different stages. Form AFRL K. L. Schepler then G. Cook where the team lead with P. A. Berry, S. A. McDaniel and J. Evans also working on the project. All of the work was made possible my continued funding form EOARD.

Cr:ZnSe waveguides laser

Introduction

There is great interest in developing laser sources in the Mid-IR region (2-5 μm) form a wide range of applications. The reason for this is the overlapping of atmospherics transmission window and many fundamental molecular absorption lines. Some examples of applications that require laser sources in this wavelength range are infrared countermeasures, laser surgery, remote sensing and non-invasive imaging. These require efficient, compact, robust and reliable Mid-IR laser sources, hence there is a great drive to develop solid-state lasers for this wavelength range.

Transition metal doped II-VI semiconductors such as Cr^{2+}: ZnSe, Cr^{2+}: ZnS and Cr^{2+}: CdSe have many desirable properties such as large absorption and gain bandwidths, large emission cross-sections, no excited state absorption and room temperature operation [1-4]. Specifically, Cr^{2+}:ZnSe lasers have demonstrated room temperature operation with CW output powers of 12.5 W [5], gain switched pulsed operation at 57 W [6] and continually tuneable CW from 1973-3339 nm [7]. IPG Photonics have commercialised Cr^{2+} doped ZnSe and ZnS laser, aided by the large number of readily available pump sources such as Er fiber, Tm fiber, Tm:YAG and InP diodes.

The limitations in further power scaling of Cr^{2+}:ZnSe has been attributed to thermal lensing caused by the materials high thermo-optic coefficient, $\left(\frac{\partial n}{\partial T}\right)$. At high pump powers thermal lensing in the gain medium leads to self-focussing and filamentation causing cavity instability and even optical damage of the laser material. An attractive method to overcome this is to use waveguide geometry, allowing a plane wavefront to be maintained through the gain medium and hence mitigate thermal lensing [8, 9]. Waveguide geometry also grants inherent vibration insensitivity in a compact system, which is paramount for the aforementioned applications.

Ultrafast laser inscription offers unique capabilities in the fabrication of low-loss channel waveguides in that it allows rapid prototyping, fabrication of truly 3-D architectures and is highly flexible across a wide range of different glass and crystal substrates [10-13]. Before the start of this project successfully developed the first directly written near-infrared waveguides in ZnSe and Cr^{2+}: ZnSe [14, 15] has been achieved. That project saw the achievement of another major milestone in creating the first mid-infrared waveguides in ZnSe and the demonstration of the first channel waveguide laser in Cr^{2+}: ZnSe. This report details the subsequent progress over the last three years on phase two, in which slope efficiency was improved by an order of magnitude and wavelength tuneability of 803 nm was demonstrated, a world record for a waveguide laser. Furthermore, we detail work on phase three of the project, demonstrating high power operation of Cr^{2+}: ZnSe waveguide laser sources. A thermal model of the system is presented indicating thermal limitations of current Cr^{2+}:ZnSe systems and providing insight on how these limitations can be overcome using ULI waveguide fabrication technology.

Ultrafast laser inscription

Ultrafast laser inscription relies on focusing ultrashort pulses of sub-bandgap radiation inside the substrate material. The high irradiances present in the focal volume induce nonlinear absorption phenomena that deposit optical energy in the form of a free-electron plasma. Following this, the plasma transfers energy to the material lattice, a transfer that may induce localized structural modifications. These modifications can manifest themselves in many ways, including a change in refractive index. If the refractive index modification is appropriately controlled, waveguides can be directly inscribed inside the material by translating it through the laser focus. A graphical representation is shown in Figure 1.

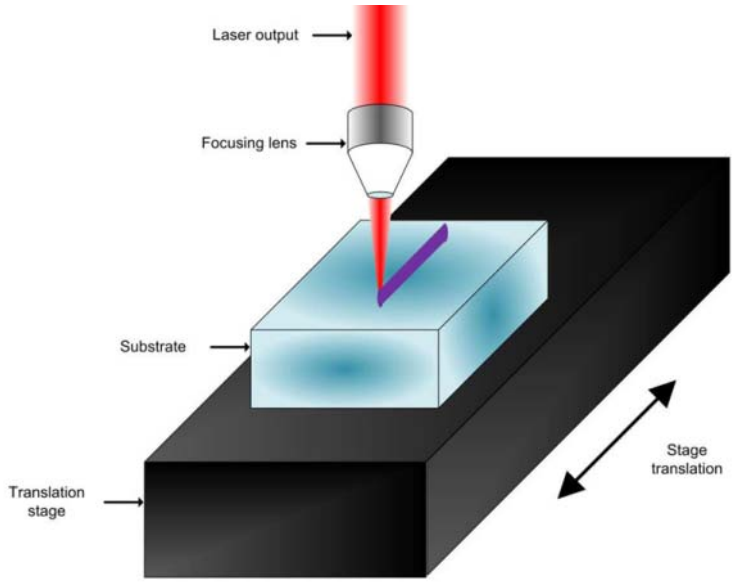

Figure 1. Graphical representation of ultrafast laser inscription of waveguides in a dielectric substrate.

Over the past decade, this technique has proven a highly flexible tool for the fabrication of a host of active and passive photonic devices in single crystal, ceramic and glass substrates. This range of devices span applications such as: astrophysics [16, 17], compact laser sources [18, 19], biophotonics and lab-on-chip technology [20, 21], sensors [11], and integrated photonics [10, 22].

At Heriot-Watt, ultrafast laser inscription of devices is performed with our state-of-the-art inscription apparatus which utilises a chirped pulse amplified, fibre MOPA (Master Oscillator Power Amplifier) system as the inscription laser (IMRA μJewel D400). This system incorporates computer control over power and polarisation and nanometer resolution XYZ air bearing stages (Aerotech) for translation of the sample substrate. Figure 2 - 4 show the arrangement of this apparatus.

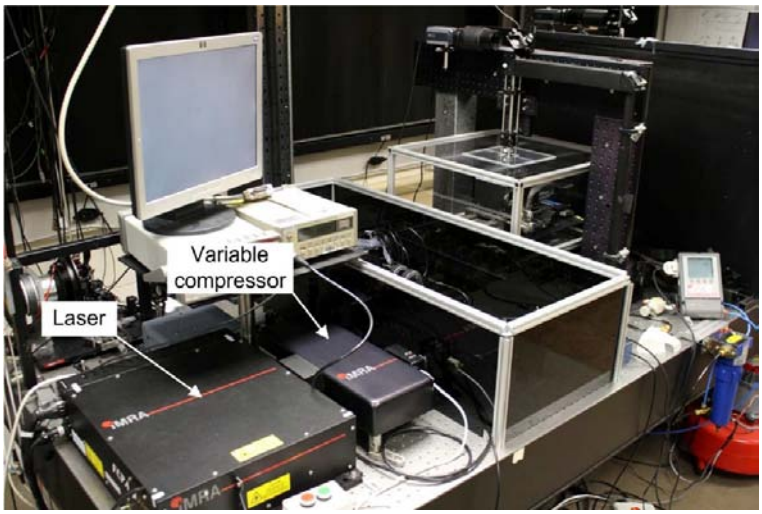

Figure 2. Ultrafast laser inscription apparatus: IMRA inscription laser and variable compressor

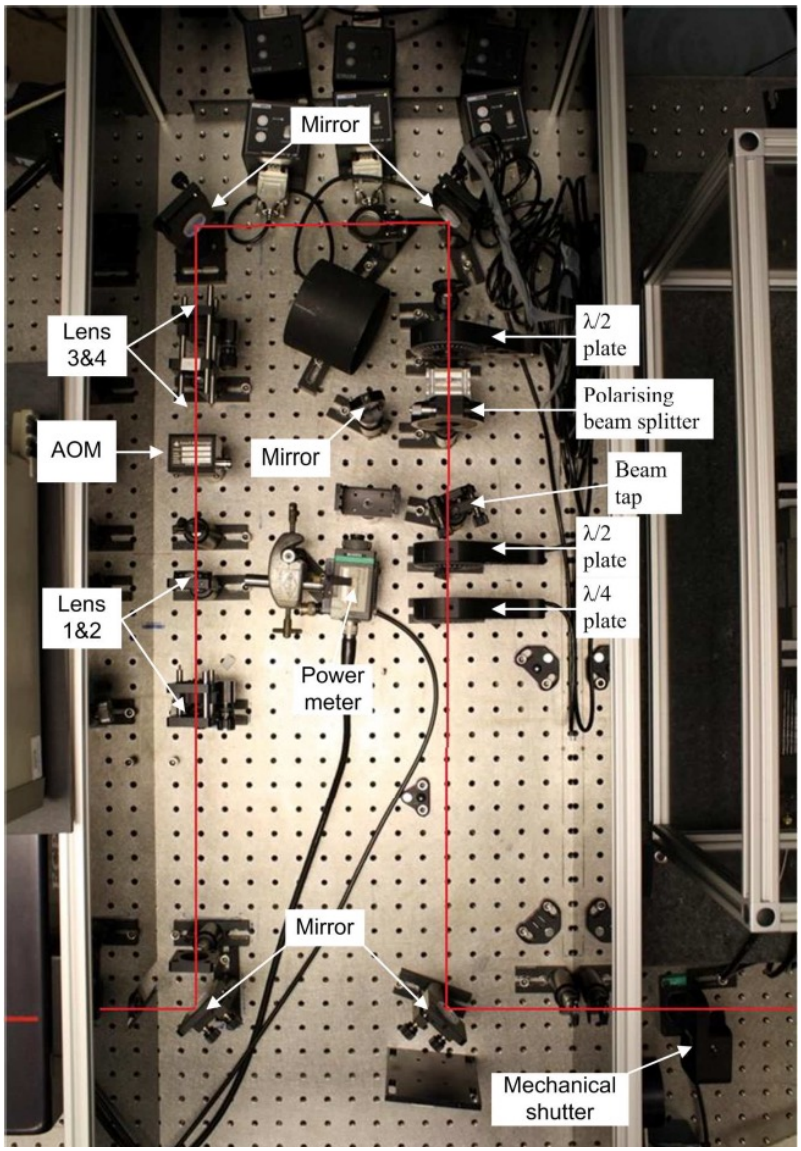

Figure 3. Ultrafast laser inscription apparatus: Power and polarisation control.

The external variable compressor (see Figure 2) allows the adjustment of the pulse duration used for inscription. Previous work on this project has highlighted this as an essential capability when working with highly non-linear materials such as ZnSe [23], and this technique has been pioneered by the project over the last four years. The acousto-optic modulator (AOM) is included in the apparatus to allow rapid modulation of the inscription beam for the fabrication of periodic features such as Bragg gratings [22].

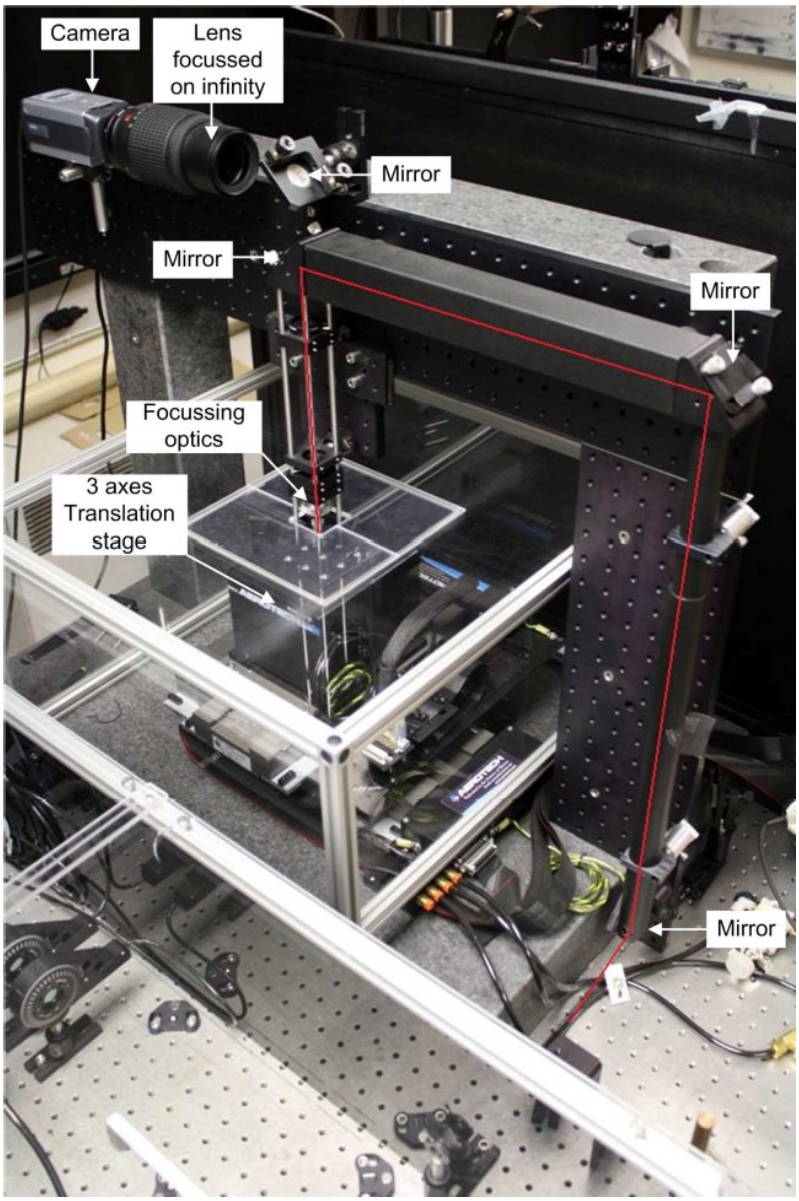

Figure 4. Ultrafast laser inscription apparatus: IMRA inscription laser beam path, focusing optics and imaging system.

An important waveguide inscription procedure utilised in the first and second phase of this project is the multiscan technique [24, 25]. This technique allows the tailoring of waveguide cross-section as well as a higher degree of control over the energy deposition within the desired waveguide volume. By overlapping multiple scans with asymmetric focal volumes, a symmetrical modified region can be created as illustrated in Figure 5.

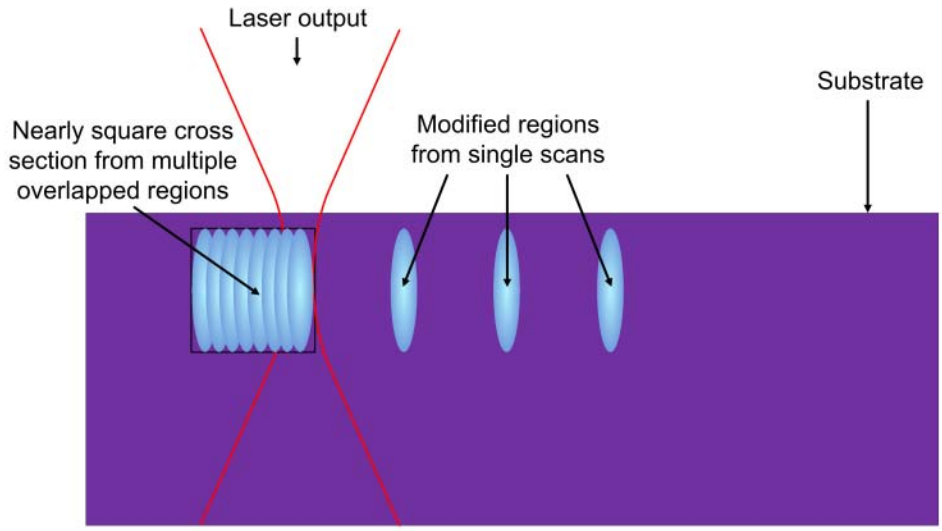

Figure 5. Multiscan technique inscription geometry. Overlapping scans are used to fabricate one near-symmetrical modified region.

First waveguides in Cr^{2+}:ZnSe and undoped ZnSe

The multiscan techniques were used to create the first waveguides in undoped ZnSe. These structures demonstrated guiding at 1550 nm but did not guide in the Mid-IR [14]. The reason for this was limitations in the maximum achievable index contrast combined with unwanted material damage adjacent to the fabricated waveguide core. This prevented an increase in cross-sectional area of the waveguides and hence they could not be optimised for the peak of Cr: ZnSe emission cross-section at 2450 nm.

The ability to achieve negative refractive index change in ZnSe was reported after an in depth investigation into a wide range of ULI fabrication parameters for ZnSe culminating in the demonstration of the first mid-IR ZnSe channel waveguide [26]. These structures used an unaltered core surrounded by a square cladding of negative refractive index change, shown in Figure 6. A multiscan technique with modified parameters was used to achieve entirely negative refractive index change. This structure demonstrated guiding at 3.39 μm which is at the long wavelength end of Cr^{2+}: ZnSe gain bandwidth, with propagation losses of 1.9 $dB \cdot cm^{-1}$. This result was a major milestone for the project and allowed progression to waveguide inscription in Cr doped ZnSe.

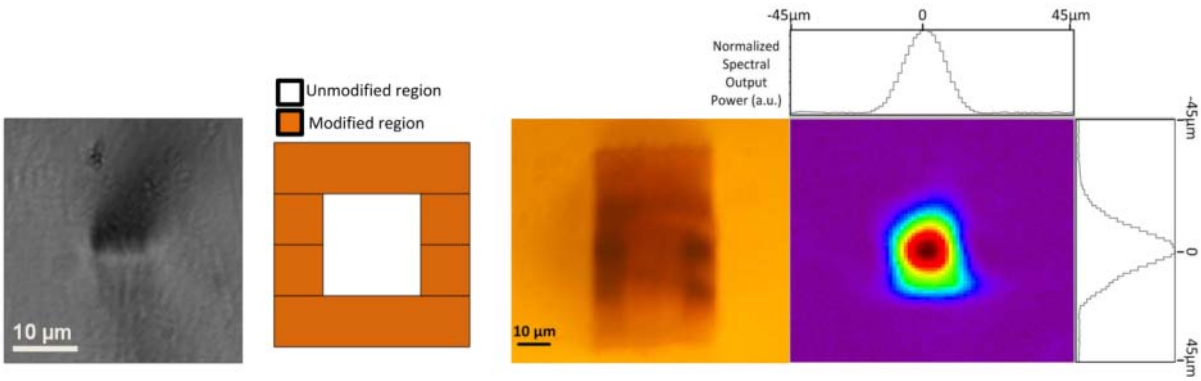

Figure 6. (a) Image of negative refractive index change in ZnSe taken using an optical microscope in transmission mode with white light illumination. (b) Map of depressed cladding waveguide design using the negative refractive index change. (c) Depressed cladding waveguide in ZnSe and associated guided mode at 3.39 µm.

The waveguide inscription parameters found to guide in the Mid-IR with undoped ZnSe where found to be unsuccessful in Cr^{2+}:ZnSe. This required a re-optimisation of the inscription parameters in order to demonstrate guiding at 3.39 µm. However, despite these changes, the propagation losses were too great to allow lasing in the waveguide cavity [27]. In order to improve the confinement a double cladding structure was utilised, this used the square cladding of the previous experiment with the addition of an outer cladding layer of grater negative refractive index change which surrounded the inner cladding. The greater refractive index change was created by the use of larger pulse energies, 0.35-0.5 µJ increasing to 0.5-1 µJ for the inner and outer cladding respectively. A diagram of the depressed double cladding waveguide designs are shown in Figure 7.

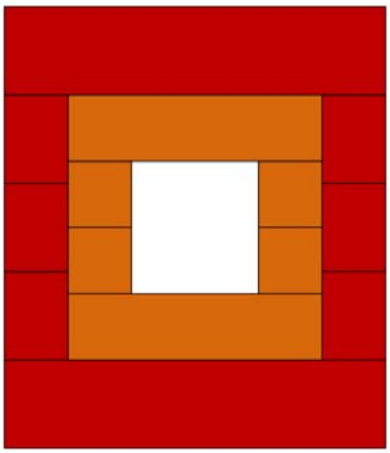

Figure 7. A schematic of a double clad depressed cladding waveguide where the red colour represents a greater change in refractive index than orange.

The waveguide structure was built into a compact cavity by butt-coupling a dichroic mirror on the input side of the waveguide and an output coupler mirror on the opposite side. Index matching gel was placed at the waveguide-mirror interface in order to reduce the losses from the fennel reflections. The output of the laser was collimated using a CaF_2 lens. The laser was pumped with a continuous wave (CW) thulium fibre laser in the configuration shown in Figure 8. Laser performance is also demonstrated in Figure 8 with an output coupling of 20 %.

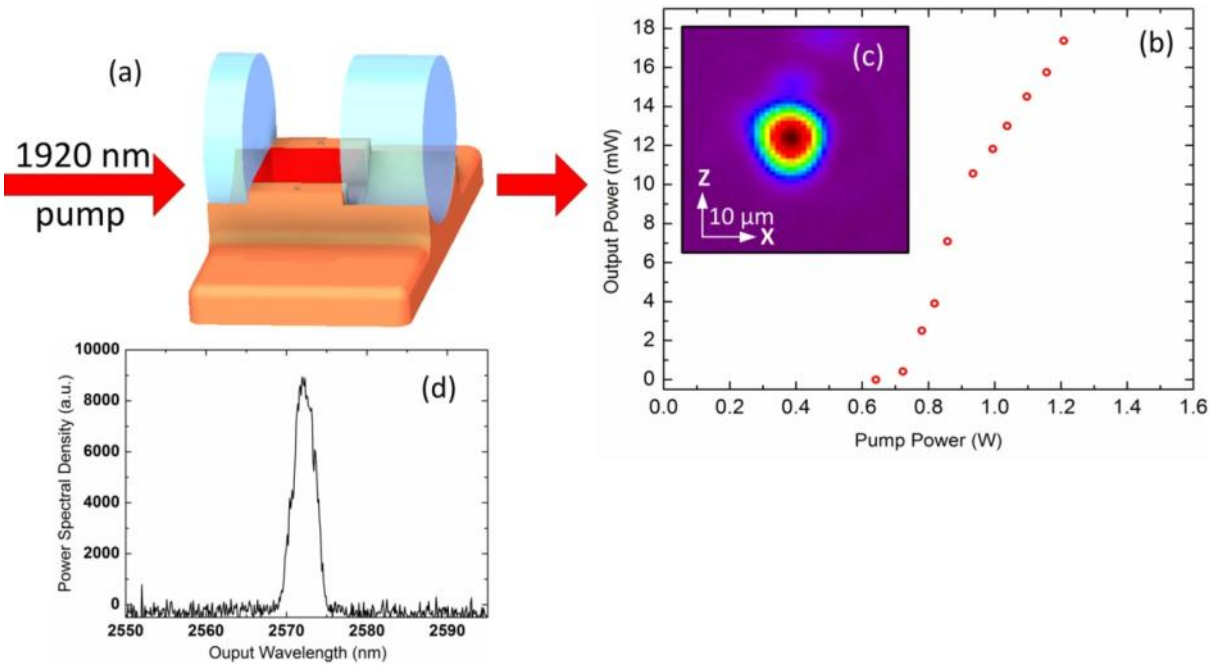

Figure 8. (a) Waveguide laser cavity assembly with butt-coupled dichroic mirror and output coupler mirror. (b) Laser output power against input pump power. (c) Near field image of the laser output mode at 2573 nm. (d) Laser output power spectral density.

The waveguide laser displayed a maximum output power of 18.5 mW for an incident pump of 1.2 W. A slope efficiency of 5 % and pump threshold power of 700 mW

were observed. This result is a major milestone in the project and also the field of mid-infrared photonics and as such the initial report of lasing in a Cr^{2+}: ZnSe channel waveguide has been published this year in Applied Physics Letters. Reference: Macdonald, J.R., et al., *Compact mid-infrared Cr:ZnSe channel waveguide laser.* Applied Physics Letters, 2013. **102**(16): p. 161110.

High efficiency circular cladding WG laser

The initial demonstration of square double clad depressed cladding waveguides where effective in demonstrating lasing, however the waveguide propagation losses were still high. Part of the reason for this was the cracks in the structure created by the large amounts of strain across the waveguide. These cracks increase the lasing threshold and hence reduced the lasers overall performance. For efficient laser performance it was clear that the waveguide losses must be reduced.

A low loss circular cladding waveguide structure has been demonstrated in YAG [28]. It was decided to see if this could be used to create low loss waveguides in Cr^{2+}: ZnSe as we have demonstrated the correct refractive index change needed for these structures. This structure will allow the use of the inscription parameters found in the previous work but will require a larger refractive index change. In order to achieve this increase the structure was fabricated with ‘overscans’, whereby we inscribe over the same line multiple times. A diagram and optical micrograph of the circular cladding structure is shown in Figure 9 where we are viewing the end facet of the waveguide.

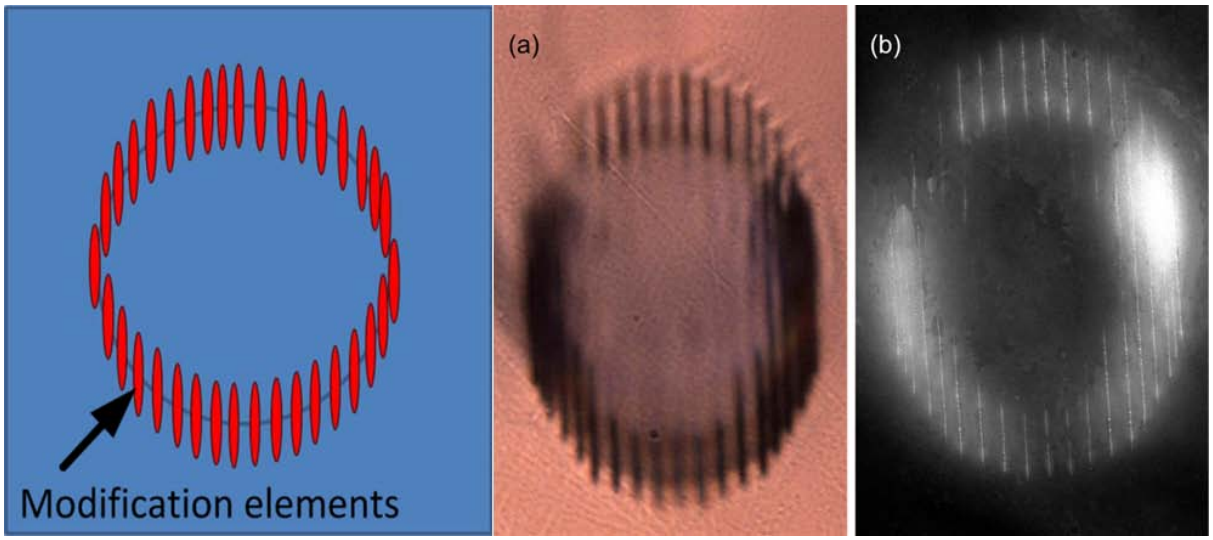

Figure 9. Left is a diagram of the arrangement of the modification elements viewed from the end facet. Middle is an optical micrograph of waveguide end facet taken in transmission mode under white light illumination. Right dark field image of the waveguide end facet.

The waveguides where then built into a laser cavity as shown in Figure 10. A 1.93 µm thulium fibre laser was used to pump the cavity with a maximum effective pump power available of 1.11 W. The beam was focused on to the waveguide end facet thought the input mirror with a CaF_2 objective of focal length 50 mm. The output of the cavity was collimated using an AR coted CaF_2 lens of focal length 20 mm. The collimated output beam was passed thought two 2000 nm long pass filters, to remove any non-absorbed pump, before being incident on a detector.

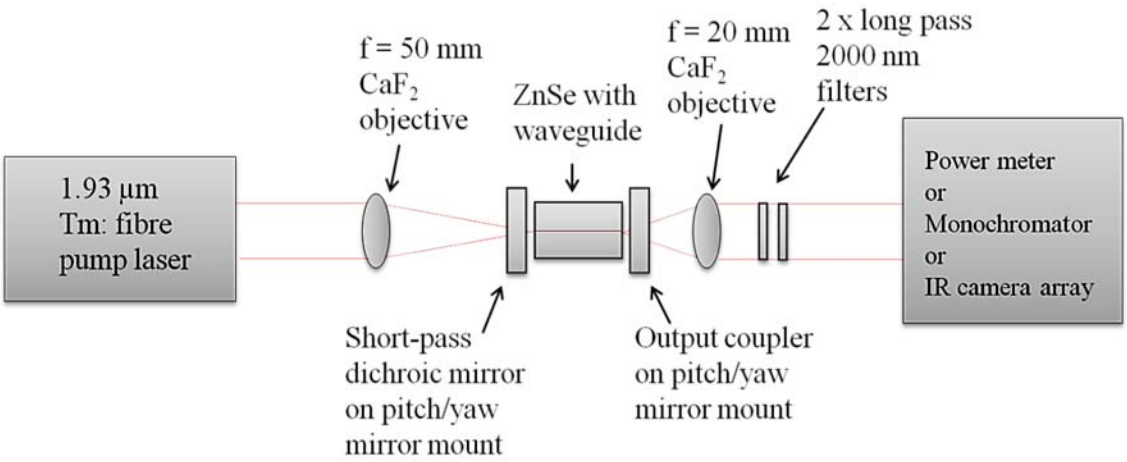

Figure 10. Schematic of Cr:ZnSe circular depressed cladding waveguide laser setup with pitch and yaw control of input and output couplers.

The laser performance was examined for a range of output couplers, 80 %, 70 % and 60 % reflectivity (R), to examine the effect of output coupling on laser performance. The laser signal with varying pump power is shown in Figure 11.

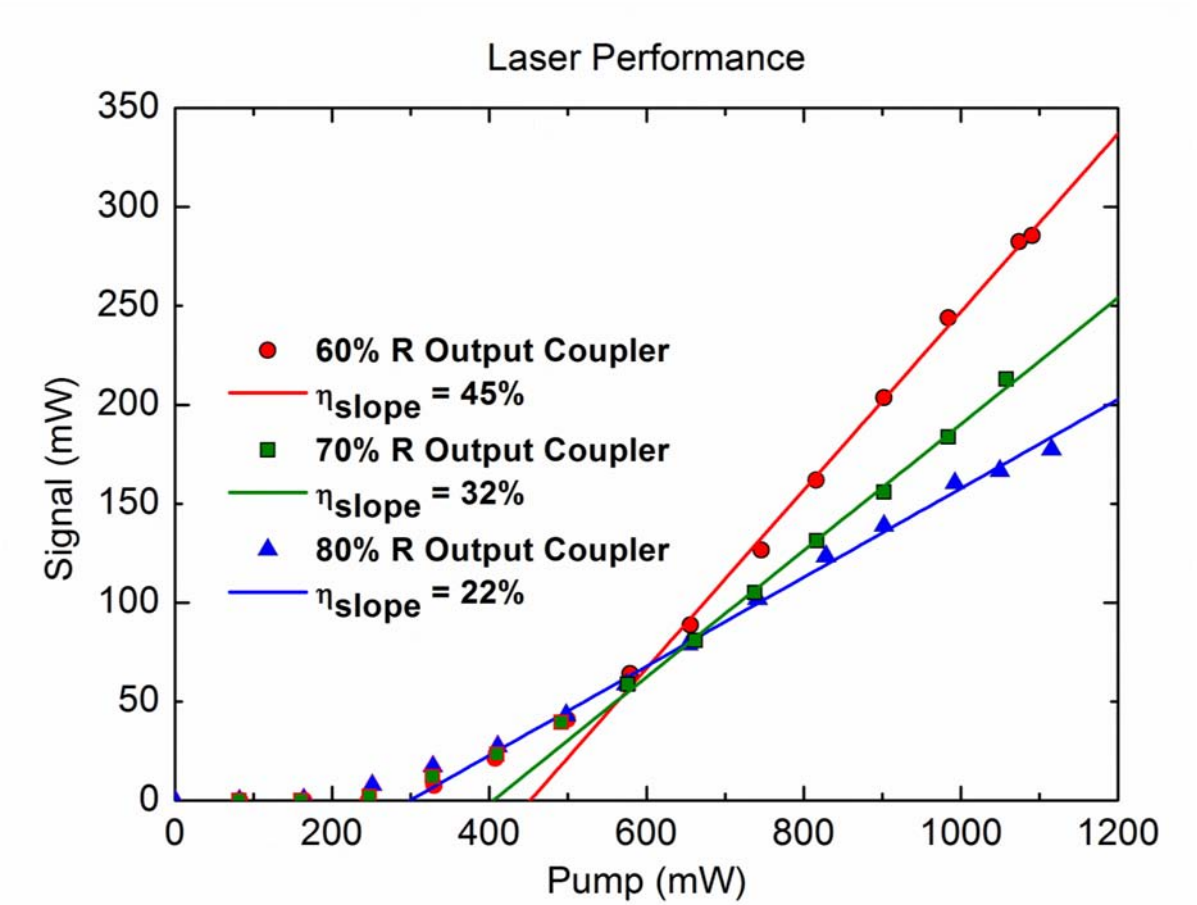

Figure 11. Cr^{2+}:ZnSe circular depressed cladding waveguide laser performance. Red line and points are for a output coupler of R 60 %. Green line and points are for an output coupler of R = 70 %. Blue line and pints are for an output coupler of R = 80%.

The laser demonstrated its best performance with a 60 % reflective output coupler where a high slope efficacy of 45 % and a maximum output power of 285 mW with a pump of 1.11 W. Figure 12 shows an optical spectrum and M^2 measurements taken of the laser with a 60 % reflective output coupler under a pump power of 1.11 W.

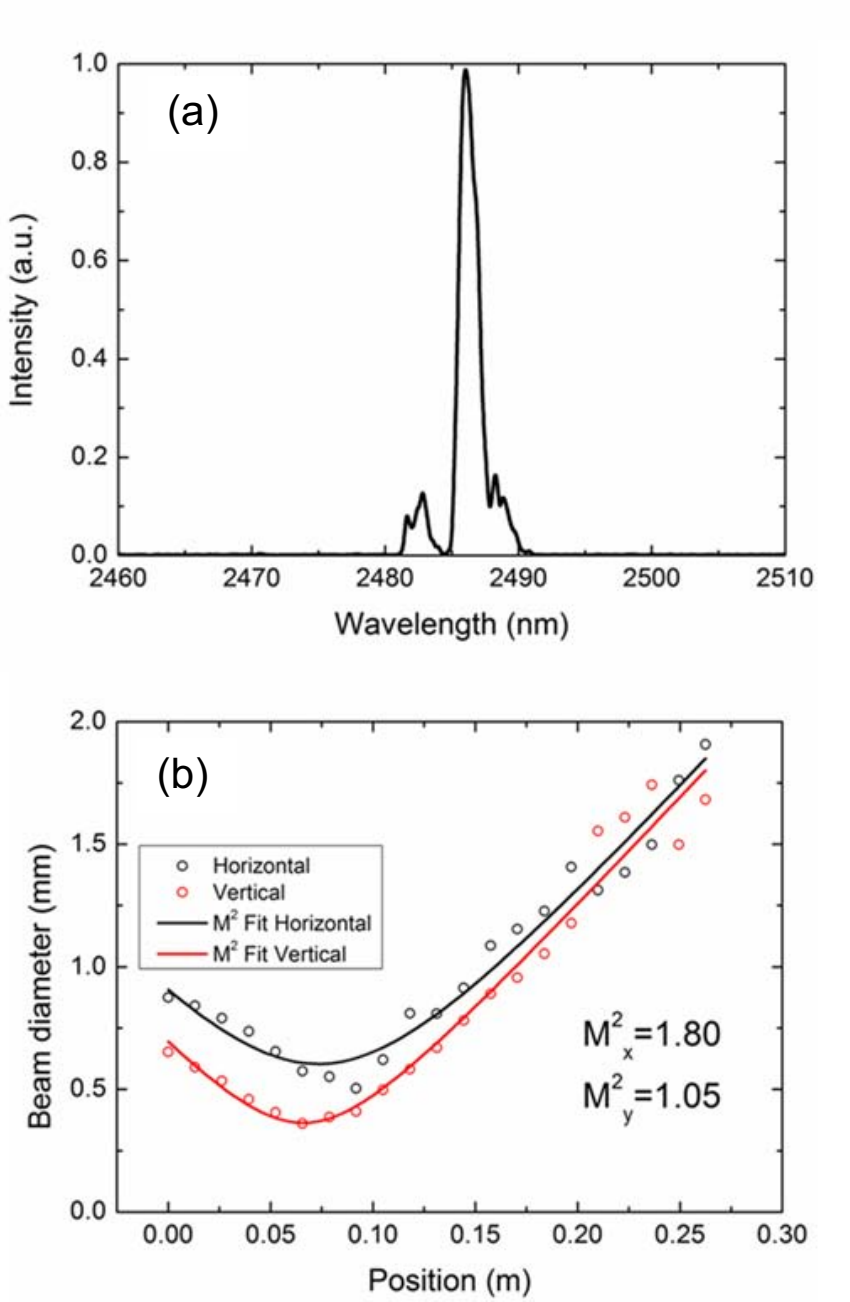

Figure 12. (a) Optical spectrum of the laser for 1.1 W of pump power. (b) M^2 beam quality for 1.1 W of pump power.

The M^2 measurement, shown in Figure 12 (b), demonstrates close to Gaussian

divergence and demonstrates the high mode quality possible with ultra-fast laser inscription. We have demonstrated an order of magnitude increase in performance with the circular cladding waveguides compared with previous work. The performance of the waveguides are now of sufficient quality to be used in creating new devises and to be sent to our collaborators at AFRL for high power testing. This work was published in Optics Letters reference: Macdonald, J.R., et al., *Efficient mid-infrared Cr:ZnSe channel waveguide laser operating at 2486 nm.* Opt Lett, 2013. **38**(13): p. 2194-6.

Tuneable waveguide laser

The demonstration of high efficiency Cr^{2+}:ZnSe waveguide laser allows research to progress to exploiting the materials broad gain bandwidth. The first investigation into tuneable continuous wave operation utilised an extended cavity design in order to incorporate a tuning element into the cavity. The external cavity used a blazed grating assembled in the well know Littman-Metcalf configuration as displayed in Figure 13. The signal wavelength coupled back into the waveguide is selected by rotating the silver tuning mirror. An advantage of using the Littman-Metcalf configuration over the Littrow configuration is the fixed output beam direction. In a Littrow configuration the output beam angle varies with the rotating grating element used for wavelength tuning. This is a particular problem when tuning across a broad wavelength range as the output angle would vary considerably. In addition to overcoming this problem, the Littman-Metcalf configuration provides greater wavelength selectivity, due to the signal preforming a double pass of the diffraction grating. This increased wavelength selectivity should lead to a narrower line width. The disadvantage of the Littman-Metcalf is the loss of the zero-order reflection upon the second pass of the grating, this increases laser threshold and potentially could limit the wavelength tuneability range of the laser.

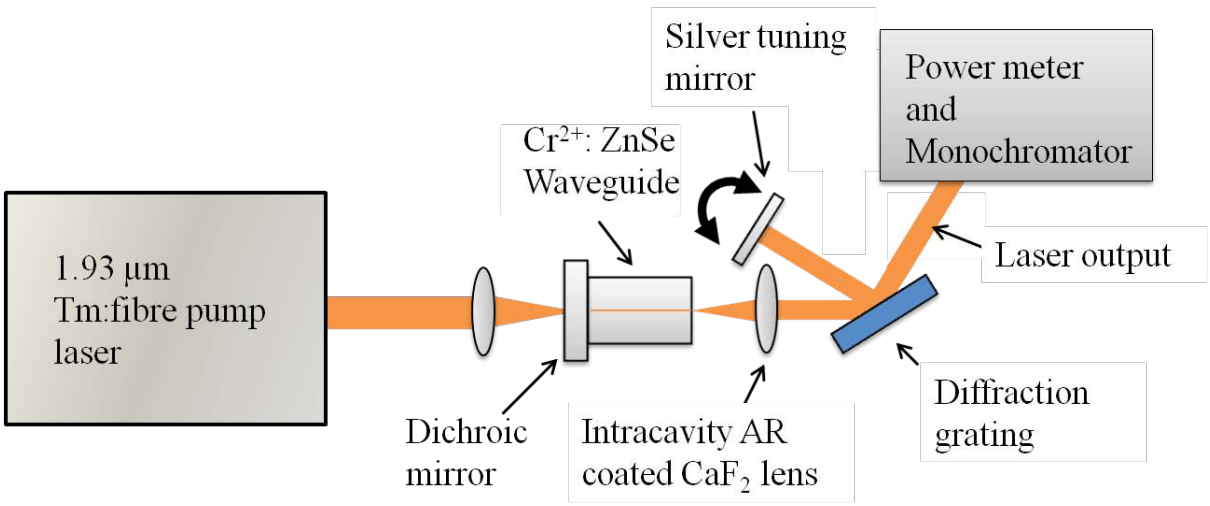

Figure 13. Experimental arrangement of the Cr:ZnSe external-cavity waveguide laser in the Littman-Metcalf configuration. The silver tuning mirror is rotated as shown to change the lasers wavelength.

The tuneable laser performance was investigated using a thulium fibre laser as an optical pump, with a maximum effective power of 1.4 W focused onto the waveguide end facet by a CaF_2 objective. A dichroic mirror was placed at the face of the waveguide and an AR coated CaF_2 lens was used to collimate the waveguide output before the beam was incident on the diffraction grating. The diffraction grating used was a Thorlabs GR13-0616 and has an efficiency of 90% across the gain bandwidth of Cr^{2+}:ZnSe.

The extended cavity demonstrated continues lasing form 2077-2777 nm, with output powers greater than 15 mW, by rotating the tuning mirror. Figure 14 shows the output power at varies wavelengths measured. This is a world record, for the widest tuning range by a waveguide laser. An impressive line with of only 0.053nm was achieved; this makes the devise suitable for chemical sensing applications. Spectra's measured across the lasers tuneable range are shown in Figure 15.

The peak of the laser output power was 120 mW at 2446 nm, which is in good agreement with the peak of gain materials emission cross section. This is an impressive result for a waveguide laser, demonstrating the low loss broadband guiding of ULI waveguide inscription. The power scaling limitations of this setup where not investigated due to the limited pump power available of 1.4 W at 1928 nm. Overall, the tuneable laser results mark a major milestone in the project and the wider photonic community as 700 nm of tuneability is a world record for a waveguide laser. As such this work along with a finite element model of the cavity was published in IEEE Journal of Selected Topics in Quantum Electronics: Macdonald, J.R., et al., *Ultrabroad Mid-Infrared Tunable Cr:ZnSe Channel Waveguide Laser.* Selected Topics in Quantum Electronics, IEEE Journal of, 2015. **21**(1): p. 375-379.

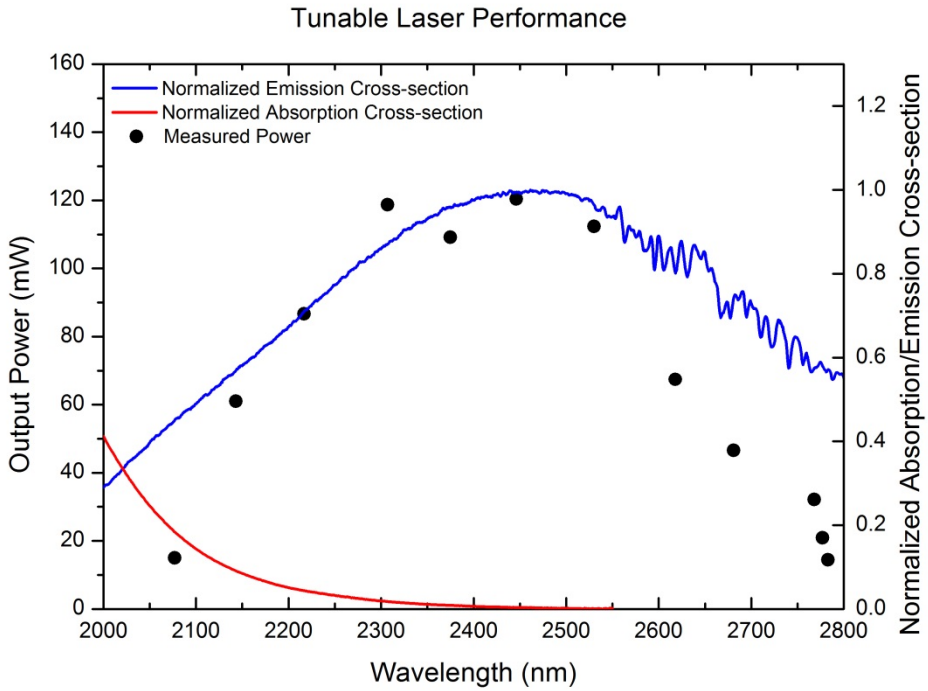

Figure 14. Tuneable waveguide laser performance utilising a diffraction grating in an extended cavity. Black dots represent measured output power at specific wavelengths. The blue and red line represent a normalized emission and absorption cross-section respectively.

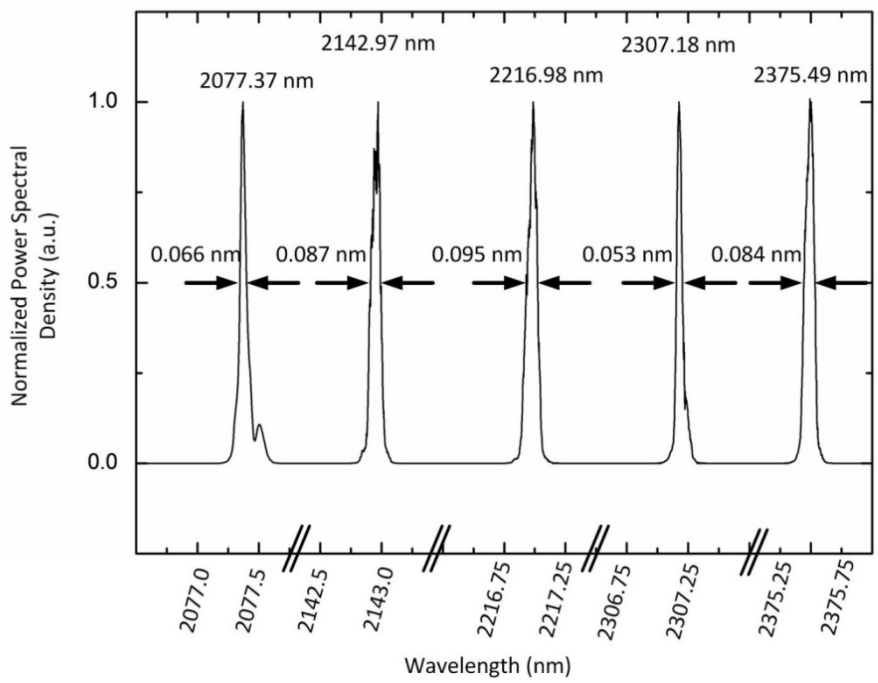

Figure 15. Narrow linewidth spectra of the tuneable Cr^{2+}:ZnSe waveguide laser measured with a mid-infrared spectrum analyser.

Finite element analysis of Cr^{2+}:ZnSe wavelength tuneable laser

To investigate limitations in the tuning performance of the laser, the system was numerically modelled using a plane wave approximation. Initially the pump and a small signal power were converted to an irradiance based on the measured mode-field diameter and are co-propagated through the gain medium, which is split into 10000 steps to allow for numerical modeling using steady state optical amplification equations adapted from Berry et al. to include signal absorption [6]. All values for the Cr: ZnSe absorption and emission cross-sections are taken from DeLoach *et al.*[1]. The signal emerging from the end of the gain medium is then multiplied by the manufacturers quoted efficiencies for the optical elements i.e. the intracavity lens = 0.99, grating efficiency at the given wavelength and the silver tuning mirror. This signal is then fed back into the amplifier in the counter propagating direction and the sum of the two counter propagating signal irradiances at each spatial co-ordinate is used. When the signal reaches the beginning of the waveguide it is multiplied by the reflectivity of the dichroic mirror and co-propagated with the pump again through the system. This process is repeated until the output power reaches a steady value. The propagation loss of the waveguide was assumed to be constant across the wavelength range of interest for the model at a value of 0.7 dB cm-1, with only the Cr: ZnSe absorption and emission cross sections and values for the grating and mirror reflectivities being varied for the different wavelengths. The experimental results and the results of this model are shown in Figure 16.

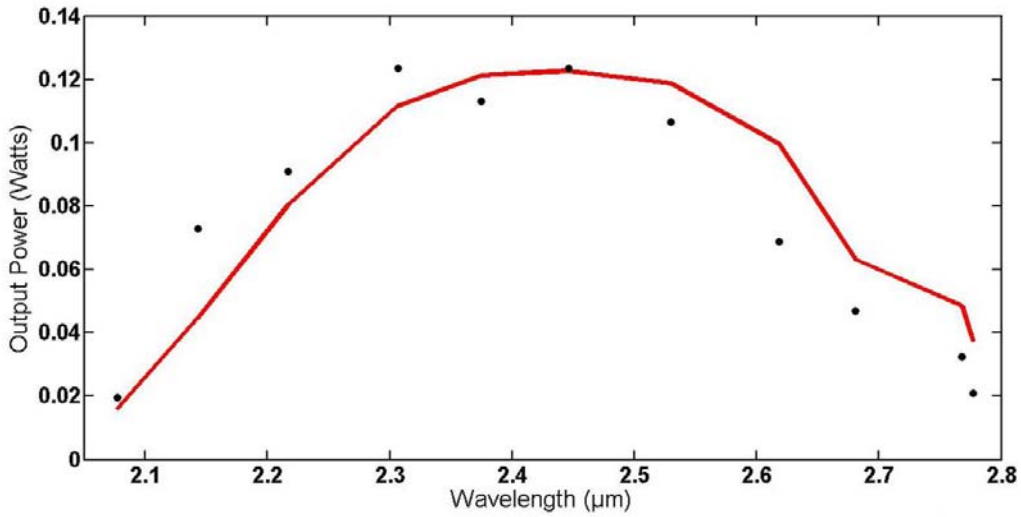

Figure 16. Finite element model of tunable laser output against experimentally obtained data. Experimental measured data shown as black points and model shown as red line.

Good agreement can be seen over the entire tuning range but some deviation between modelled and experimental data can be seen, predominantly at the edges of the tuning range. This discrepancy is likely due to spectral dependence in the

guiding characteristics of the waveguide. For short lasing wavelengths mode overlap between the pump and signal modes is better than at longer wavelengths and propagation losses due to waveguide radiation losses are likely to increase for the longer lasing wavelengths [29, 30]. Water absorption also increases for the recorded wavelengths beyond 2600 nm. These factors account for the model over predicting the output powers for long wavelengths. This model can be used to simply and quickly investigate the potential capabilities of similar systems built from different components, or different experimental configurations e.g. a Littrow configuration built from the same components would be capable of 900 nm tuneability, however the laser output changing direction with wavelength tuning significantly complicates the Littrow configuration integration into compact sensing systems.

Tuneable Cr^{2+}:ZnSe waveguide laser with a Si prism

The finite element analysis showed that the grating was reducing the tuneability range particularly at higher wavelengths. This arises from the loss of the gratings zeroth order and the poor grating efficiency at longer wavelengths. A Si Brewster cut prism was proposed to expand the tuneability range and increases overall laser performance. The prism has the advantage of not having an efficiency drop off at 3 μm. The large Fresnel losses from the air Si interface can be mitigated by placing the prism at Brewster's angel. The extended prism cavity, shown in Figure 17, was built into a similar cavity arrangement as that of the grating.

A Thulium fibre laser was used as the pump source with a maximum pump power of 1.4 W. The pump was focused through the dichroic mirror onto the facet of the waveguide using a CaF^{2+} lens. The large gain bandwidth of Cr^{2+}: ZnSe spanning approximately 1950 to 3350 nm [31], is much larger than the flat reflection response of the mirrors available to us. Therefore, the mirror set needed to be changed as the laser output was tuned. A list of the mirrors used and there wavelength ranges are given in Table 1. The Si prism was aligned at close to Brewster's angle. An intracavity AR coted CaF_2 lens was used to collimate the output of the waveguide on to the prism. The output coupler was rotated in order to change the wavelength of the cavity. This rotation deflected the output beam slightly, this meant the alignment of the power meter and monochromator had to be optimised for each different wavelength measurement. The tuneable laser output power plotted against wavelength is shown in Figure 18.

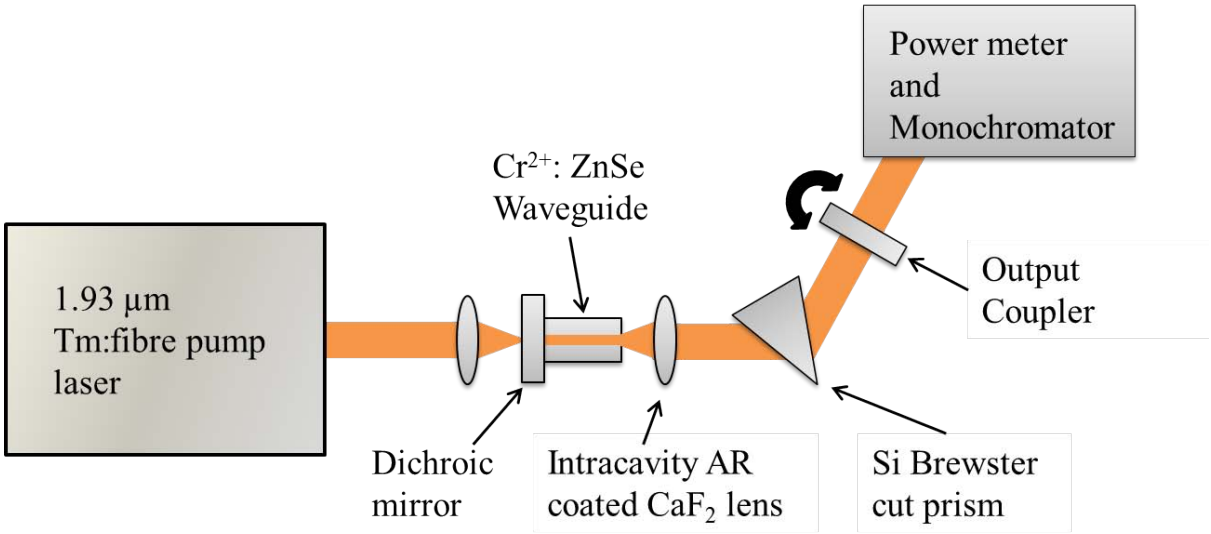

Figure 17. Experimental arrangement of the wavelength tuneable Cr^{2+}:ZnSe external-cavity waveguide laser using a Si prism. The Output Coupler is rotate to change the lasing wavelength.

Mirror Type	Reflectance (%)	Wavelength range (nm)	Use In
Dichroic mirror	> 99.9	2000-2500	Set 1
Dichroic mirror	> 99.6	2500-3000	Set 2 and Set 3
Output Coupler	80 ± 5	1700-2700	Set 1 and Set 2
Output Coupler	89 ± 1	2800-3070	Set 3

Table 1. List of mirrors used in tuneable Cr^{2+}:ZnSe external-cavity waveguide laser using a Si prism.

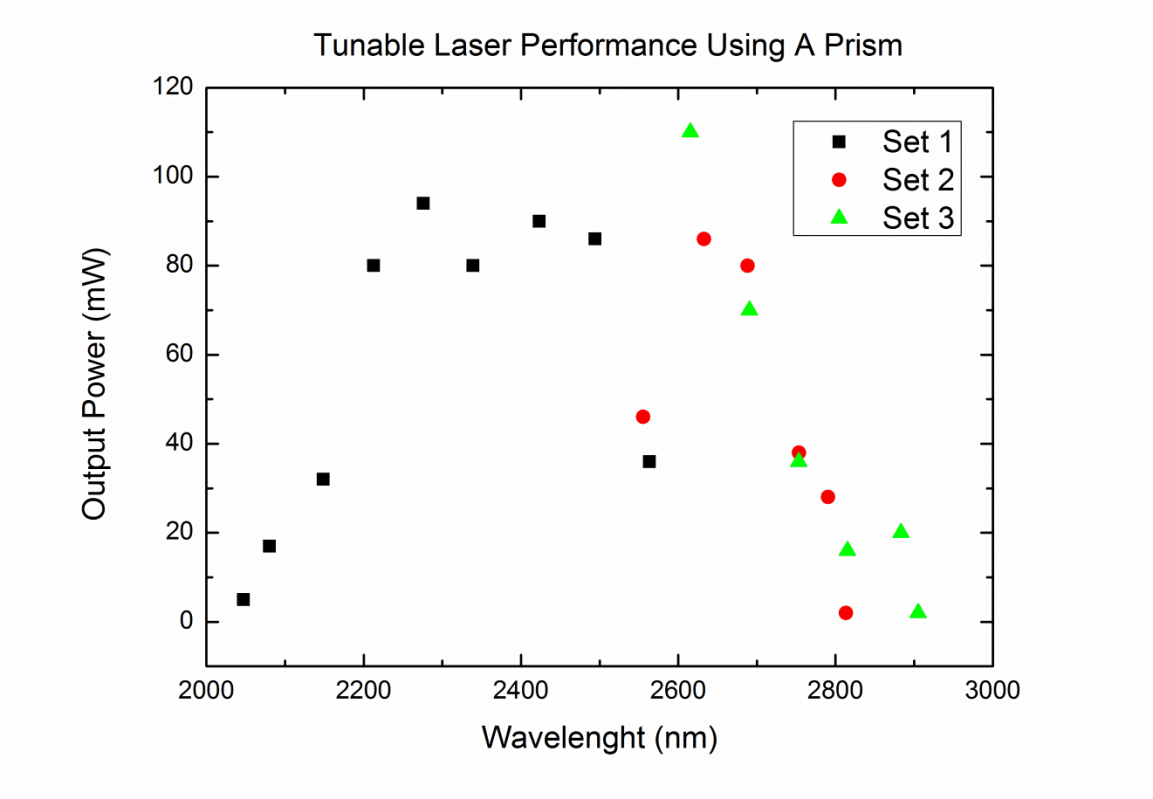

Figure 18. Wavelength tuneable Cr:ZnSe laser performance using a Si prism. Set 1 used a dichroic mirror with reflectance > 99.9 % for a range of 2000-2500 nm and an output coupler with reflectance 80 ± 5 % for a range of 1700-2700 nm. Set 2 used a dichroic mirror with reflectance > 99.6 % for a range of 2500-3000 nm and an output coupler with reflectance 80 ± 5 % for a range of 1700-2700 nm. Set 3 used a dichroic mirror with reflectance > 99.6 % for a range of 2500-3000 nm and an output coupler with reflectance 89 ± 1 % for a range of 2800-3070 nm.

The extended cavity demonstrated continuous lasing over 2080-2883 nm with an output power greater than 15 mW over the whole wavelength range. The maximum output power of 110 mW was measured at a wavelength of 2615 nm. A notable improvement in performance was observed using the Si prism tuning element which achieved an additional 101 nm of tuneability over the results obtained using the blazed grating. However, in order to create a robust, integrated system, more appropriate cavity mirrors are required. The output couplers differed in Set 3 compared with Set 1 and 2. Set 3 utilised an 89% reflectance output coupler compared with the 80% in the other sets, this means the lasing threshold of Set 3 should be lower than that of the others. The laser slope efficiency will also be different. These discontinuities in the cavity properties make modelling of the system challenging and a complete characterisation with fewer mirror sets would be preferable to understanding the waveguide gain medium. These initial results remain significant and warrant further investigation and modelling. This work was presented at Photon 12 conference in the UK: A. Lancaster, J. R. Macdonald, S. J. Beecher, P. A. Berry, K. L. Schepler and A. K. Kar, “Broadly tuneable Cr^{2+}:ZnSe channel

waveguide laser," Fibre Optics and Waveguides symposia, Photon 14, 2014, London, UK.

High power waveguide laser

The key objective of this project is to power scale Cr^{2+}: ZnSe by overcoming the limitations of thermal lensing. Waveguide geometry was proposed as a method of overcoming the limiting factor thermal lensing. The pump source available at Heriot-Watt is a 1.4 W thulium fibre laser which is not adequate to demonstrate tens of watt laser output power. As such, this work is being continued in collaboration with AFRL at Wright-Patterson Air Force Base. The above described circular cross-section depressed cladding waveguides where sent to AFRL in order to be operated with a high power Tm: fibre pump source capable of 38 Watts CW output at 1908 nm.

For high power operation the laser cavity setup was similar to the one used in Figure 10 with the addition of a water cooled heat sink kept at a constant 15°C. The cavity was optically pumped with an IPG thulium fibre laser at incident powers up to 9.3 W at 1908 nm. Lasing was observed for many of the structures but the most effective waveguide had a designed diameter of 80μm consisting of 60 elements each of which had be overwritten 25 times. The laser performance using a variety of output couplers is shown in Figure 19.

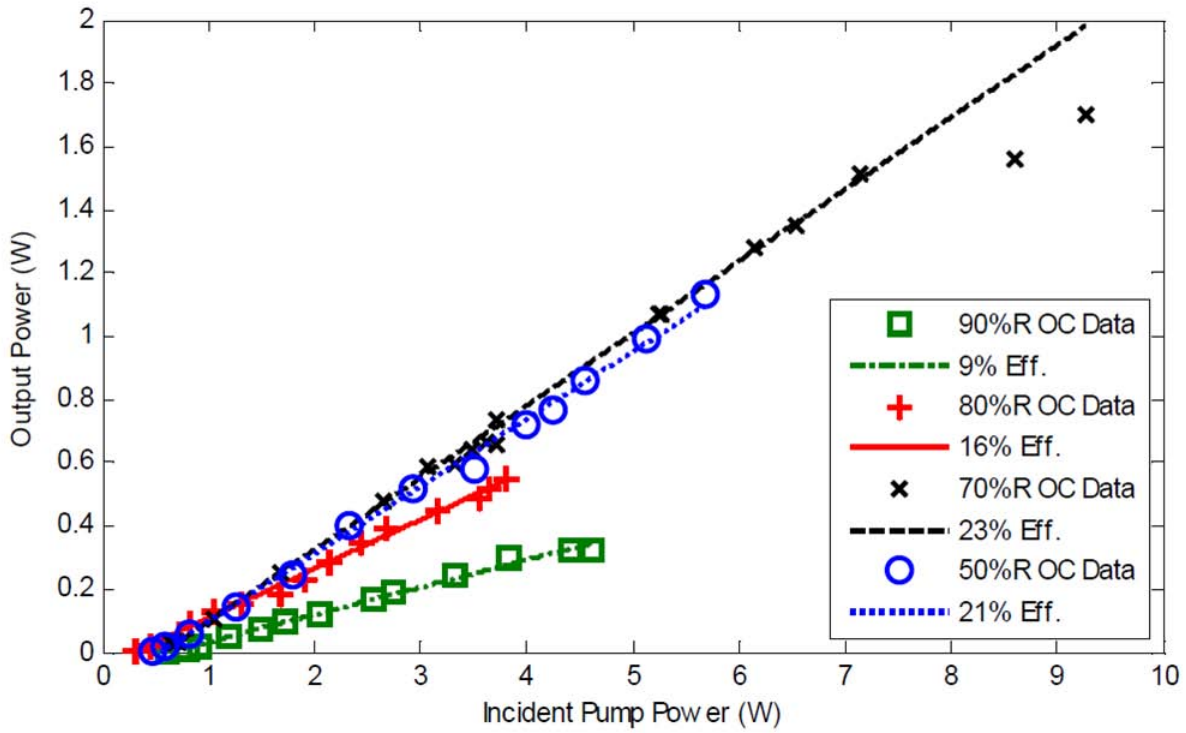

Figure 19. Depressed circular cladding waveguide Cr^{2+} laser performance for different output coupler reflectivity under high pump power [32].

As can be seen from Figure 19 the largest slope efficiency was 23 %, achieved with a 50 % reflective output coupler. A maximum output power of 1.7W was observed for

9.3 W of incident pump power. This impressive result demonstrates a 6 fold increase in output power compared with previous work in Cr^{2+}: ZnSe waveguide lasers. As such this work along with a thermal model was published in Optical Materials Express reference: Berry, P.A., et al., *Fabrication and power scaling of a 1.7 W Cr:ZnSe waveguide laser.* Optical Materials Express, 2013. **3**(9): p. 1250-1258.

This initial result for mid-IR depressed clading waveguide lasers with a maximum output power of 1.7 W remains substantially lower than the tens of watts demostrated in bulk Cr:ZnSe laser systems [33]. Significant improvements are expected, however, as the waveguide structures are optimised for lower propagation losses and more effective thermal management . In order to understand the thermal limitations of the waveguide structures a thermal model was proposed with a view to investigating the effect of waveguide cross-section, waveguide depth within the bulk crystal, waveguide length and dopant concentration of the Cr^{+2}: ZnSe gain medium. This model is presented in the following section.

Modelling of Cr^{2+}:ZnSe waveguide laser performance

The current limitations in power scaling of Cr^{2+}: ZnSe have been attributed to thermal lensing within the gain medium as a result of the high thermo-optic coefficient of ZnSe. While a waveguide geometry offers a means of mitigating thermal lensing, the effect of thermal quenching of upper state lifetime must be considered. This problem can be exacerbated by the high confinement of the laser beam with non-radiative decay quenching caused by increased temperature of the host material in the waveguide. The reason for this is there is always some pump power converted into heat (even when lasing) and as the material heats up above room temperature the non-radiative relaxation rate rises rapidly [2].

The accumulated temperature increase in the waveguide was modelled using the computer package COMSOL[32]. The waveguide structure analysed was similar to that used in the high power studies it had a diameter of 80 μm and was located 200 μm from the singular cooled surface (shown in back in Figure 20). Laser pumping was modelled as a Gaussian beam with a $1/e^2$ radius of 40 μm and the Cr^{2+} doping was model as 320 ppm. Beer's law of heat deposition was calculated using an absorption cross section of 1×10^{-18} cm^2 for a 1.9 μm pump source. The temperature in the waveguide was calculated to increases by 19 K per watt of pump power. The largest irradiance in the system is at the front facet of the waveguide and hence this is the worst case scenario and is shown in *Figure 20*.

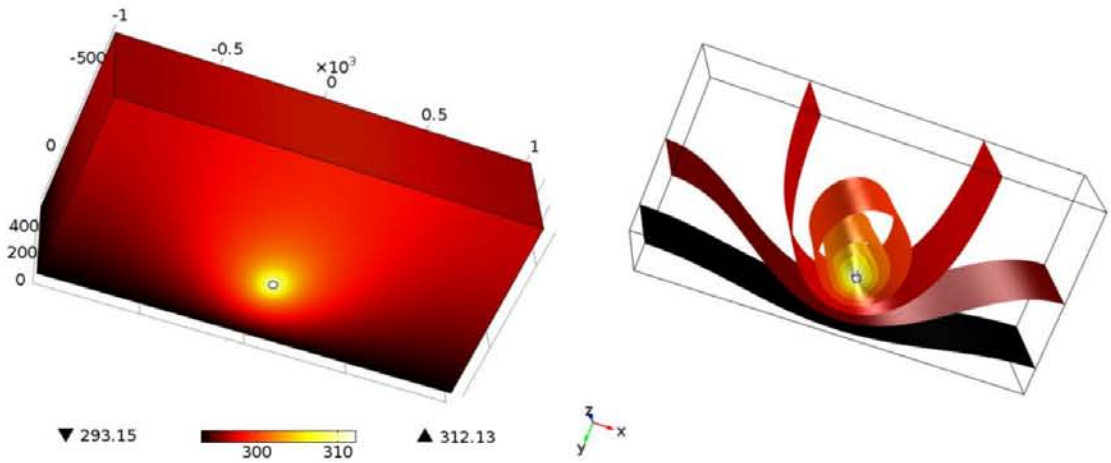

Figure 20. Plots of calculated temperature of Cr^{2+}:ZnSe slab pumped by a Gaussian beam with 40 μm $1/e^2$ radii propagation along a 40 μm radius waveguide structure. The bottom dark surface was fixed at room temperature to simulate mounting on a heat sink. The left plot is a surface plot of temperature: the right plot is an isosurface plot of the region near the waveguide region. The dimensions and location of the waveguide region were chosen to match those of the actual waveguide sample used to demonstrate lasing except for the waveguide propagation length (0.5 mm rather than the actual 6 mm length).

The modelling is for the cavity when it is not lasing, lasing operation should reduce the heat load but at a certain amount of pump power, the oscillator will become unstable. The models was used along with lasing stability arguments detailed in [32] to produce a calculation for the critical pump power shown in Equation 1.

$$P_{crit} = \frac{\Delta T_{crit} - S P_{th} \frac{dT}{dP_{in}}}{(1 - S)\frac{dT}{dP_{in}}}$$

Equation 1. Calculation for the critical pump power (P_{crit}) at which instability's arise form high temperature increases in the waveguide cavity. ΔT_{crit} is equal to the critical temperature minus the heat sink temperature. S is the laser slope efficiency, P_{th} is the laser threshold and P_{in} is the laser pump power.

This calculation is for the front of the waveguide, further downstream will have a higher critical pumping but quenching at the start of the cavity will still be detrimental to the whole lasers performance. Using a 70% reflective output coupler the model gives a value of 6.8 W for P_{crit} and this agrees well with the experimental roles off observed at 7W shown in Figure 19. Thus the model and experimental results are in good agreement and hence the model can be used analysed the limits of power scaling with a Cr^{2+}:ZnSe waveguide laser.

From this model and the experimental results, it is clear that further scaling of power will require mitigation of thermal quenching of lasing. Using the model Berry, et al [32] was able to make several recommendations for overcoming this problem. The first was to increase cooling by the use of liquid nitrogen cryogenics but this would only increase the temperature change need to reach instability by a factor of 3.2. Another method would be to increases the waveguide area to reduce dT/dP_{in} by a factor proportional to the square of the diameter. Cr^{2+} doping concentrations could also be reduced to allow higher pump powers. This would reduce the overall gain per unit length of the system therefore the losses of the waveguide would need to be reduced to make this an effective option. Another and effective solution is to bring the waveguides closer to the surface of the material and hence closer to the heat sink. There is a problem with waveguide asymmetry and ablation when doing this, which has been observed in previous work with waveguides close to the surface. Overall reduction in waveguide losses would improve system efficiency and the ability to increase power scaling further makes it clear that it should be a mean focus for future work.

Modelocking of Cr:ZnSe waveguide laser

There has been a considerable body of work by different research groups in the development of bulk Cr:ZnSe mode-locked laser. There reason for this is Cr:ZnSe gain bandwidth spans 1.95 to 3.35 μm [34] which is unprecedented in the spectra range it operates. Indeed Cr:ZnSe is often referred to as the "Ti:Sapphire of the mid-infrared". In this work we am to combine the work in bulk Cr:ZnSe femtosecond lasers with the waveguide technology we have developed at HWU [35]. The main

advantages of a Cr:ZnSe waveguide laser is high pulse repetition frequency (PRF) in the tens of GHz [36, 37] and vibrational insensitivity available to a monolithic laser geometry.

A schematic of the CW mode-locked Cr:ZnSe waveguide laser cavity is given in Figure 21. The Cr:ZnSe waveguide was optically pumped with a 1.5 W CW Tm: Fiber laser. The end facets of the Cr:ZnSe waveguides where anti-reflection coated. For this work we used a SESAM (Del Mar Photonics SAM-2400-1-25) with a saturation fluence, relaxation time constant and modulation depth of 90 μJ/cm^2, 500 fs and 0.6 % respectively to passively mode-lock the laser. Our initial investigations used a two mirror butt-coupled cavity design with resonator length 6.5 cm, similar to Ref [38], but no modulation was observed and the laser was found to operate in pure CW. The cavity of the laser was then extended to 34.5 cm, with the cavity configuration shown in Figure 21, the laser was found to be mode-locked with a PRF of 580 MHz but there was also an overlapping Q-switched envelope with a frequency of 2.5 MHz at 1.3 W of pump power. The cavity of the laser was then extended to 50 cm. In this configuration the laser was found to reach laser threshold at 300 mW of incident pump power. Modelocked operation was not started until the pump power was increased to 800 mW. Stable self-starting CW Modelocking was observed from 800 nm to the limit of the available pump power 1300 mW. CW Modelocking was confirmed using a CMT detector (VIGO system PVM−10.6) with a 1 ns time constant and a 13.2 GHz RF spectrum analyser (Agilent E4405B). From laser threshold to 800 mW pure CW operation was observed with no transition into Q-switched Modelocked operation observed. The RF spectrum of the laser operating under 1.3 W of pump power is shown in Figure 22.

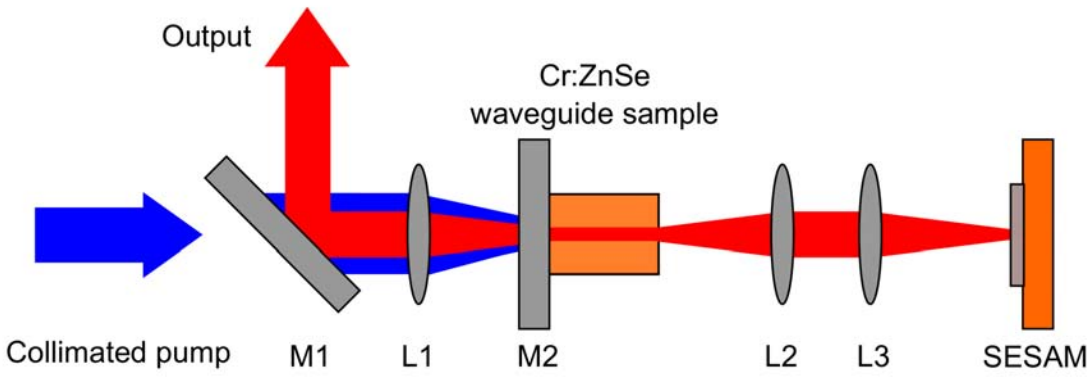

Figure 21: Schematic of Modelocked Cr:ZnSe waveguide laser. M1 is 45^0 dichroic mirror AR 1.9 μm and HR 2.3 – 3 μm. M2 is a dichroic mirror with AR at 1.9 μm and 98 % reflecting at 2-3μm coatings. L1, L2 and L3 are 50 mm plano-convex CaF_2 lenses AR coated from 1.65 to 3.0 μm.

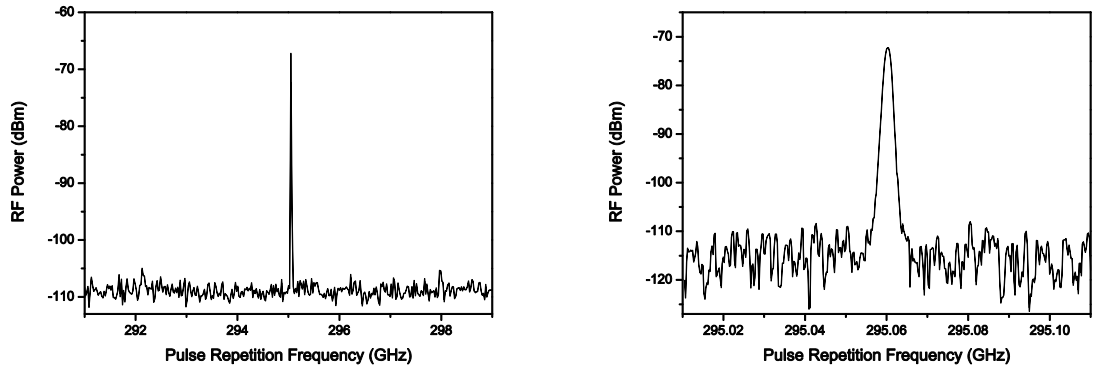

Figure 22: RF spectrum of CW Modelocked Cr:ZnSe waveguide laser operating with 1.3 W of pump power. In (a) the span was 9 MHz with a resolution bandwidth of 1 kHz. In (b) the span was 100 kHz with a resolution bandwidth of 1 kHz.

The maximum average power of the laser was measured to be 5 mW with a pump power of 1.3 W. The slope efficiency of the laser in the CW modelocked regime was calculated to be 0.63 %. A plot of pump power v.s. output power is shown in Figure 23 (a). From this figure we observe that the onset of modelocking at 800 mW of pump power results in the slope efficiency increasing from the reduction in cavity loss created by the saturating of the SESAM. Future work will use higher average power pump laser. Not only will this allow access of higher output powers than with the current cavity configuration but it will also allow sufficient saturate of the SESAM with larger output coupling rustling in better laser efficiency. The mode field diameter of the laser was imaged using a 500 mm lens and a Mid-IR camera (Flir SC7000), shown in Figure 23 (b). The MFD of the waveguide laser was found to be single mode with diameters of 60.0 μm and 57.7 μm in the x-axis and y-axis respectively.

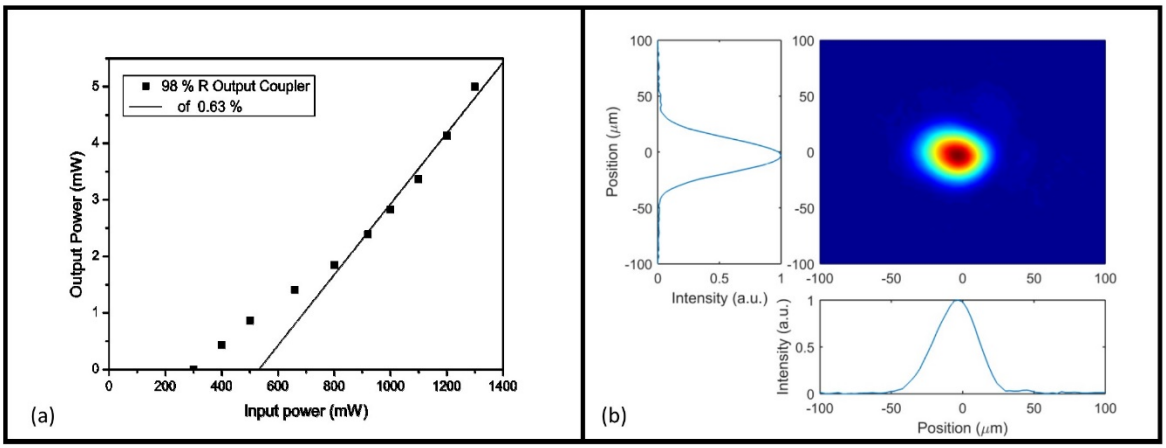

Figure 23: (a) Input power – Output power graph of 50 cm long Modelocked Cr:ZnSe waveguide laser. (b) Mode image of the waveguide during Modelocked operation.

The output spectrum of the laser was measured using an Optical Spectrum Analyser (Thorlabs OSA205). The Cr:ZnSe laser operating in CW Modelocked with 1300 mW of incident pump power is shown in Figure 24 (a). As can be seen from this figure the laser has the majority of its spectra emission centered at 2475 nm with two other

smaller emission centered at 2530 and 2550 nm this multi peck spectra is common feature for free running bulk Cr:ZnSe lasers [33]. Figure 24 (b) shows an expanded view of the spectrum centered at 2475 nm with clearly visible fringes. This fringe effect was confirmed not to be form the modelocking of the laser as the same result is observed when the SESAM is replaced with a 100 % reflecting dichroic mirror and the laser is operated in CW mode. The fringes are formed from by a Fabry-Perot etalon created from the end facets of the Cr:ZnSe waveguide sample inside the extended laser resonator. The Cr:ZnSe sample is anti-reflective coated but this coating is not sufficient to remove the etalon effect when you take into account that there is gain in the etalon. Development of polarization maintaining waveguides to allow the use of Brewster cut waveguide end facets will eliminate this problem and make more of the available bandwidth available for the creation of ultra-short pules. Characterization of the pulse width of the laser where investigated using two autocorrelators. The first was a commercially available system that used a frequency doubling crystal (APE pulse Check) and the second was a homemade system that detected the nonlinear absorption in a InGaS detector to autocorrelate the laser. An autocorrelation trace could not be obtained with either of this systems. The reason for this is the low average power, relatively high repetition rate and long pulse width of the laser. Setting a lower bound on the pulse width by calculating the transform limited pulse from the 2475 nm spectral peck gives a pulse width of 2.8 ps. This results in a peck power of only 5.34 W at a pump power of 1.3 W. This is not sufficient for frequency doubling in a crystal or two photon absorption in an InGaS detector.

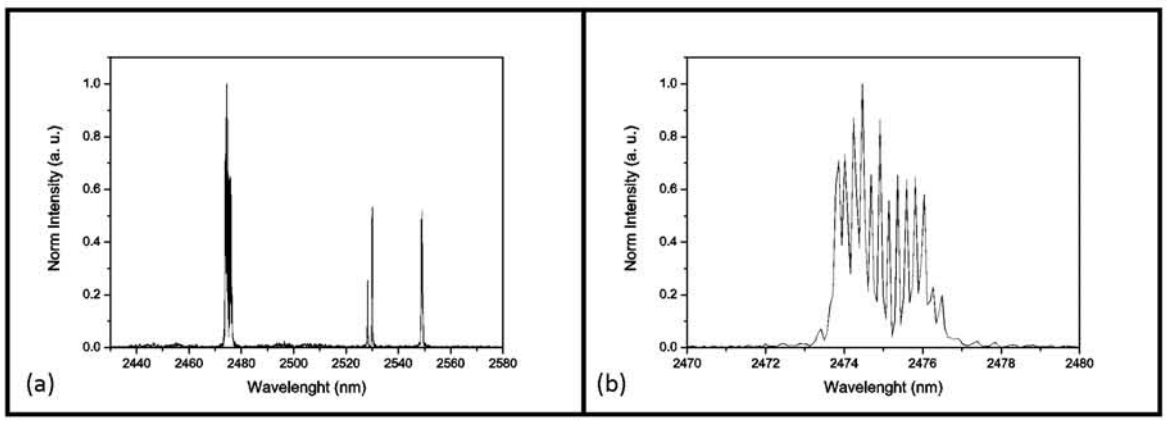

Figure 24: (a) Wavelength spectrum of CW ML Cr:ZnSe waveguide laser with 1.3 W of pump power. (b) Zoomed in view of lasers main spectral emission peck.

We have demonstrated a the first CW Modelocked Cr:ZnSe waveguide laser. The cavity length was extended beyond that the of the laser sample length in order to demonstrate CW Modelocked operation with the available SESAM and laser pump power. The main spectra emission peck of the Modelocked laser was centered at 2475 nm with a FWHM of 2.3 nm when operated with the maximum available pump power of 1.3 W. Form this a lower bound on the pulse width of the laser is calculated

to be 2.8 ps. The laser demonstrated an output of 17 pJ at a fundamental pulse repetition rate of 295 MHz.

Further work in dispersion compensation and improved laser efficiency are need to facilitate a successful autocorrelation of the lasers pulse width. Once this is done we will work on reducing the cavity length to produce an ultra-short pulsed laser in the 2 – 3 μm spectra region with tens of GHz PRF.

Summary

This project saw the fabrication of low loss (0.7 $dB \cdot cm^{-1}$) circular cladding waveguides in Cr^{2+}:ZnSe, marking a major milestone for the project. This allowed the creation of a compact Mid-IR source with 285 mW of output power and 45% slope efficiency. A world record was broken with the demonstration of a waveguide laser with 803nm of wavelength tuneability. The initial high power testing was performed with an impressive 1.7 W of output power. The thermal limitations of the waveguide laser design were modelled and this gives a clear direction for the future the project. That is to bring the waveguides closer to the surface, reduce the waveguides propagation losses and use lower doping concentrations in conjunction with longer waveguides. These modifications will open the door to an order of magnitude increase in output power of Cr:ZnSe lasers in a compact and robust laser system suitable for real world applications.

Fe:ZnSe waveguide laser

Introduction

This investigated was performed at Heriot-Watt University in close collaboration with Gary Cook from AFRL WPAFB. For this work G. Cook spent 5 weeks in the summer of 2014 working in the labs at Heriot Watt with our research team developing the Fe:ZnSe waveguide laser. G. Cook's trip was founded by EOARD through the window on the world program.

Iron-doped ZnSe (Fe:ZnSe) is another promising broad-band gain medium with luminescence from 3.5 to 5.2 μm at room-temperature [6]. This lines up well with the second atmospheric transmission window. The absorption and emission bands of Fe:ZnSe are shifted to longer wavelengths than that of Cr:ZnSe because the d6 electron configuration of the Fe2+ ion experiences a 4/9 reduction in the magnitude of the crystal field splitting in ZnSe when compared to the d4 configuration of the Cr^{2+} ion. The first Fe:ZnSe laser was demonstrated by Adams et al. [39]. Since then, CW output powers of >1.5 W, 35 W of average output power in gain switched operation and tunable operation from 3770 to 5050 nm has been demonstrated in bulk Fe:ZnSe lasers [40-42]. One of the limitations of the Fe:ZnSe laser transition is the short upper-state lifetime at RT due to multi-phonon quenching [39]. The practical implication of this quenching is that Fe:ZnSe must be cryogenically cooled to achieve CW laser operation. However room temperature operation has been demonstrated in gain switched operation with laser efficiencies of up to 34 % [43].

In this work we want to combing the excellent bulk properties of Fe:ZnSe with that of a waveguide geometry with the aim of being able to have a fully monolithic Fe:ZnSe laser. We will use our experience waveguide fabrication using ULI in in Cr:ZnSe and apply it to Fe:ZnSe waveguide fabrication.

Waveguide fabrication

Fabrication of depressed cladding waveguides where using ULI where investigated in Fe:ZnSe. The Fe:ZnSe sample used in this work had dimensions 1.82 mm × 4.76 mm × 6.94 mm and an Fe^{2+} -ion concentration of 8.88×10^{18} cm^{-3}. The samples where purchased form IPG Photonics. The inscription parameters investigated are given in Table 2. In this investigation it was found that the modification parameters for Fe:ZnSe are different from that of Cr:ZnSe but are similar to that of ZnSe. Further investigations at WPAFB by S. McDaniel and G. Cook found the larger pulse energy needed for modification in Cr:ZnSe arises from residual liner absorption from the Cr atoms at the inscription laser wavelength. An transmission microscope image of a depressed cladding waveguide fabricated in Fe:ZnSe is give in Figure 26 (a).

Waveguide fabrication parameters investigated in Fe:ZnSe	
Inscription laser	Amplitude Systems Satsuma
Laser wavelength	1047 nm
Laser polarization	Horizontal
Laser pulse width	750 and 1000 fs
Laser repetition rate	100 kHz
Inscription lens	0.6 NA
Pulse energy	1.8 to 2.1 µJ
Sample translation speed	9 $mm \cdot s^{-1}$
Waveguide diameter	100 to 200 µm
Number of inscription elements	100 to 200
Number of element overwrites	1 to 9

Table 2: Waveguide fabrication parameters investigated in Fe:ZnSe for CW laser applications.

Waveguide laser

Laser operation of the Fe:ZnSe waveguides where investigated. A schematic of the laser cavity is given in Figure 25. The pump source of this laser was a 1.5 W CW Er:YAG thin disk laser. To achieve laser operation in Fe:ZnSe with a CW pump source the sample was cooled with liquid nitrogen to 77 K. This added extra complication to the laser cavity as the sample has to be under vacuum and there is an addition of two CaF_2 windows and two optics in the cavity. Even with these addition components of loss inside the cavity the Fe:ZnSe waveguide was found to lase at a central wavelength of 4122 nm with a FWHM of 6 nm. A characterisation of the lasers performances and a graph of emission spectra is given in Figure 26. The optimum waveguide demonstrated an output power of 76 mW with a slope efficiency of 11.0% using an output coupler with R = 80%. The threshold of laser action was

found to be 210 mW. The lowest threshold of the waveguide laser was measured to be 153 mW with an output coupler with R = 90%. There was no observed rollover at the highest pump power of 908 mW and thus, we can infer that that laser performance was pump limited and further power scaling is possible. In addition, for optimal laser performance, the end facets of the Fe:ZnSe sample should be AR coated.

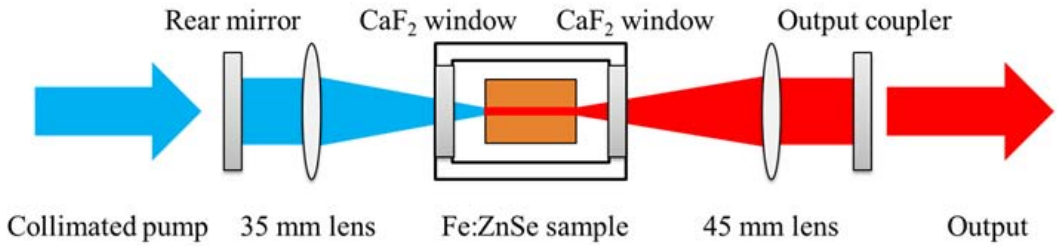

Figure 25: Schematic of Fe:ZnSe waveguide laser in a cryostat cooled by Liquid nitrogen.

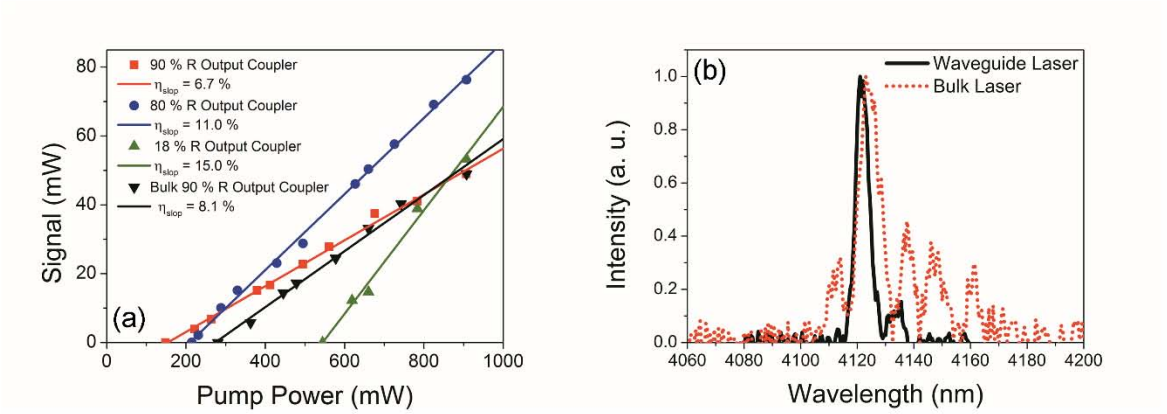

Figure 26: Fe:ZnSe waveguide and bulk laser characterization. (a) Laser performance of waveguide and bulk Fe:ZnSe laser with different amounts of output coupling. (b) Spectrograph of Fe:ZnSe waveguide and bulk laser under 908 mW of pump power with a 80%R output coupler.

The performance of the waveguide laser with was compared with that of a bulk laser using a 90 % reflective output coupler. For bulk laser operation the focus of the two lens shown in Figure 25 where translated to the centre of the Fe:ZnSe sample and the sample was translated so that the laser operated in unmodified region of the sample. The laser performance and emission spectra of the bulk Fe:ZnSe laser is given in Figure 26. From this it can be seen that the slope efficiency of the bulk laser is 8.1 % compared with 6.7 % of the waveguides laser. The reduced efficiency of the waveguide laser is from the propagation and coupling loss induced by the waveguide. The waveguide was found to reduce the lasing threshold of the laser by 44% compared with the bulk system using the same inter cavity optics. This reason for this is because of the increased overlap and interaction length between the pump

and signal in the waveguide. This result is important for future low power application and could open the possibility of direct diode pumping. Laser mode images of the Fe:ZnSe waveguide and bulk lasers are shown in Figure 27.

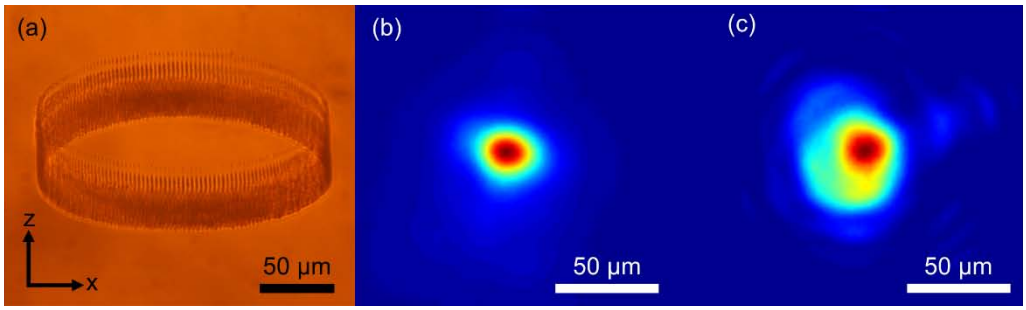

Figure 27: (a) Optical micrograph of end facet of 200 µm wide waveguide. (b) Waveguide laser mode image at 4122 nm imaged at end facet when lasing from Fresnel reflection at output facet. (c) Bulk laser output mode at centered at 4135 nm lasing from Fresnel reflection at output facet.

Waveguide losses

Waveguide losses are often difficult to accurately measure without using destructive methods, for example the cut back method, because of the relative short propagation length. In order to have confidence in our measurements we used three different methods. Direct comparison of the transmitted pump light under guiding and non-guiding conditions allowed an estimate of the waveguide losses due to increased scattering by the inscribed structures. With the pump laser operating at 450 mW and the Fe:ZnSe crystal cooled to 77 K, the pump light was launched into the inscribed waveguide. The power exiting the sample compartment was measured to be 0.865 mW. The sample compartment was translated, so that the beam propagated along a section of bulk Fe:ZnSe. In this configuration, the power exiting the sample compartment was measured to be 1.00 mW. The loss due to all effects, most notably, Fresnel effects and absorption of the pump radiation by the Fe^{2+} ions are the same in both configurations, so the difference in transmitted power is attributable to waveguide effects exclusively. Thus, the waveguide losses were calculated to be 0.91 dB/cm.

Additionally, the method of Findlay and Clay was used to find a value of the waveguide loss at the signal wavelength [44]. The modified Findlay–Clay equation was fitted to the threshold and output coupler reflectivity data for the waveguide laser. Accounting for Fresnel reflectivity losses of 17.5% and 1.3% transmission losses of the CaF_2 windows, the propagation loss is calculated to be 0.16 dB/cm.

The scattering loss of the waveguide was also measured using the technique demonstrated by Okamura et al. [45]. The output of a free-running Fe:ZnSe laser operating at approximately 4050 nm was launched into the waveguide, and the scattering from the side of the guide was imaged using a FLIR mid-IR camera. Image analysis of the scattered light enables a non-destructive technique for

estimating losses from a waveguide structure. This image analysis technique eliminates the need to carefully factor out entrance and exit coupling losses required for input/output measurements. We also note from Ref. [39] that the absorption coefficient of Fe:ZnSe at 4050 nm at 77 K is negligible, so all the light image by the camera is from scattering processes. Using this method, the propagation loss in the waveguide at the signal wavelength is measured to be 0.46 dB/cm. The fidelity of this technique deteriorates when the signal to noise ratio is small, which is the case when the scattering losses are low. Consequently, the propagation losses calculated here should be interpreted as an upper-bound of the waveguide losses.

In summary, the value of the total waveguide loss was calculated using three methods. Direct measurement of the total loss at the pump wavelength gave a value of 0.9 dB/cm. Extrapolation of the value in situ with the laser running using the Findlay–Clay method gave a value of 0.16 dB/cm. The method of imaging scattered light at approximately the laser wavelength with an IR camera gave a value of 0.46 dB/cm. So, we see that each method indicates the total losses are <1 dB/cm, which is negligible compared with the small signal gain coefficient for our laser material, which is typically >20 dB/cm. Propagation losses of <1 dB/cm demonstrated in this paper are comparable to previous demonstrations of ULI passive waveguide devices at 4 μm [46, 47].

Summary

We have demonstrated the first Fe:ZnSe waveguide laser. The waveguide structure was an annular depressed cladding structure fabricated by ULI. The inscribed waveguides were found to have a low propagation loss of <1 dB/cm at the lasing wavelength of 4122 nm. The laser emitted at a maximum output power of 76 mW, which was limited by the available pump power of 906 mW. The tighter confinement of the pump and laser signal beams by the waveguide resulted in a low laser threshold of 154 mW, which is a 44% reduction compared to an otherwise identical bulk system with a laser threshold of 274 mW. A narrow spectral linewidth of 6 nm was demonstrated by the waveguide laser. To the best of the authors' knowledge, this is the narrowest linewidth demonstrated in any free-running Fe:ZnSe laser. Demonstration of an Fe:ZnSe laser in a guided-wave configuration will enable the creation of compact, all solid-state laser systems for commercial and laboratory use.

This work as a result of close calibration between HWU and WPAFB, funded by EOARD, resulted in a conference paper at CLEO15 [48] and a journal paper in Applied Physics Letters [49].

CaF_2 waveguides

Introduction

For the generation of ultra-short pulses, of femtosecond to few picosecond, it is paramount that the cavity round trip time of all the of the modelocked pulse frequency components are the same. Thus there is no phase change of each

frequency component with respect to each other after one round trip of the cavity. The reason for this is if there is a phase change of some of the frequency components they will not constructively interfere with the other components. This will limit the available gain bandwidth of the system and lead to pulse width broadening. In most bulk laser cavities this problem can be resolved by the simple addition of a Brewster cut prism pair. This system allows positive and negative group velocity dispersion (GVD) compensation by changing the distance between the prim pair. N. Tolstik et al. [50] used a YAG prism pair to demonstrate a CW Modelocked Cr:ZnS bulk laser with a pulse width of 41 fs and a pulse repetition frequency (PRF) of 108 MHz. A schematic of the laser cavity used by N. Tolstik is given in Figure 28. The disadvantage of GVD compensation from prim pars is the requirement for free space beam propagation which is not compatible with compact fully monolithic lasers cavities.

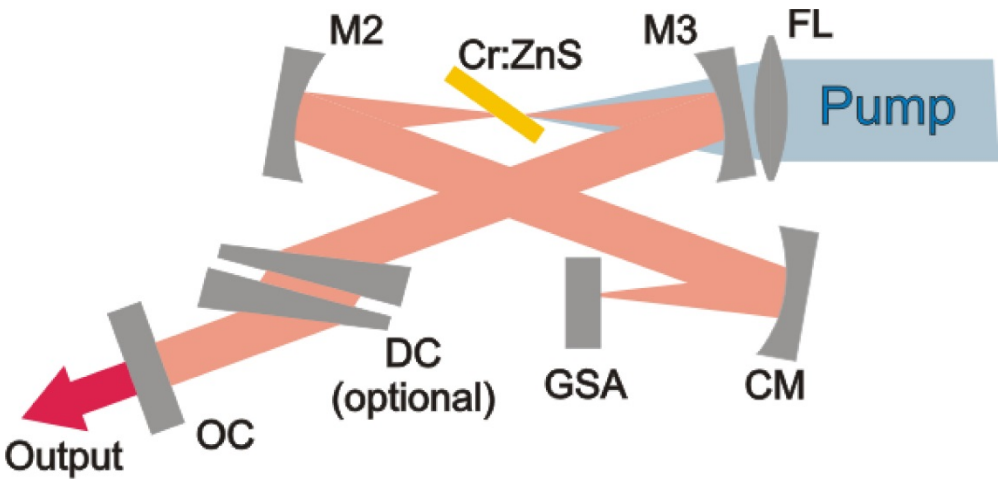

Figure 28: Schematic of CW modelocked Cr:ZnS laser operating with a pulse width of 41 fs at a PRF for 108 MHz. FL is the pump focusing lens (f= 40 mm), M2 and M3 are HR dielectric mirrors, CM is a concave chirped mirror, GSA is a graphene-based saturable absorber mirror, DC is the YAG prism pair and OC is the output coupler. This diagram has been reproduced for N. Tolstikc et al. [50].

Chirped or dispersive cavity mirrors are one alternative method of GVD compensating which is combatable with a monolithic laser cavity. These mirrors use brag stacks to phase shift some frequency more than others thus allowing for GVD compensation. The issue is these mirrors work by the use of bragg stacks and thus the bandwidth of frequencies that they support is fundamentally limited. Many high quality low loss and large bandwidth GDD mirrors have been developed for Ti:Sapphire lasers but they are not as well developed for the 1.9 to 3.4 μm range needed to utilise the full bandwidth of Cr:ZnSe. The GVD compensation of the mirrors is also set on fabrication and does not allow for any optimisation once fabricated. This is not a problem for a bulk laser cavity because you can compensate for most of the GVD with the chirped mirrors and then optimise the GVD with a prism pair. This is however an issue for monolithic lasers.

A small gap between an uncoated waveguide end facet and a plan mirror can create negative GVD by forming a Gires-Tournois interferometer structure [51]. A. A.

Lagatsky et al. [36] demonstrated the effectiveness of the method with a 15 GHz fundamentally CW mode-locked ytterbium doped glass waveguide laser. A. A. Lagatsky showed that tuneable GVD control can be achieved in a quasi-monolithic flat mirror butt-coupled waveguide laser by adjusting the gap between one of the mirrors and the waveguide end facet. Figure 29 shows a diagram of an ytterbium doped bismuthate glass waveguide laser that has demonstrated CW modelocking using the Lagatsky method in our research group at Heriot Watt University. This method has been found to be very effective in the demonstration of compact CW modelocked lasers. There is one issue however, the air gap must be controlled to a precision of a less than a micron and because of this gap the laser is no longer a truly monolithic system. This means that this method is very sensitive to vibrations thus remove the main advantage of using a waveguide laser cavity is lost.

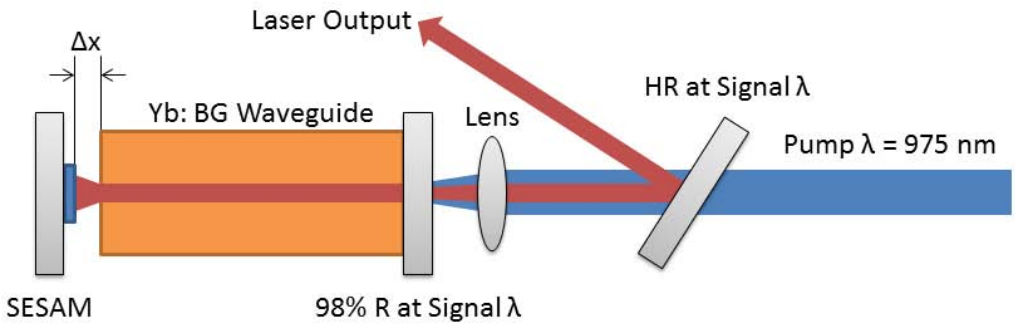

Figure 29: Diagram of CW modelocked ytterbium doped bismuthate glass waveguide laser with GVD compensation form adjusting the gap Δx.

We have started to develop a different approach to GVD compensation in Cr:ZnSe/ZnS mode-locked lasers using CaF_2. At a the peak of Cr:ZnSe emission cross-section, 2.45 μm, CaF_2 is an anomalously dispersive material and ZnSe is a normally dispersive media. Thus by inserting a sufficient length of CaF_2 inside the cavity we can compensate for GVD induced by the Cr:ZnSe/ZnS waveguide. In order to do this and still have a fully monolithic laser system waveguides must be fabricated in CaF_2 with mode field diameters (MFD) and numerical apertures (NA) that are similar to that of the current ultra-fast inscribed waveguides in Cr:ZnSe/ZnS which have a MFD of around 50 μm [35, 52]. We are using ultrafast laser inscription to fabricate depressed cladding waveguide in CaF_2. The advantage of using ultrafast laser inscription instead of the more common lithographic methods is ability to fabricate fully 3D structures and the low index contrasts of negative index change. Using this method facilitates relatively large (50-100 μm) single mode MFDs needed for efficient butt-coupling to Cr:ZnSe waveguides [53]. Low loss single mode waveguides in CaF_2 waveguide could be placed inside a Cr:ZnSe/ZnS waveguide laser for dispersion compensation as shown in Figure 30.

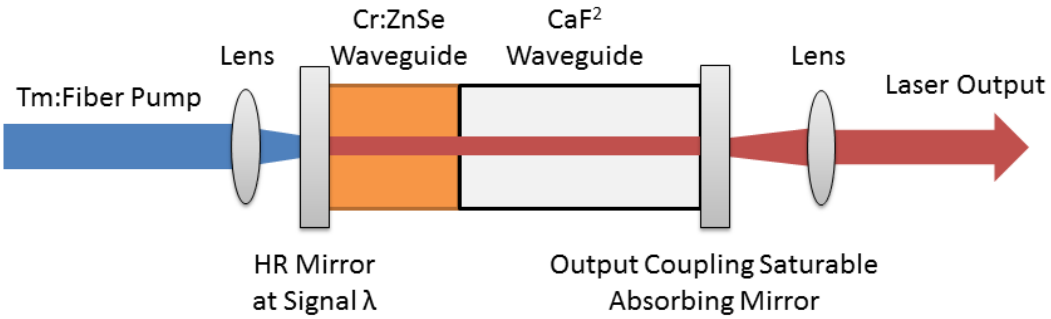

Figure 30: Schematic of cavity design for a monolithic passively Modelocked Cr:ZnSe waveguide laser. GVD control is manage with a ULI inscribe waveguide in CaF_2. Passive modelocking is achieved using a SESAM or few layer graphene saturable absorber.

Assuming the mode-locked Cr:ZnSe (217.8 fs^2/mm) laser operates at the peck of the emission cross-section (2.45 µm) the CaF_2 (-51.7 fs^2/mm) waveguide would need to be 4.2 times longer than the Cr:ZnSe waveguide. This would lead to a CaF_2 waveguide of 25 mm if we use a 6 mm Cr:ZnSe waveguide which is what was used in past CW Cr:ZnSe waveguide lasers [35]. It can often be beneficial to operate a mode-locked the laser in the soliton mode-locked regime this is achieved by having a slightly anomalous GVD cavity, we can achieve this by increasing the length of the CaF_2. Using the proposed Cr:ZnSe and CaF_2 waveguides lengths will lead to a Modelocked laser with a fundamental PRF of 3 GHz. Post waveguide fabrication adjustment of the negative GVD of the CaF_2 waveguide can be accurate adjusted by polishing the end facet of the sample. This makes the CaF_2 an attractive alternate to the use of Chirped mirrors in monolithic mode-locked waveguide lasers systems.

CaF_2 Waveguide fabrication and characterisation

There has been no reports of ULI waveguide fabrication in CaF_2 thus an initial parameter scan is needed. The polycrystalline CaF_2 used in this investigation was UV grade polished and sourced form Crystran Ltd. In order to investigate the effect of femtosecond laser pulses on the refractive index of CaF_2 a range of single line scans with different laser parameters where used. The inscription parameters investigated are given in Table 3.

CaF_2 single line modification parameter range investigated	
Inscription laser	IMRA 400 µJewel
Laser wavelength	1047 nm
Laser polarization	horizontal, vertical and circular
Laser pulse width	370 fs
Laser PRF	500 kHz
Inscription lens	0.4 NA
Pulse energy	40 to 840 nJ
Sample translation speed	1 to 25 $mm \cdot s^{-1}$

Table 3: Ultra-fast laser inscription parameters investigated in single line modification of CaF_2.

The end facet of the sample was image with a transmission microscope to get an indication of if there was any permanent refractive index modification and if so if it is type I (increase in n) or type II (reduction in n). A transmission microscope image of single line scans in CaF_2 are shown in Figure 31. From this figure it can be seen that the modification elements are anti-guiding thus could be suitable for type II or depressed cladding waveguides.

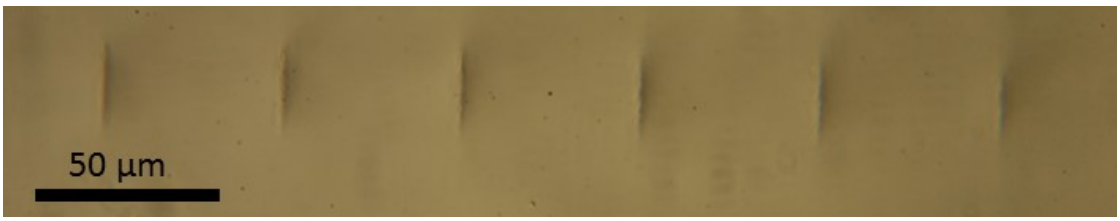

Figure 31: Transmission microscope image of end facet of single line scans in CaF_2. The modification elements shown where fabricated with pulse energies of 220 nJ.

The feasibility of depressed cladding waveguides where investigated over that of type II to facilitate effective integration with the current Cr:ZnSe depressed cladding waveguide laser sources. A wide range of parameters where used for fabrication of CaF_2 waveguides at a depth of 250 µm below the surface of the sample. A list of the parameters investigate are given in Table 4. The pulse energy of the laser was reduced to below 220 nJ to stop the sample from cracking during inscription and the subsequent polishing stage. It was found that pulse energy of less than 140 nJ did not modified the CaF_2. Form this the waveguides parameters where optimized within this pulse energy envelop. A transmission microscope image of CaF_2 depressed cladding waveguides are show in Figure 32.

CaF_2 cladding waveguides inscription parameters	
Laser	IMRA 400 µJewel
Laser wavelength	1047 nm
Laser polarization	horizontal
Laser pulse width	370 fs
Laser PRF	500 kHz
Inscription lens	0.4 NA
Pulse energy	40 to 300 nJ
Sample translation speed	10 to 25 $mm \cdot s^{-1}$
Waveguide diameter	20 to 120 µm
Number of elements per waveguide	20 to 90

Table 4: Range of inscription parameters investigated in the fabrication of CaF_2 waveguides.

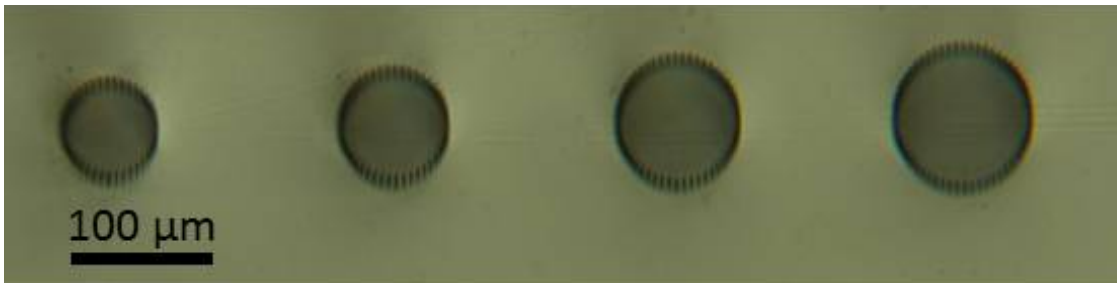

Figure 32: Transmission microscope image of CaF_2 cladding waveguides. The diameters of the waveguides left to right are 65, 75, 85 and 95 µm.

The application for these waveguides needs to have efficient coupling with Cr:ZnSe waveguides with this in minded a Cr:ZnSe waveguide laser was used to characterise the insertion losses of the CaF_2 waveguides. A schematic of the Cr:ZnSe waveguide laser signal source and the coupling setup used for testing the CaF_2 is shown in Figure 33. Insertion loss measurement of the waveguides where found to be sub 1 dB for a 10 mm sample which is promising for future integration in a Cr:ZnSe resonator. The output mode of the waveguides where imaged with a Flur Mid-IR camera. A typical mode images is shown in Figure 34. It was found that waveguides of 75 µm in diameter or less are single mode. This is a promising result as this is very closes to the waveguide diameter of the optimum single mode Cr:ZnSe waveguides and thus should allow good coupling.

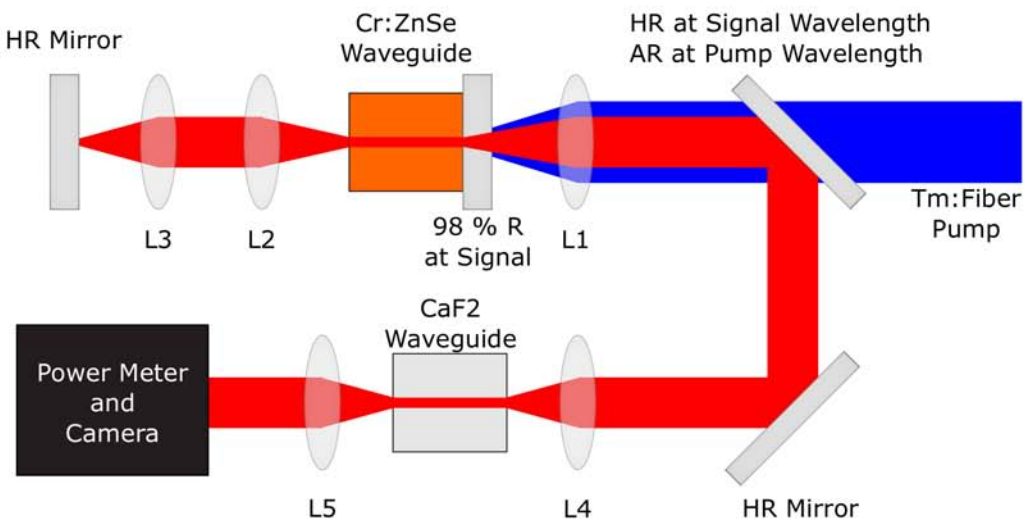

Figure 33: Schematic of CaF_2 waveguide characterisation setup used for insertion loss measurement with Cr:ZnSe as the signal source.L1 to L5 are AR coated CaF_2 Lenses with 50 mm focal lengths.

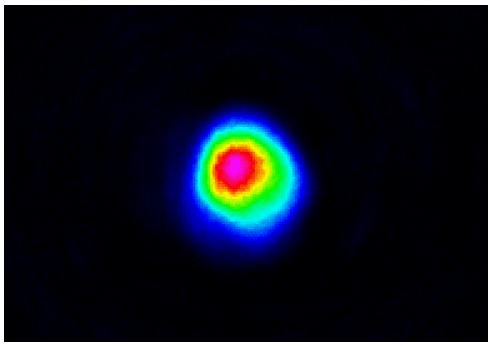

Figure 34: Mode image of CaF_2 waveguide laser guide the signal of the Cr:ZnSe waveguide laser emitting at 2.45 µm. The inscription parameters of the waveguide where diameter 75 µm, number of elements 45, inscription speed 10 mm·s^{-1}, pulse energy 0.2 µJ, NA of inscription lens 0.68 and horizontal inscription laser polarization .

Summary

The initial work in ULI fabricated waveguides in CaF_2 has been successful with low insertion loss and MFDs comparable to that of Cr:ZnSe waveguide lasers. The next stage for this project will be to insert the CaF_2 waveguides into a laser resonator and investigate the losses it adds to the cavity when butt coupling to a Cr:ZnSe waveguide. Once the losses are reduced to a sufficient level we will investigate the suitability of the CaF_2 waveguide for dispersion compensation in a Modelocked Cr:ZnSe waveguide laser resonator.

SBN Waveguides

Introduction

Inscription parameters for the fabrication of cladding waveguide where investigated at Heriot-Watt university in close collaboration with Gary Cook from WPAFB. For this work G. Cook spent 6 weeks working in the labs at Heriot Watt with our research team developing the waveguides. This G. Cooks trip was founded by EOARD through the window on the world program.

Strontium-Barium Niobate (SBN) is in my ways a wonder material in photonics because of its nonlinear, electro-optic and photorefractive properties. For our investigation we will focus on its electro-optic and photorefractive properties. The main reason for developing waveguides in SBN is to develop non-mechanical phase modulators and wavelength tuning elements for Transition Metal doped ZnSe waveguide lasers. The advantage of the monolithic laser cavity design has been commented on at length earlier in this report. SBN is available in different Strontium (Sr) and Barium (Ba) ratios the two most common are $Sr_{0.61}Ba_{0.39}Nb_2O_6$ (SBN:61) and $Sr_{0.75}Ba_{0.25}Nb_2O_6$ (SBN:75), in this report we investigate both types to judge there suitability. All the SBN:61 and SBN:75 used in our investigation was purchased from Altechna and fabricated using the Stepanov technique [54].

Waveguide fabrication in SBN:61

An initial investigation of ULI on SBN:61 was investigated with a range of single line modification elements. The SBN:61 samples where not poled before this test. The

inscription beam was incident parallel to the c-axis of the SBN:61 crystal to allow access to the strongest electro-optic coefficient, a schematic is show in Figure 35. The range of inscription parameters investigation are given in Table 5. Imaging the end facet of the sample with a transmission microscope, as shown in Figure 36, can give a lot of information of the delta n induced by the inscription process. For example Figure 36 (b), 500 kHz 0.4 NA, we can see that the modified regions are brighter than the surrounding unmodified region this indicates an increases in refractive index has been induced. This type of modification, type I, can be used to build up a waveguide core with square cross-section. This is achieved by passing the sample through the focus of the inscription beam multiple times with a small lateral offset to form a multiscan waveguides, as shown in Figure 35. The multiscan method has proven to be very effective in fused silica and Yb:Bismuthate glass because of their single mode operation with MFDs in the 5-10 μm range which is well matched to SMF 28 fibre at 1.5 μm [55]. Propagation losses at 1.5 μm of less than 1 dB/cm can be easily achieved with this method. The MFD of type I waveguides, single element and multiscan, are often in the few μm to 20 μm this might not provide efficient coupling with the comparatively large Cr:ZnSe waveguides which are around 60 μm. From Figure 36 (e), 100 kHz 0.68 NA, the black lines show clear type II modification which is a localised reduction in refractive index. Using the lower pulse energy inscribed elements and arranging them in an annular pattern my produce an effective depressed cladding waveguides. The parameters investigated in Figure 36 (c) & (b), 500 kHz and 200 kHz with 0.68 NA respectively, show the transition from type I modification to type II. This investigation has shown that SBN61 is a promising material for both increased and decreased in delta n based waveguides. This adaptability will be very useful for many different application in the future.

SBN single element ULI modification parameter scan	
Inscription Laser	IMRA 400 μJewel
Laser wavelength	1047 nm
Laser polarization	horizontal
Laser PRF & pulse width	100 kHz at 1.1 ps, 200 kHz at 447 fs, 500 kHz at 359 fs & 1 MHz at 373 fs
Pulse energy	0.05 to 2.5 μJ
Inscription lens	0.4 & 0.68 NA
Inscription depth below sample surface	200 μm
Sample translation speed	3, 5 & 10 $mm \cdot s^{-1}$

Table 5: Inscription parameters investigated in single scans of non-polled SBN:61 with inscription beam parallel to the c-axis.

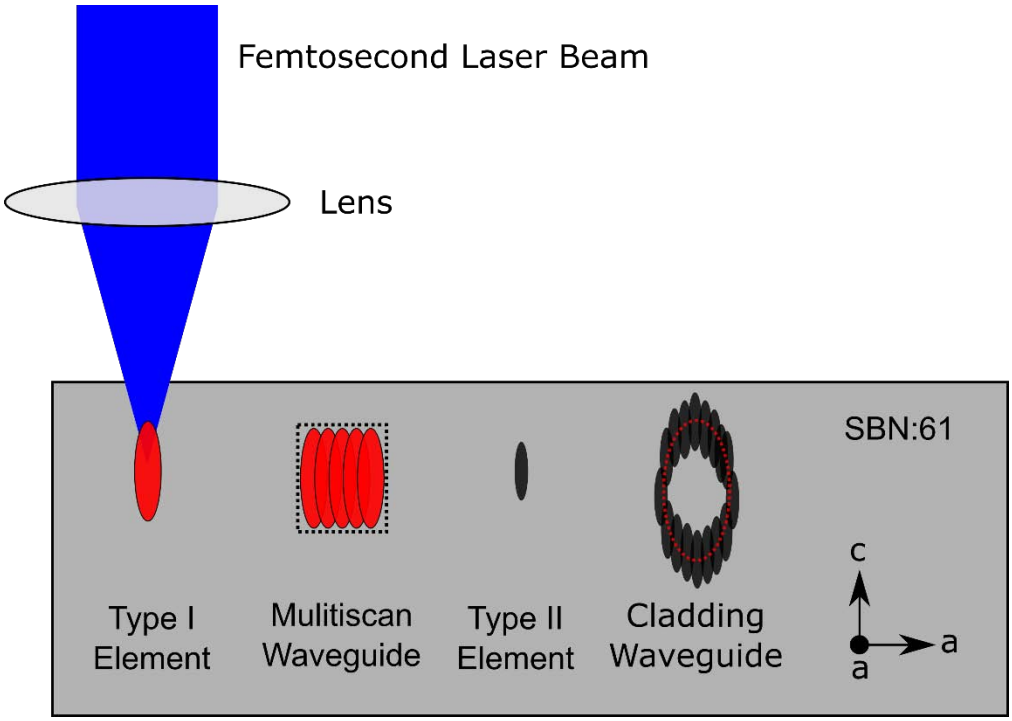

Figure 35: Schematic of multiscan and depressed cladding waveguides fabricated using ULI in SBN:61 with crystal axis given.

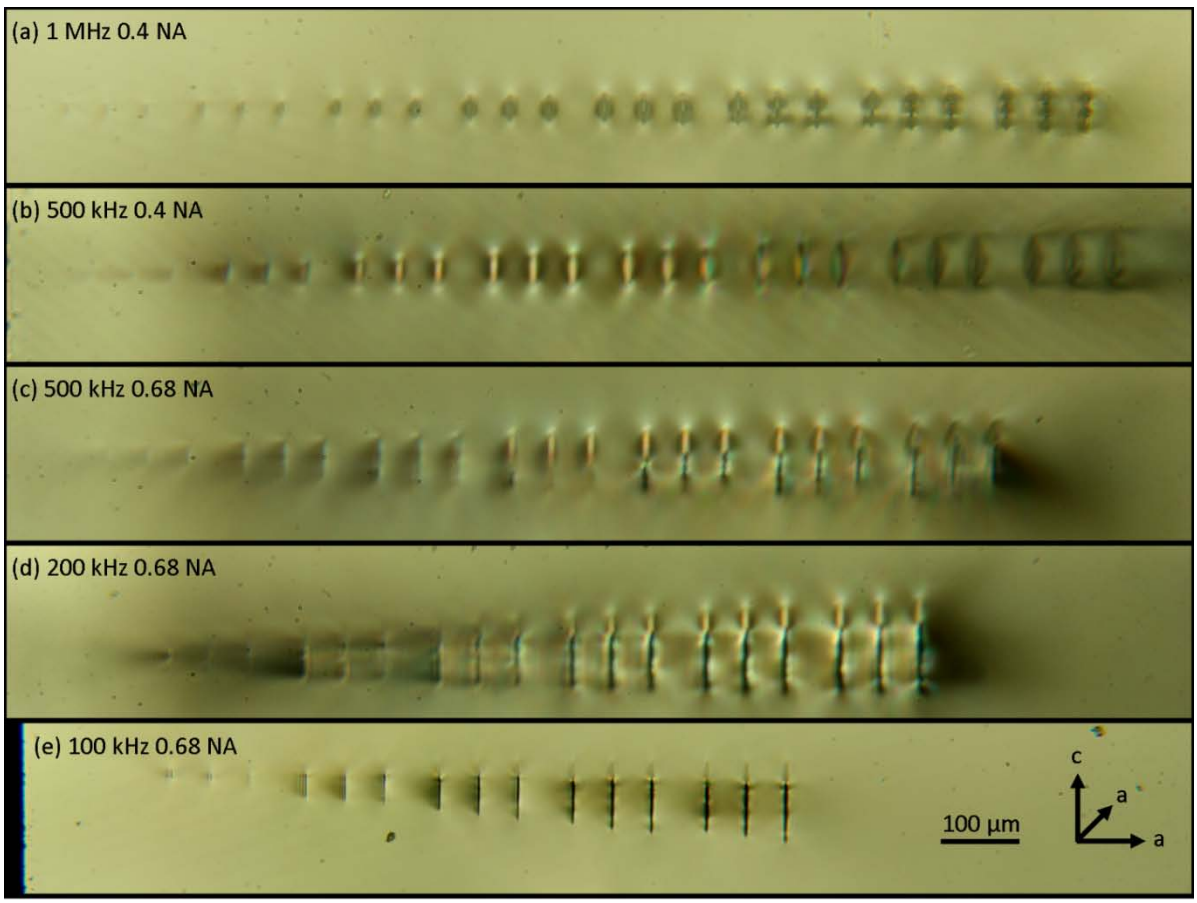

Figure 36: Transmission microscope image of single line modification elements in SBN:61 with a range of laser PRF and inscription lens.(a) 1 MHz with 0.4 NA form left to right there is banks of 3 lines with 10 , 5 and 3 mm·s^{-1} translation speed

respectively. The inscription pulse energy of each bank from left to right is 0.05 to 0.25 μJ increasing in 0.05 μJ steps. (b) 500 kHz with 0.4 NA using the same parameter pattern as (a) but with pulse energies of 0.1 to 0.8 μJ. (c) 500 kHz with 0.68 NA parameter pattern as (a) but with pulse energies of 0.2 to 0.8 μJ. (e) 100 kHz 0.68 NA parameter pattern same as (a) but with pulse energies of 0.25 to 1.75 μJ. (e) 200 kHz 0.68 NA parameter pattern same as (a) but with pulse energies of 0.5 to 2.5 μJ

Before the inscription of waveguides in SBN: 61 the samples where electrically poled to create a single ferroelectric domain before the waveguides where inscribed. The sample was heated in a pottery furnace from room temperature to 150 ^{0}C at a rate of 50 ^{0}C per hour. The furnace was then held at 150 ^{0}C for 15 minutes during which 1 kV DC (5000 V/cm) was applied across the c-axis. The sample was then let to cool with the voltage sill applied to force all the domains to be in the same direction.

Form the single element modification investigation there was not a clear path for which type of waveguide to investigate because of this we decide to investigate multiscan waveguides and depressed cladding waveguides, as shown in Figure 35Figure 21. The inscription parameters used for the depressed cladding waveguides are given in Table 6. The effect of inscription depth was investigated by inscribing the waveguides with the centre of the waveguide at 250 and 700 μm below the samples surface. Figure 37 is a transmission microscope image of the cladding waveguides inscribed at different depths. It is very clear from comparing Figure 37 (a) and (b) that there is a large modification dependence on inscription depth. The waveguides inscribed at 700 μm where barely visible. It is also worth noting that the modification on the top and bottom of the waveguide inscribed at a depth of 250 μm is different. This presents some challenges in creating a symmetrical waveguide in the vertical axis. Nether the less the 250 μm depth waveguides appeared viable for testing the guiding properties of SBN:61 cladding waveguides.

SBN:61 depressed cladding waveguides ULI parameters	
Laser	IMRA 400 μJewel
Laser wavelength	1047 nm
Laser polarization	horizontal
Laser PRF & pulse width	100 kHz at 1.1 ps
Pulse energy	1 μJ
Inscription lens	0.68 NA
Inscription depth below sample surface	250 μm
Sample translation speed	10 mm·s^{-1}
Waveguide diameter	50 , 75 & 100 μm
Number of elements	Equal to the diameter in μm

Table 6: Inscription parameters used in investigation of SBN:61 depressed cladding waveguides.

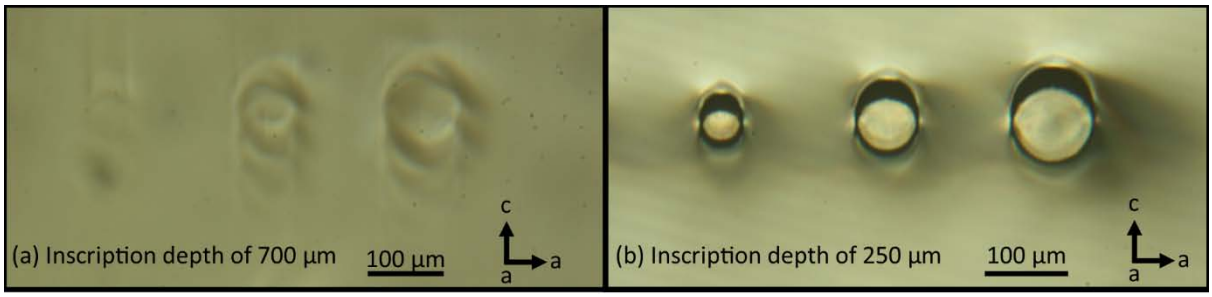

Figure 37: Pre-poled SBN:61 depressed cladding waveguides. The inscription laser was operated at 100 kHz with a pulse energy of 1 µJ and a 0.68 NA lens was used to focus the light into the positive c-axis. (a) Inscription depth was 700 µm from surface of the sample. (b) Inscription depth was 250 µm from surface of the sample.

Multiscan waveguides were also investigated using the parameters given in Table 7. A transmission microscope image of the multi-scan waveguides inscribed using a pulse energy of 0.3 µJ are given in Figure 38 (a). Form this figure you can see that the waveguides do guide light in the modified core wich is expected for an increase in the refractive index. What is interesting is the gap between the waveguides and above each waveguide also appear to be guiding light. This would suggest that there is also a reduction in the refractive index by the laser. Similar results have has also been found in GLS glass ate Heriot-Watt. This effect can be due to the moving of material in the modified region. With a densification of material in the modified area lending to an increase in refractive index and a reducing of refractive index form the surrounding region. To investigate this further depressed cladding waveguides where inscribe using the same laser parameters as that of the multi-scan waveguide. Figure 38 (b) show depressed cladding waveguides fabricated using a laser PRF of 500 kHz, pulse width of 359 fs and a pulse energy of 0.3 µm. It can be seen form this figure that the cladding waveguides are guiding light in the central unmodified region therefore a positive and negative change is refractive index is being induced with this set of inscription laser parameters.

SBN:61 depressed cladding waveguides ULI parameters	
Laser	IMRA 400 µJewel
Laser wavelength	1047 nm
Laser polarization	horizontal
Laser PRF & pulse width	500 kHz at 359 fs
Pulse energy	0.3 to 0.5 µJ in steps of 0.1 µJ
Inscription lens	0.40 NA
Inscription depth below sample surface	200 µm
Sample translation speed	10 mm·s^{-1}
Number of elements	1 to 31 in steps of 10
Space between elements	1 µm

Table 7: ULI parameters used for the fabrication of multiscan waveguides in pro-poled SBN: 61. The inscription beam was parallel to the c-axis of the crystal.

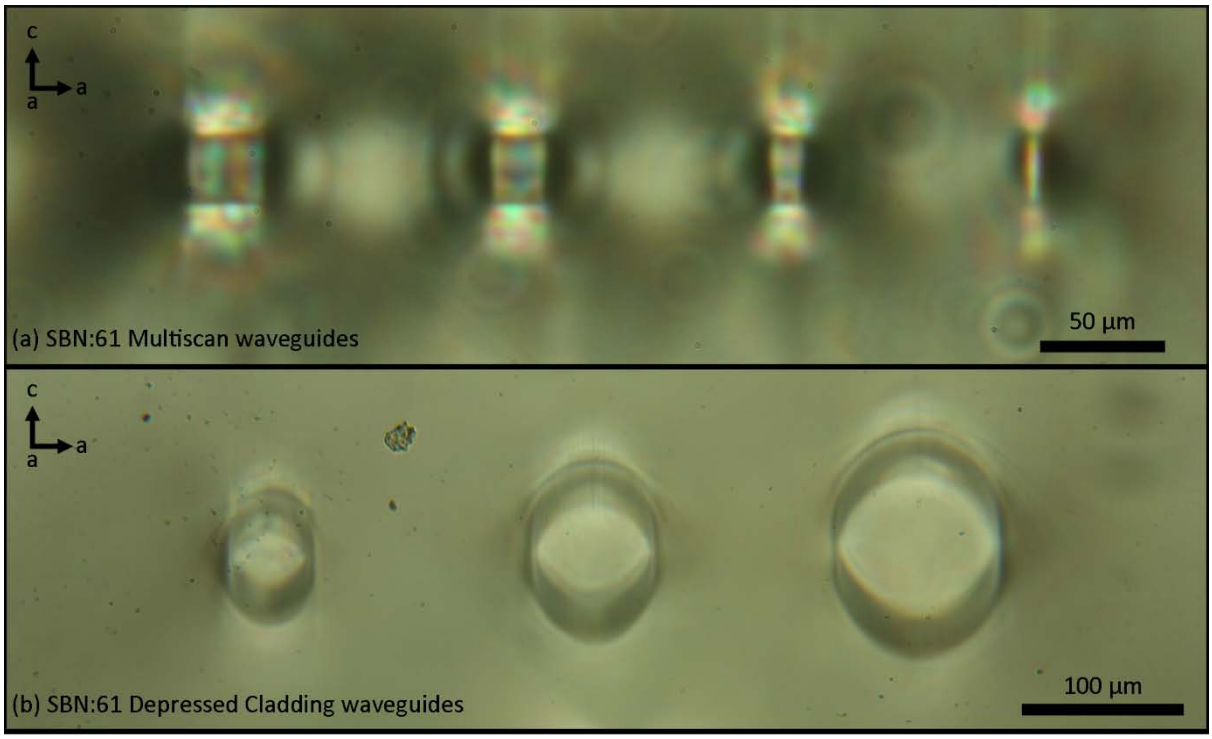

Figure 38: Transmission microscope image of SBN:61 waveguides. The inscription laser was operated at 500 kHz with a pulse energy of 0.3 µJ and 0.4 NA lens was used to focus the laser beam onto the sample. (a) Multiscan waveguides with 31, 21, 11 and 1 elements respectively form left to right. The spacing between each element was 1 µm and the waveguide where inscribed at a depth of 200 µm. (b) Depressed cladding waveguides with diameters 50, 75 and 100 µm respectively form left to right. The number of elements in cladding waveguides was equal to their diameter in µm.

Waveguide fabrication in Ce doped SBN:61

Doping SBN:61 with Ce greatly increases the photorefractive properties of SBN. Photorefractive materials have been proposed for a number of different application most notably data storage because of the relatively long time scales involved in the process. The application we have in mind is forming a Bragg grating in the waveguide by using to intersecting green laser beams. This will allow the creating of a tuneable Bragg grating because the grating period is proportional to the angel between the intersecting green laser beams. An example diagram, given in Figure 39, of this taken form Ref. [56] shows how this being implemented at 1550 nm. Cladding waveguides fabricated at 100 kHz with 0.68 NA where investigated using the parameters developed in SBN: 61, given in Table 6 . On inspection of the end facet with a transmission microscope, shown in Figure 40, the waveguides where all found to be over exposed by using too much pulse energy.

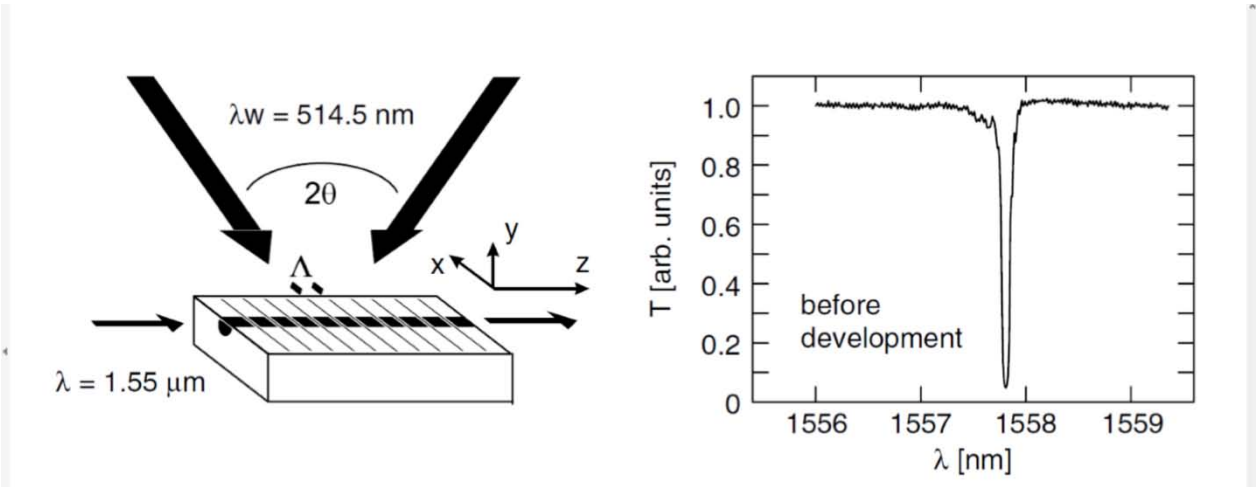

Figure 39: Holographically recorded reflection filters in $LiNbO_3$:Ti:Cu channel waveguides. (a) Geometry for recording and red-out of the grating, and (b) typical transmission spectrum T(λ) of a 15 mm-long filter. The c-axis referred to in the report is the z-axis in this schematic.

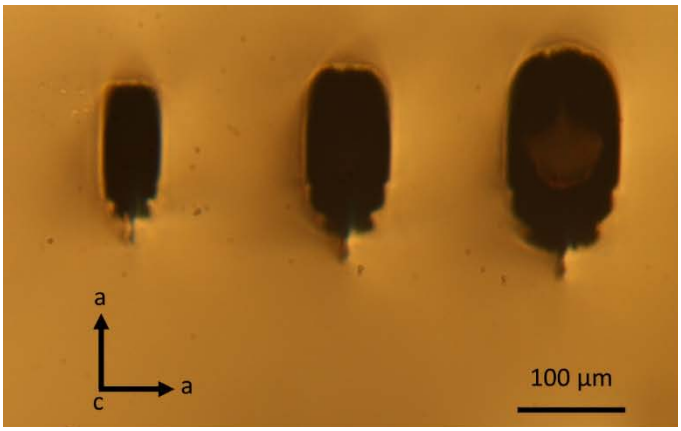

Figure 40: Ce:SBN61 depressed cladding waveguides inscribed using 100 kHz, 0.68 NA, 1 μJ and 10 mms^{-1}. Inscription beam was parallel to an a-axis of the crystal.

There are two initial thoughts as to what could be the reason for the discrepancy in inscription "recipes" between SBN:61 and Ce:SBN:61. Cr dopant in ZnSe have been show to change the inscription "recipe" of ZnSe drastically [27]. The reason for this was that there is a small linear absorption of the Cr at 1047 nm which is the emission wavelength of the inscription laser. This absorption reduces the amount of modification for a given pulse energy which is not observed thus it is not the Ce ions that are casing the difference in ULI parameters. A more likely reason for the increased inscription sensitivity is therefore thought to be associated with the change in the effective polarization properties of the inscription process with respect to the crystal c-axis. Previous inscriptions have been designed to produce waveguides where access to the r_{33} coefficient is possible (polarization propagation issues aside). This required creating waveguides with the crystal c-axis perpendicular to the waveguide direction. In order to minimize the external voltage needed to modulate the refractive index of the waveguides, the crystals were cut with the c-axis in the thinnest dimension, which, in turn, necessitated writing the waveguides through the

crystal c-face. In this orientation, linearly polarized inscription light experiences progressive radial birefringence for all optical vectors in the a-c crystal plane with a resolved component along the c-axis. This creates a radially dependent progressive phase retardation for opposite segments of the focused light cone, while not introducing any phase delay for the remaining orthogonal segments of the focused inscription light. Figure 41 illustrates this concept. The presence of this type of radial and directionally dependent birefringence will cause the focal spot to become distorted, resulting in a reduction in reduction in the focused intensity compared with identically focused light in the absence of any such phase distortion. Conversely, the use of horizontally polarized light, where the polarization vector is perpendicular to the crystal c-axis, does not create any radial dependent birefringence and so the focal spot is likely to be much smaller than the previous case, with a corresponding increase in the apparent inscription sensitivity.

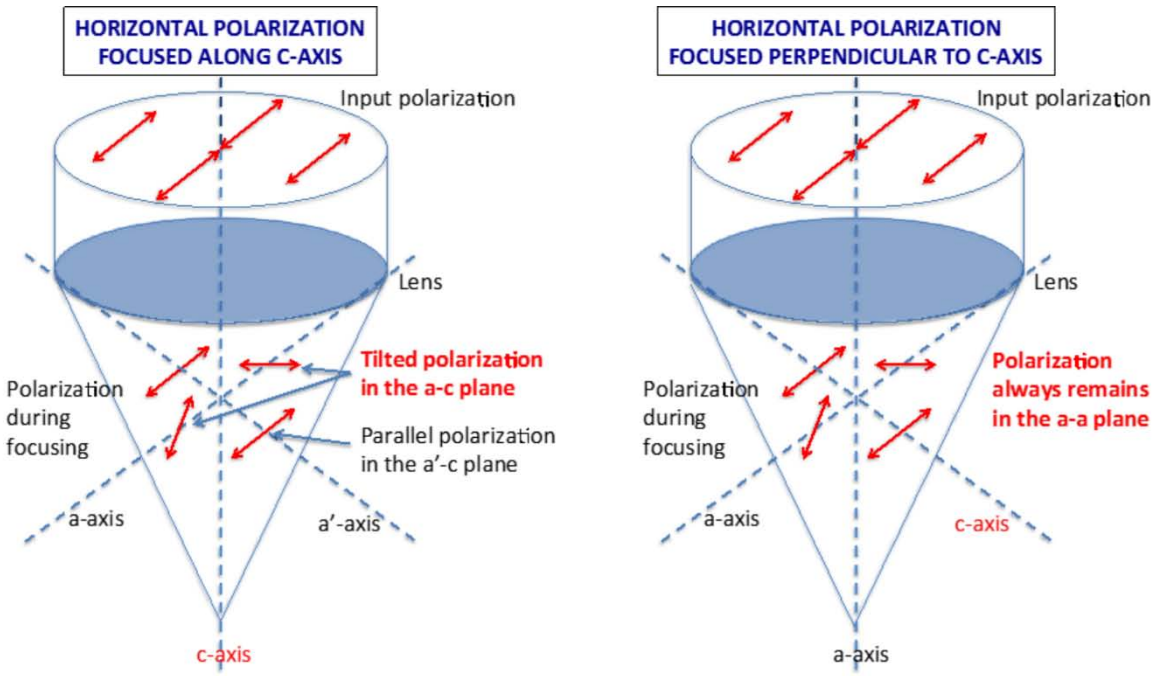

Figure 41: – Birefringence issues with focusing in SBN. Focusing along the c-axis causes tilting of the polarization vector for light a-c plane (left), while the polarization vector always remains in the a-a plane when focusing along the a-axis with the input polarization perpendicular to the crystal c-axis (right). The two a-axes have been distinguished with ' symbol in the left hand image, for clarity.

The birefringence issue was confirmed by inscribing parallel to an a-axis of non-doped SBN:61. Inscription in parallel to the a-axis of SBN:61 was then used to optimises the inscription "recipe" for Ce:SBN:61. The reason for using SBN:61 to developed the parameters was the higher cost and reduced availability of Ce:SBN:61. The parameter range found to give viable depressed cladding waveguides in Ce:SBN:61 is given in Table 8. It is worth noting that to reduce the difference in modification element high with depth the top of the waveguides where inscribed will less pulse energy than the bottom of the waveguides, this is discussed

further in the SBN:75 section of this report. A transmission microscope image of Ce:SBN:61 waveguides is given in Figure 42.

SBN:61 depressed cladding waveguides ULI parameters	
Laser	IMRA 400 µJewel
Laser wavelength	1047 nm
Laser polarization	horizontal
Laser PRF & pulse width	100 kHz at 1.1 ps
Pulse energy	0.3 to 0.35 µJ for top of waveguide 0.35 to 0.4 µJ for bottom of waveguide
Inscription lens	0.68 NA
Inscription depth below sample surface	250 µm
Sample translation speed	10 $mm \cdot s^{-1}$
Waveguide diameter	30, 40, 50 , 60 & 75 µm
Number of elements	Equal to the diameter in µm and it multiplied by 3/5

Table 8: Inscription parameters for Ce:SBN:61 depressed cladding waveguides. Note the change in modification with depth is compensated by reducing the pulse energy for the top of half of waveguide.

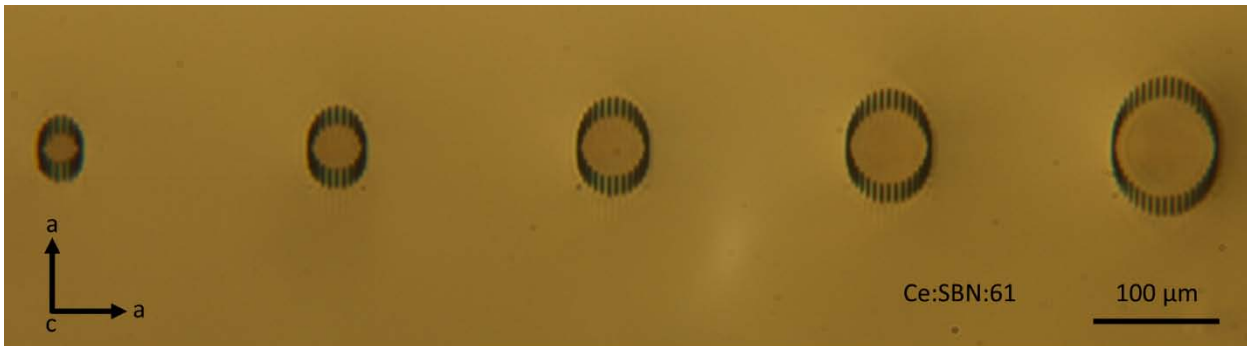

Figure 42: Transmission microscope image of depressed cladding waveguides in Ce:SBN:61. The inscription laser was parallel to the a-aixs of the crystal. Inscription parameters where 100 kHz, 1.1 ps, 0.3 µJ for top half, 0.35 µJ for bottom half, number of elements are equal to diameter in µm multiplied by 3/5 and 0.68 NA lens. The waveguides had a diameter of 30, 40, 50, 60 & 75 µm respectively from left to right of the figure.

Depressed cladding waveguides have been fabricated and are ready for using in applications. There first will be too insert the waveguide inside an extended cavity Cr:ZnSe laser resonator to use as a wavelength tuning element. This is achieved by a tuneable Bragg grating created by interfering green laser beams inside the photorefractive Ce:SBN:61 waveguide. Our research group at Heriot-Watt University does not have a high power green laser with a long coherence length that is suitable so the sample has been sent to WPAFB for this experiment to be done there. This experiment is currently being setup by S. McDaniel and G. Cook with initial results expected in the near future.

Waveguide fabrication in SBN:75

$Sr_{0.75}Ba_{0.25}Nb_2O_6$ (SBN:75) r_{33} elector-optic coefficient is 1340 pm/V which is ≈ 6 times that of SBN:61. However SBN:75 has a low curie temperature of 56 ^{0}C which might make it not suitable for applications in warm environments. It is also more challenging to manufacture single crystal SBN:75 than SBN:61. This knock-on effect of this for us is our supplier (altechna.com) has a 4-6 week lead time on ordering SBN:75 which is why we investigated SBN:61 before starting this investigation. A summary of the material properties of SBN:75 and SBN:61 for comparison purposes is given in Table 9.

Strontium-Barium Niobate Material Parameters		
Material Parameters	SBN:61	SBN:75
Electro-optic coefficients	r_{33} = 235 pm/V	r_{33} = 1340 pm/V
Curie temperature	80 ^{0}C	56 ^{0}C
Pyroelectric coefficient	0.065 μC per cm^{2}K	0.28 μC per cm^{2}K

Table 9: SBN material properties (source Altechna.com).

The SBN:75 samples used in this investigate had dimensions 10x10x2 with the c-axis alone the 2 mm length. Before any laser inscription the samples where poled in our furnace at Heriot-Watt. The samples were heated to 100 ^{0}C at a rate of 50 ^{0}C/hour, then held at 100 ^{0}C for 30 minutes and then allowed to passively cool to room temperature. Once the sample reached 100 ^{0}C a Voltage of 1kV was applied across the c-axis to pole the ferroelectric domains. The voltage was left on until the sample returned to room temperature. The electrodes (silver paint) on the positive and negative c-axis surfaces where removed with acetone before inscription.

In order to access the strongest electro-optic coefficient of SBN:75 (r_{33}) the inscription laser beam was incident on the sample parallel to the c-axis. This is the same geometry as discussed in the SBN:61 waveguide fabrication section of this report, a schematic is give in Figure 35. Depressed cladding waveguides where fabricated in SBN:75 using the same parameters used in SBN:61, given in Table 6. The ULI parameters used for cladding waveguides in SBN:61 ,100 kHz PRF and 0.68 NA lens, where found to induce larger amounts of modification than expected in SBN:75. Figure 43 show the in modification induced using the same ULI “recipe” as SBN:61. In order to find more optimum inscription pulse energys for SBN:75 a set of 50 μm diameter depressed cladding waveguides where inscribed with a range of pulse energies, 0.2, 0.3 and 0.4 μJ as shown in Figure 43 (c).

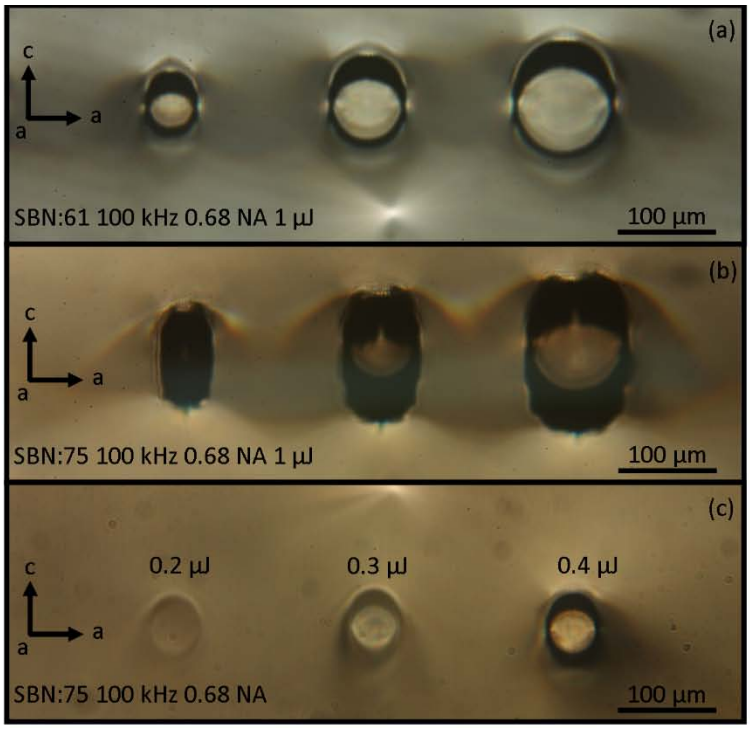

Figure 43: Transmission microscope images of SBN end facets. (a) SBN:61 with waveguides of diameter 50, 75, 100 µm form left to right respectively. (b) SBN:75 with waveguides of diameter 50, 75 and 100 µm from left to right respectively.(c) SBN:75 with waveguides that are 50 µm in diameter. Pules energy of 0.2, 0.3 and 0.4 µJ where used for inscription from left to right respectively.

From Figure 43 (c) it is clear that the optimum pulse energy needed for fabricating cladding waveguides in SBN:75 is between 0.3 and 0. 4 µJ. There is however still a clear difference in the waveguides between the modification at the top of the waveguide and the bottom. This is more apparent with the 100 µm waveguides but is still visible in the 50 µm guides. To counter this effect the pulse energy was reduced for the top half of the waveguide compared with the bottom elements. The exact amount of compensation need was not known so this was investigate with a parameter scan, shown in Figure 44. The laser parameters used, apart from the pulse energy, where the same as the 100 kHz depressed cladding waveguides inscribed in SBN:61, given in Table 6. From our earlier work in SBN it was clear that larger waveguide will need more compensation that smaller ones thus a wider range of waveguide diameters was investigated. Figure 44 (a) shows depressed cladding waveguides, with diameters form 50 to 150 µm, all elements where inscribed with a pulse energy of 0.4 µJ. This run was used as a control to compare the compensated waveguides too. A range of pulse energy's where investigated the optimum of which , for the 75 µm waveguide, was 0.45 µJ for the bottom half of the waveguide and 0.4 µJ for the top half, shown in Figure 44 (b). It can be noted that for the 125 and 150 µm dimeter waveguides a higher inscription energy is need for the bottom to make the modification more even. Nether the less compensating with different inscription powers appears to be an effective way of countering the depth dependence in the modification of SBN when inscribing along the c-axis of the crystal. The waveguide

have now been developed sufficiently to investigate the guiding properties at different wavelengths.

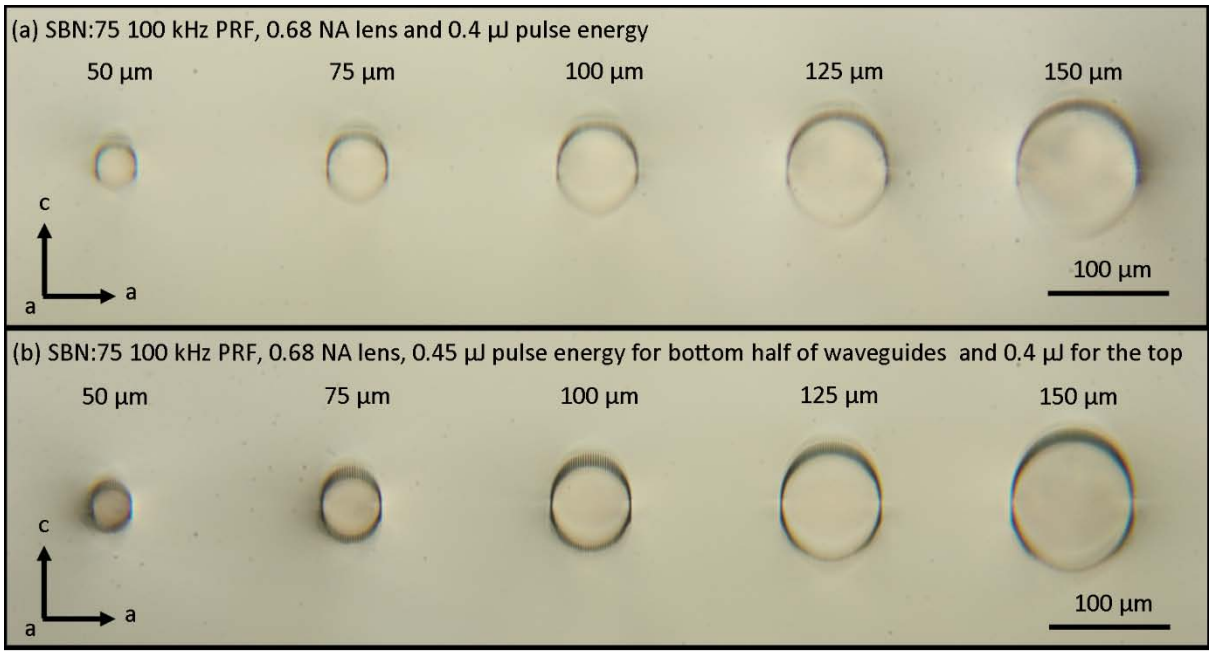

Figure 44: Depressed cladding waveguides fabricated at a depth of 250 µm in SBN:75 using a 100 kHz PRF, 1.1 ps pulse width, 0.68 NA lens. (a) 0.4 µJ of pulse energy is used to fabricate all elements that make up the waveguide. (b) 0.45 µJ pulse energy's are used to fabricate the elements in the bottom half of the waveguides and 0.4 µJ for the elements in the top half of the waveguide.

Passive guiding properties at 1550 nm

The passive guiding properties of the SBN:61 waveguides where investigated at 1550 nm. The 1550 nm light was coupled into the waveguides by butt-coupling a SMF-28 fibre to the end facet of the waveguide. The waveguide where found to guild 1550 nm but it was difficult to couple the light in and there was a large difference in light coming out of each waveguide. One reason for this could be a large NA mismatch between the fibre and the SBN:61 waveguides. To check this the NA of the waveguides we measured at 1550 nm. The beam profiles of the SBN:61 waveguides in the far-field and there NA are given in Figure 45.

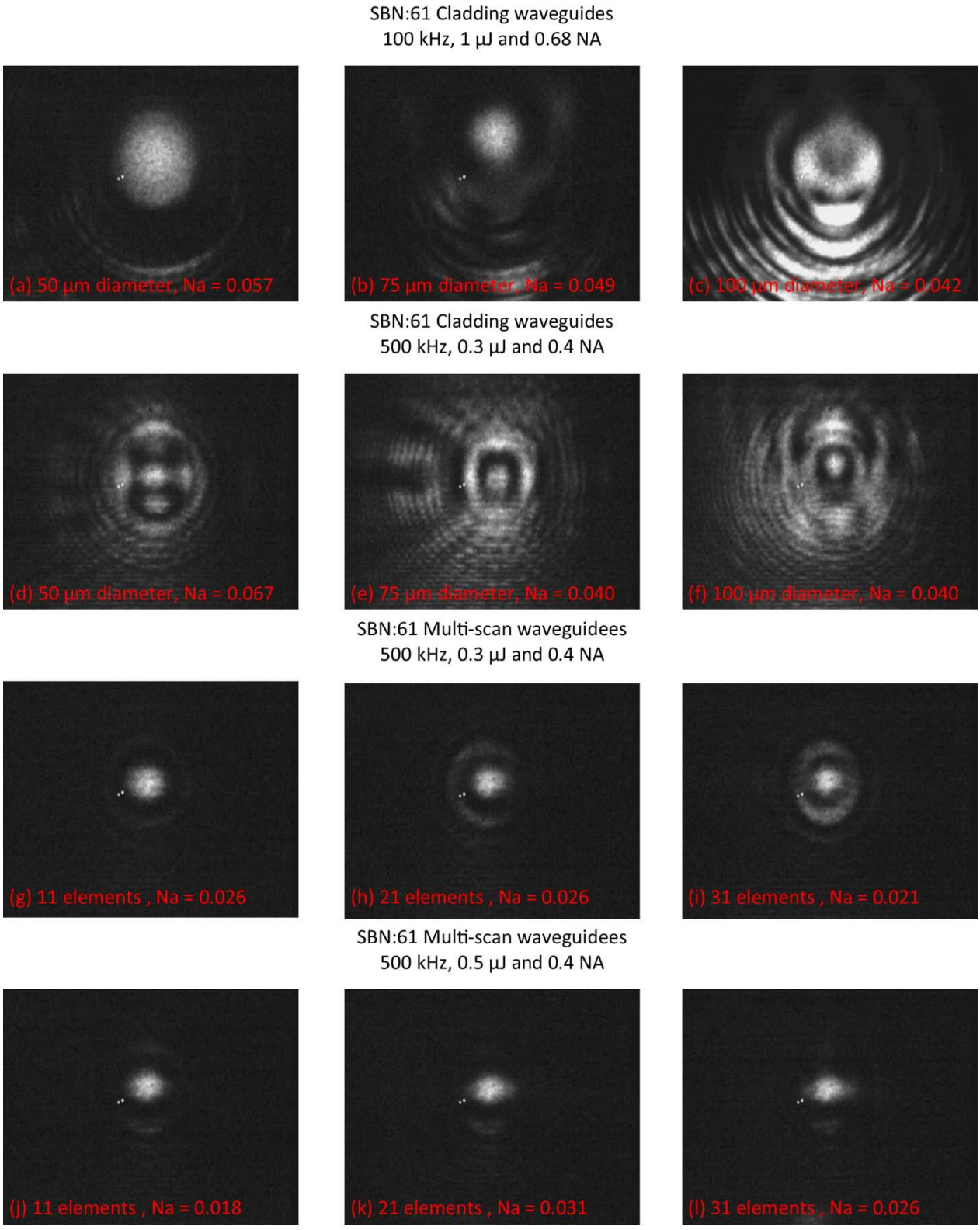

Figure 45: Far field images of SBN:61 waveguides at 1550 nm.

The NA of SMF-28 at 1550 nm is 0.14 which is much larger than any of the SBN waveguides. To get an accurate loss measurement the output of the SM-28 fibre was collimated with a 0.25 NA lens and focused onto the end facet of the waveguide with a 0.07 NA lens. This lens has a larger NA than the waveguides but is more

comparable then the SMF-28. Using this method the lowest loss of 0.08 dB/cm was measured with the 75 µm depressed cladding waveguide inscribed with a laser at 100 kHz. A more typical value for the rest of the waveguides was found to be 0.3 dB/cm. This is a very impressive result for a ULI waveguide loss which is typically around 1 dB/cm in ZnSe cladding waveguides [35, 49]. To confirm this measurement we used a different method that images the sample form above to directly detect the scattering loss. This method is a common techniques used at AFRL. This method give a typical loss of 2.5 dB/cm. the reason for the discrepancy was thoght to be mode striping at the input of the waveguides. To remove this effect form the propagation loss calculation the start of the waveguide was removed from the modelling which resulted in losses that agree with the first method. The waveguide loss being very low at 1550 nm is very promising for future work in the Mid-IR as the scattering loss is proportional to $1/\lambda^4$.

The guiding properties of SBN:75 depressed cladding waveguides fabricated with a laser PRF of 100 kHz and 0.68 NA lens with reduce inscription pulse energy where visually very similar to SBN:61. The waveguides where also very similar to the SBN:61 equivalent in terms of beam quality at 1550 nm. It was there for surprising to find out that the SBN:75 cladding waveguides only propagated linearly polarized light that is parallel to the c-axis (vertically polarized light). The SBN:75 cladding waveguides did not support the propagation of horizontally polarized light. The scattering losses of the waveguides where investigated by imaging the scattering of the light as it propagates along the waveguide. At 1550 nm no scattering was observed along the SBN:75 waveguide, this suggest a very low scattering loss. However calculation of the propagation losses form this method needs some measurable loss above the noise flower to give accurate results. A comparison of 50 µm cladding waveguides guiding 1550 nm light in SBN:61 and SBN:75 is shown in Figure 46. A graph showing the normalised scattering loss, for each curve, of each waveguide is given in Figure 47. This graph and the calculation of the losses form the images where done by Sean McDaniel at AFRL/RYDH.

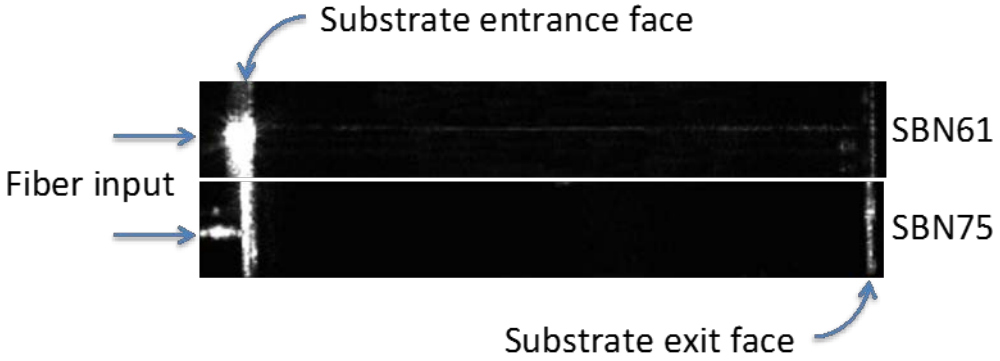

Figure 46: Exterior scattering comparison for SBN61 (top) and SBN75 (bottom) 50 µm waveguides at 1550 nm. Scattering is clearly visible for the SBN61 waveguide, but is not visible in the equivalent waveguide in SBN75.

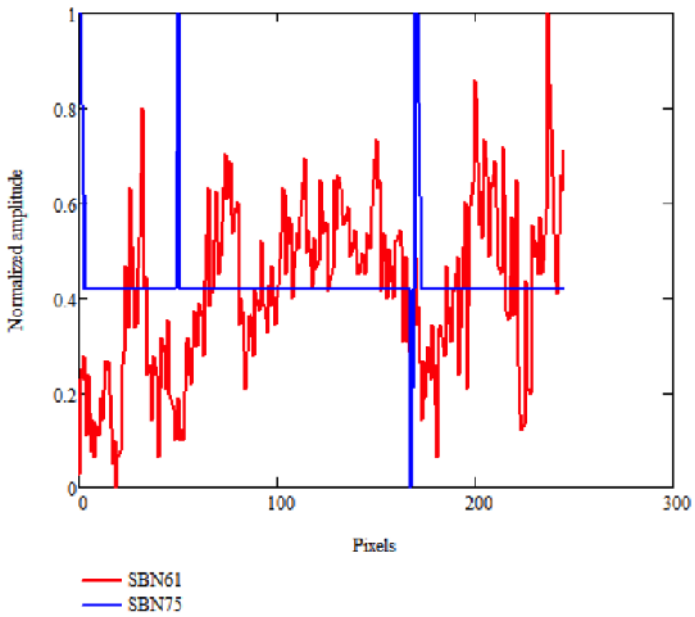

Figure 47: Local scattering intensity comparison for SBN61 and SBN75 50 µm waveguides at 1550 nm. Scattering is clearly negligible for SBN75 and no discernible slope in the scattered light intensity with distance is apparent.

Effect of ULI on SBN elector-optic properties

The main reason for developing SBN waveguides is to use them as phase modulators and Mid-IR laser tuning elements. The effect of ULI on material properties is not fully understood because of the many different non-linear process involved. Therefor it cannot be assumed that the electro-optic properties of SBN will be conserved in the modified region. To investigate this a simple method is to insert the SBN waveguides into one arm of a Mach-Zender interferometer, as shown in Figure 48. The phase delay induced by applying an electric field to the SBN can be monitored by the change in the inference pattern at the output of the interferometer. To make monitoring the fringes possible by human eye a HeNe laser, emitting 633 nm, was used.

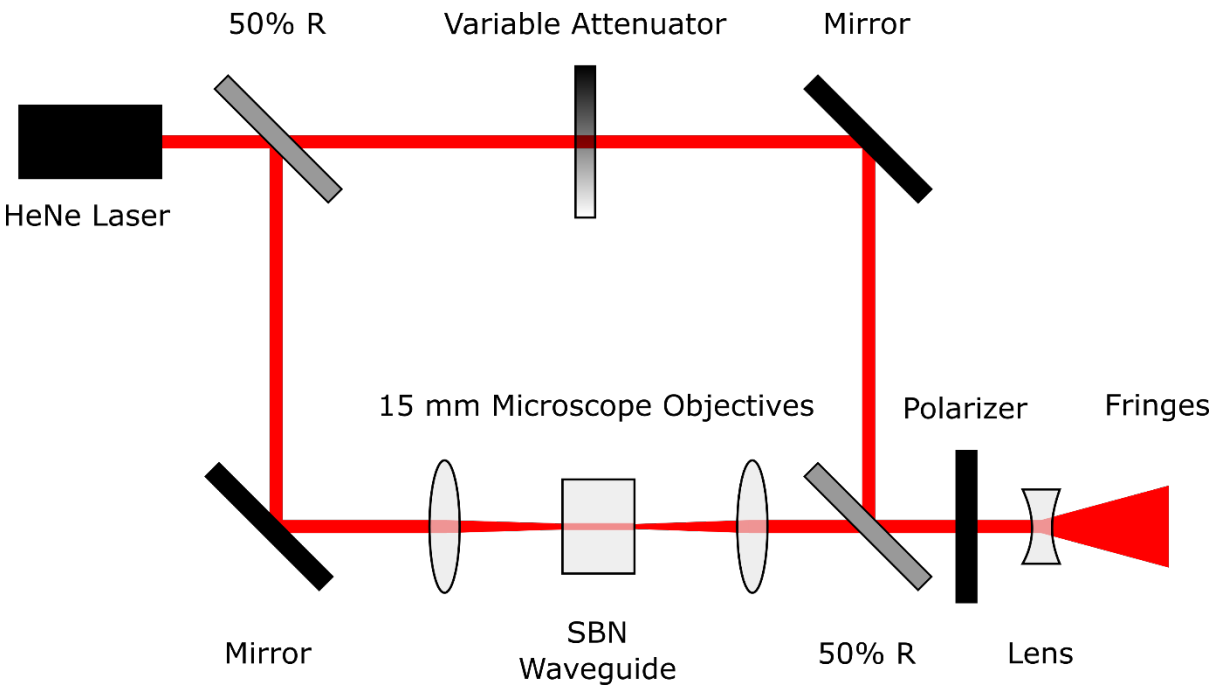

Figure 48: Mach-Zender interferometer with SBN waveguide forming a delay line in one of the arms.

The full wave voltage, corresponding to the field required to induce a 2π (whole fringe in the Mach-Zender interferometer) is given by:

$$V_{2\pi} = \frac{2d}{L}\frac{\lambda}{r_{eff}n^3}$$

where d is the crystal thickness along the c-axis (2 mm), L is the optical path length (10 mm), λ is the laser wavelength (632.8 nm) and n is the refractive index (2.3103 for light polarized parallel to the crystal a-axis, 2.2817 for light polarized parallel to the crystal c-axis, both at 632.8 nm). r_{eff} is the effective electro-optic coefficient, which depends on the crystal orientation, the direction of the applied electric field and the direction of the optical polarization with respect to the crystal orientation. The effective electro-optic coefficient is described by the tensor sum:

$$r_{eff} = \dot{e}\,\ddot{\varepsilon}\,\dddot{r}\,\dot{E}$$

where *e* is the unit vector for the optical polarization, *ε* is the dielectric permittivity tensor, *r* is the electro-optic tensor, and *E* is the applied field unit vector. The superscript dots represent the rank of the individual tensors, ˙ = vector, ¨ = second rank tensor, ⃛ = third rank tensor. For waveguides along one of the a-axes with the applied electric field along the c-axis, the effective electro-optic coefficients equate to $r_{eff} = \varepsilon_c r_{33}$ for light polarized parallel to the crystal c-axis, and to $r_{eff} = \varepsilon_a r_{23}$ for light polarized parallel to the crystal a-axis orthogonal to the waveguide direction. The electro-optic coefficients for SBN61 ($Sr_{0.61}Ba_{0.39}Nb_2O_6$)are:

$$r_{13} = r_{23} = 55 \text{ pm/V}$$

$$r_{42} = r_{51} = 80 \text{ pm/V}$$

$$r_{33} = 225 \text{ pm/V}$$

This gives full wave voltages, for a 2 mm thick c-axis orientation, of 95.13 V and 373.21 V for light polarized parallel to the c-axis and orthogonal to the c-axis, respectively.

Having established the linear electro-optic r_{13} and r_{33} coefficients for our material, the electro-optic properties of the three types of waveguides written in the same sample of SBN: 61 were measured. These are shown in figures 50 – 59. Because earlier it was noted that type 1 modification generated strong guiding immediately above and below the targeted inscription region, the electro-optic properties of these regions were also measured, defined as region A and region B, depicting the targeted inscription region and the adjacent guiding regions, respectively. These are shown in Figure 49.

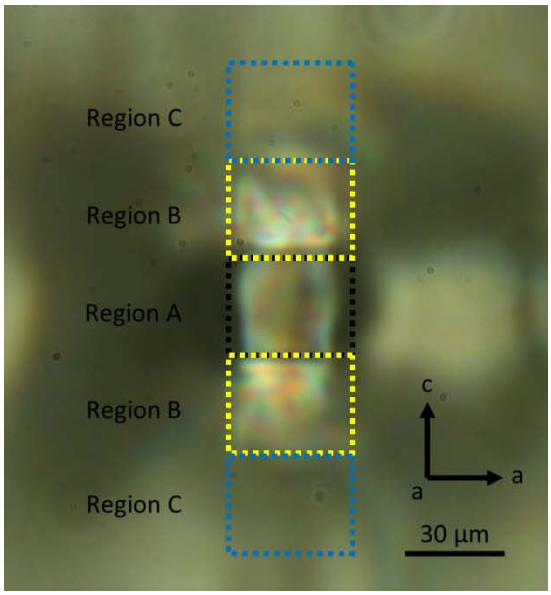

Figure 49: Defined regions for the type 1 modification. Region A- targeted inscription region. Region B – induced guiding regions immediately above and below the targeted inscription region. Region C – area of induced photorefractivity.

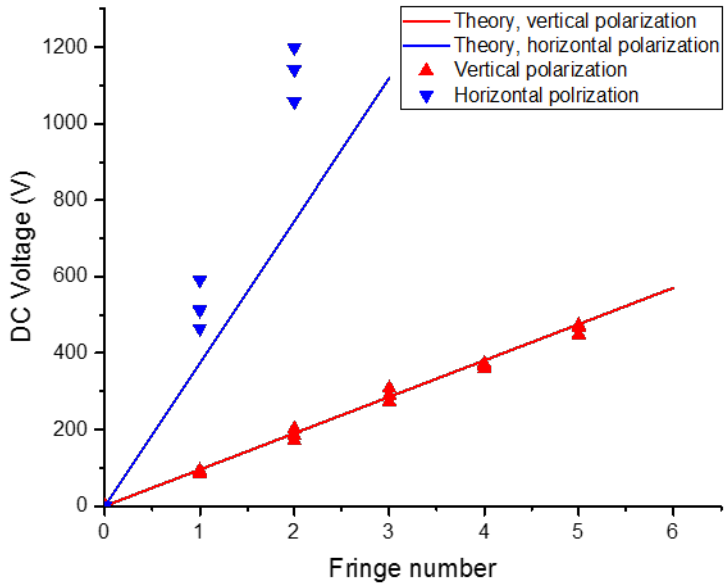

Figure 50: Measured linear electro-optic response in bulk SBN:61. In this sample, vertical polarization accesses the r_{33} coefficient, while horizontal polarization accesses the r_{13} coefficient. The r_{42} coefficient is inaccessible for this geometry.

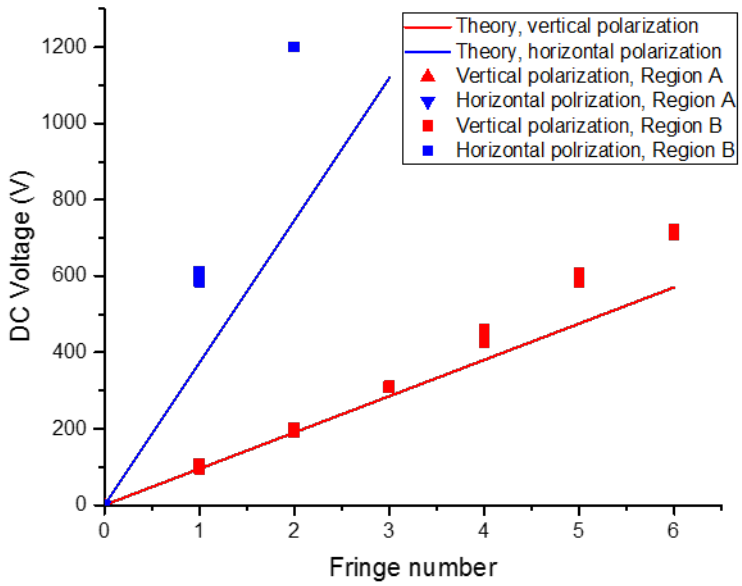

Figure 51: Measured linear electro-optic response for single stripe type 1 waveguides in SBN61. The material sample and theoretical values are the same as in figure 50.

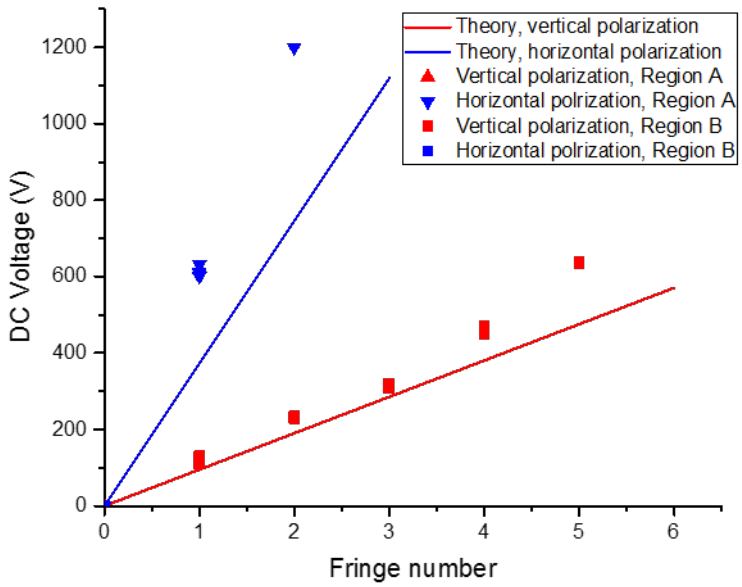

Figure 52: Measured linear electro-optic response for 11 stripe type 1 waveguides in SBN61. The material sample and theoretical values are the same as shown in figure 50.

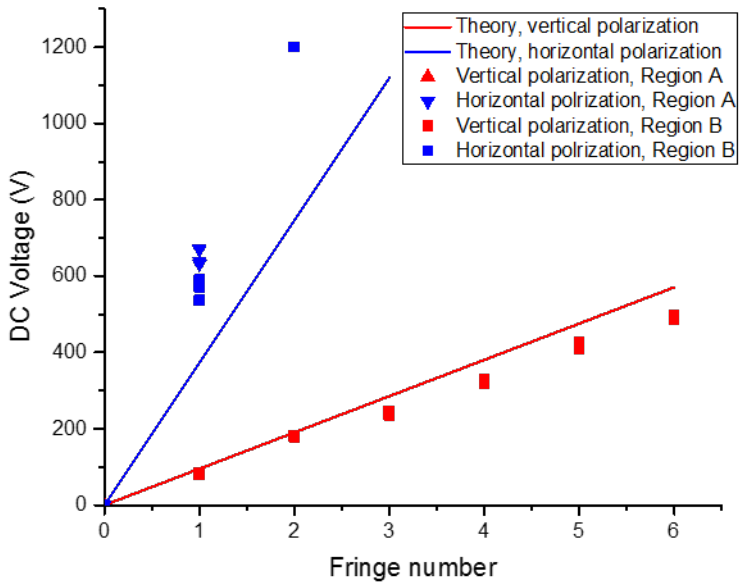

Figure 53: Measured linear electro-optic response for 21 stripe type 1 waveguides in SBN61. The material sample and theoretical values are the same as shown in figure 50.

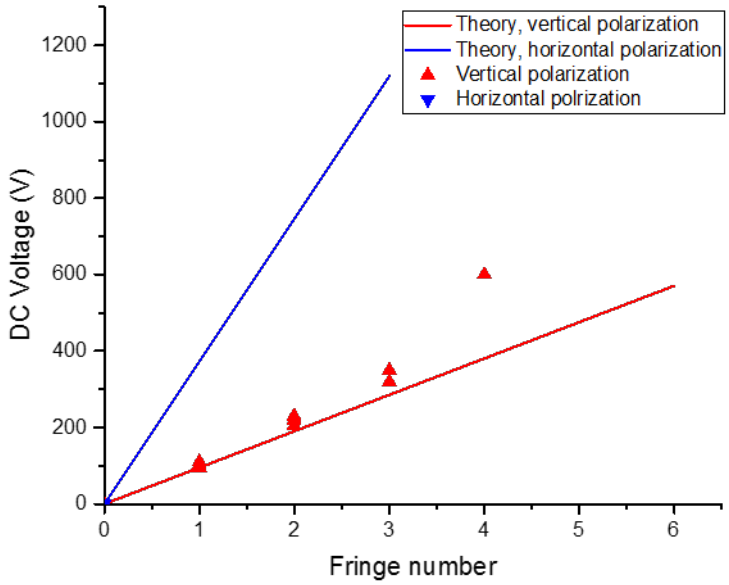

Figure 54: Measured linear electro-optic response for 50 μm type 1 cladding waveguides in SBN:61. The material sample and theoretical values are the same as shown in figure 50.

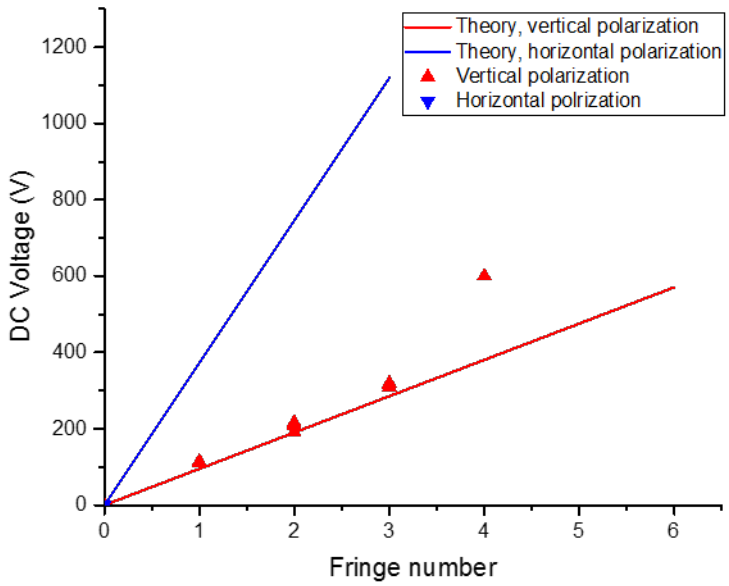

Figure 55: Measured linear electro-optic response for 75 μm type 1 cladding waveguides in SBN:61. The material sample and theoretical values are the same as shown in figure 50.

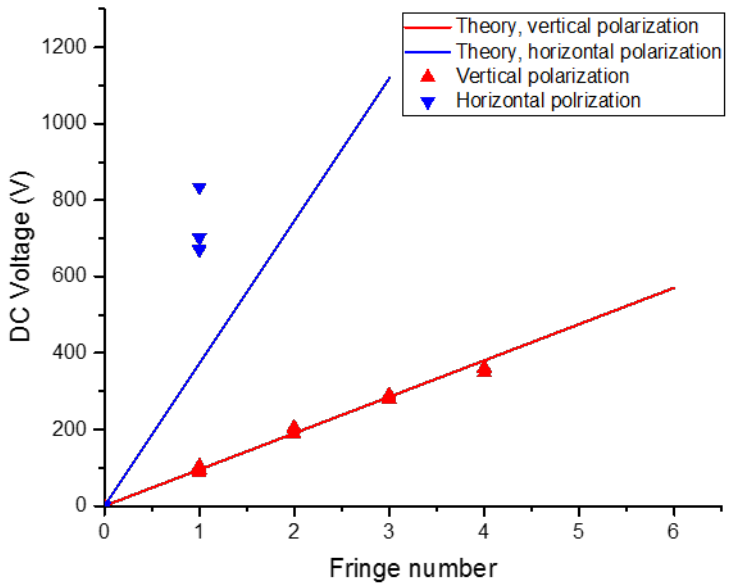

Figure 56: Measured linear electro-optic response for 100 μm type 1 cladding waveguides in SBN61. The material sample and theoretical values are the same as shown in figure 50.

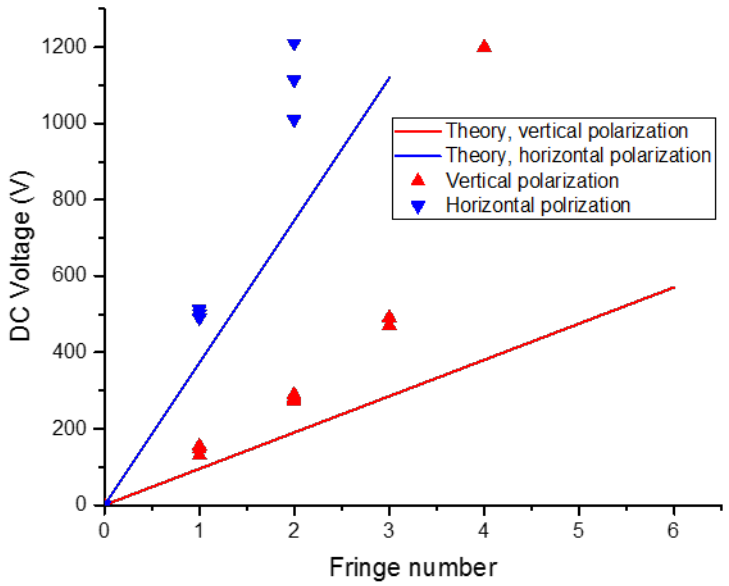

Figure 57: Measured linear electro-optic response for 50 μm type 2 cladding waveguides in SBN61. The material sample and theoretical values are the same as shown in figure 50.

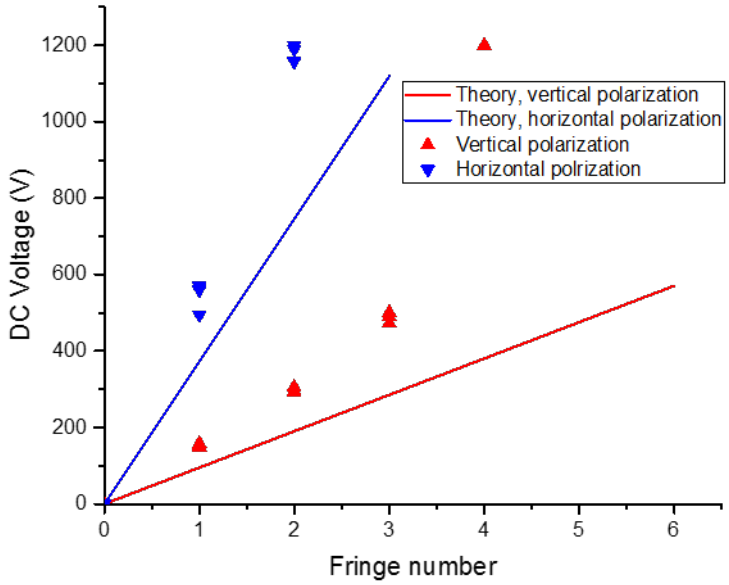

Figure 58: Measured linear electro-optic response for 75 μm type 2 cladding waveguides in SBN61. The material sample and theoretical values are the same as shown in figure 50.

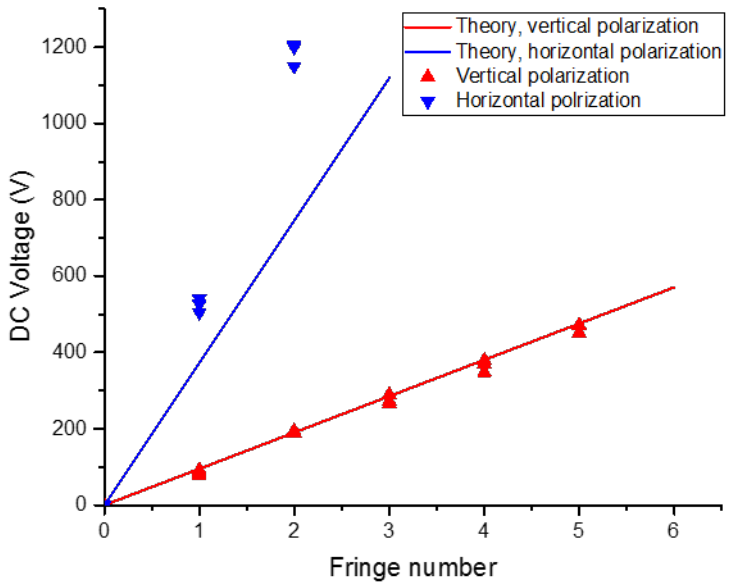

Figure 59: Measured linear electro-optic response for 100 μm type 2 cladding waveguides in SBN61. The material sample and theoretical values are the same as shown in figure 50.

Each of the three types of modification had distinct characteristics in terms of their polarization properties. However, all of the inscription types, including the anomalous type 1 region B guides, demonstrated strong electro-optic properties which generally followed the electro-optic response noted earlier in bulk material. This was a very

important result as it clearly demonstrated the ability of SBN:61 to retain its electro-optic properties after the fast laser inscription procedure had been accomplished. The only caveat to this result is that the waveguides needed to be relatively large to match the electro-optic response of the bulk crystal. If the guide regions were made too small, the electro-optic response became progressively nonlinear with the applied field, as if the guide walls presented a physical boundary to the distortion of the electron orbitals that give rise to the linear electro-optic effect. This was particular noticeable with the type 2 cladding waveguides which showed a progressive deviation compared with the bulk field induced birefringence. However, the 100 μm diameter type 2 cladding waveguide behaved identically to bulk SBN61. If small diameter waveguides were required, this might present a significant problem. However, since the waveguide numerical apertures are relatively large, the single mode diameter in the mid IR is likely to be around 100 μm diameter (or larger), meaning the electro-optic properties of these waveguides are likely to be the same as the bulk material.

Although the electro-optic properties seem to be suitable for device fabrication and laser use, care must be taken in selecting the appropriate waveguide type for the intended laser use. This is because the polarized light propagation properties of the waveguides vary considerably. Most of the waveguides only propagate one linear polarization state and so this introduces two primary considerations. If the propagated polarization does not correspond to the state required to access the largest electro-optic coefficient, the device electro-optic response will be small. Use of a polarization dependent waveguide in a laser resonator that contains a non-polarization preserving waveguide element (such as most Cr:ZnSe and Fe:ZnSe waveguides) will result in a 50 % optical loss per round-trip pass through the resonator, which is clearly unacceptable. If a polarized SBN waveguide has to be used, then polarization preserving waveguides need to be developed in Cr:ZnSe and Fe:ZnSe. This is not necessarily a daunting challenge, but it certainly something that needs to be carefully considered.

Table 10 summarizes the polarization properties of the individual waveguide types. Clearly, type 2 cladding waveguides seem to offer the greatest compatibility with existing Cr:ZnSe and Fe:ZnSe waveguide lasers. However, if a polarized laser were required, then type 1 region B waveguides would be preferred. Note that type 2 cladding could also be used with horizontally polarized light, as this is preserved on propagation through the waveguide, but this would give access only to the small r_{13} coefficient. It is interesting to note that the depolarization of vertically polarized light on passage through the type 2 waveguides does not seem to affect the apparent EO properties. This is somewhat surprising and the most likely explanation is that the depolarization occurs only towards the end of the waveguide, perhaps through a defect or local strain. Reversing the direction of beam propagation through the waveguide would provide a definitive confirmation as the apparent EO properties

may be different in each direction; if any depolarization occurred first, then only part of the resulting optical field would be able to interact with the larger r_{33} coefficient. There was insufficient time during the WOW to investigate this aspect and this will be followed up later.

Waveguide type	Polarization guiding	Accessible EO coefficients
1, region A	Guides horizontally polarized light only (polarized parallel to the c-axis).	r_{13} only.
1, region B	Guides vertically polarized light only (polarized parallel to the c-axis).	r_{33} only.
1, cladding	Guides only vertically polarized light (polarized parallel to the c-axis). Larger diameter guides may *weakly* guide horizontally polarized light.	r_{33} only.
2, cladding	Vertical (polarized parallel to the c-axis) and horizontal (polarized parallel to the a-axis) guiding possible. Guide diameter needs to be ≥ 100 µm diameter to avoid nonlinearity for EO effect for vertically polarized light. Horizontally polarized light appears to be unaffected by the guide diameter. Note: Although both polarization states are guided, vertical input polarization is depolarized on exit, while horizontal polarization is preserved.	r_{33} (light polarized long the c-axis); r_{13} (r_{23}) (light polarized along the a-axis). Note: in principal the r_{42} (r_{51}) coefficients are accessible if the field is applied along the crystal a-axis.

Table 10: Polarization dependence of waveguides in SBN:61. For these characteristics, the crystal c-axis is perpendicular to the waveguides and the field is applied along the c-axis. Vertical polarization is defined here as being parallel to the c-axis orientation, while horizontal polarization is defined as being parallel to the a-axis orientation.

The SBN:75 depressed cladding waveguides, fabrication at 100 kHz PRF with a 0.68 NA lens, electro-optic (EO) properties were also investigated. The SBM:75 was inserted into the Mach-Zender interferometer and then poled on the rig, with a standard hair dryer, at around 100 ^{o}C. The reason for re-poling is initial measurements of the EO properties where lower than expected. The bulk EO properties where then fond to be r_{33} = 900 pm/V and r_{13} = 106 pm/V. The values are within the range normally expected for SBN:75 with a slightly higher r_{13} coefficient. This results where repeatable thought-out the sample inside and outside the waveguides. However some of the higher power written guides, had slight lower EO properties than the bulk of around 10%. Unlike SBN61, no “clamping” of the EO coefficients was observed, even for the smallest waveguides. Both SBN substrates showed some degree of photorefractivity, but this was most noticeable with the SBN:75 material and caused disruption of the transmitted HeNe laser beam quality and also introduced significant cylindrical lensing in the bulk SBN75. Neither of these issues associated with photorefractivity were expected to be a problem in the IR as

photorefractivity requires photoionization of absorbing centres, which is unlikely with the relatively low photon energies encountered in the IR compared with using visible light.

From this work we have found that ULI waveguides in SBN still retain their EO properties. Form an EO point of view the ULI waveguide fabrication method is suitable to create elector-optic modulators in a no free space components format. There is additional interest in the discovery of the photorefractive properties induced by the ULI process. This does not affect our applications in the Mid-IR but could be very useful to create devises in the visible wavelength range.

Mid-IR waveguides in SBN

The passive guiding properties of the SBN waveguides at 1550 nm and the EO properties at 633 nm have been discussed earlier in this report. Both of these investigations have shown SBN to be suitable for its our desired application but the waveguides ability to support the Mid-IR waveguide lengths of a Cr:ZnSe laser has not yet be demonstrated. In this section the guiding properties of the SBN waveguides at 2.45 μm are discussed. For this work a Cr:ZnSe waveguide laser was used as the signal source. The Cr:ZnSe waveguide laser used with its emission peck at 2.45 μm. A 50 mm CaF_2 lens was used to couple the Cr:ZnSe laser beam into the SBN waveguides and a Mid-IR camera was used to image the end facet of the waveguide. A schematic of the setup is given in Figure 60. The modified region of the multiscan waveguides inscribed at 500 kHz with 0.4 NA lens where found not to guide 2.45 μm light. The most likely reason for this is the mode field diameter of the waveguides where to small. The area above and below the multiscan waveguide, region B Figure 49, was found to guide. However on application of the electric field the waveguide output was found to heavily distort and also move. The reason for this is thought to be strain induced guiding created from the piezoelectric effect induce by the applied electric field. This makes type I waveguides most likely not suitable for our intended future applications. It could be possible to compensate for the strain effect by inscribe a sandwich waveguide where the bread is Muitiscan and the filling is unmodified material. This idea is shown to be correct in the fact that the 500 kHz 0.4 NA cladding waveguide do guide the Mid-IR light of the Cr:ZnSe laser. The depressed cladding waveguides inscribed at 100 kHz with a 0.68 NA lens in SBN:61 are also found to guide. Applying a positive electric field was found to increases the NA of the waveguide. As the electric field was increases further it would reach a point at which a single mode waveguide would become multimode. Mode images of the end facet of the SBN:61 cladding waveguide with and without an applied electric field are shown in Figure 61. In particular the 75 μm dimeter waveguide clearly shows the transition from single mode at V = 0 to Multimode at V = + 1400 V.

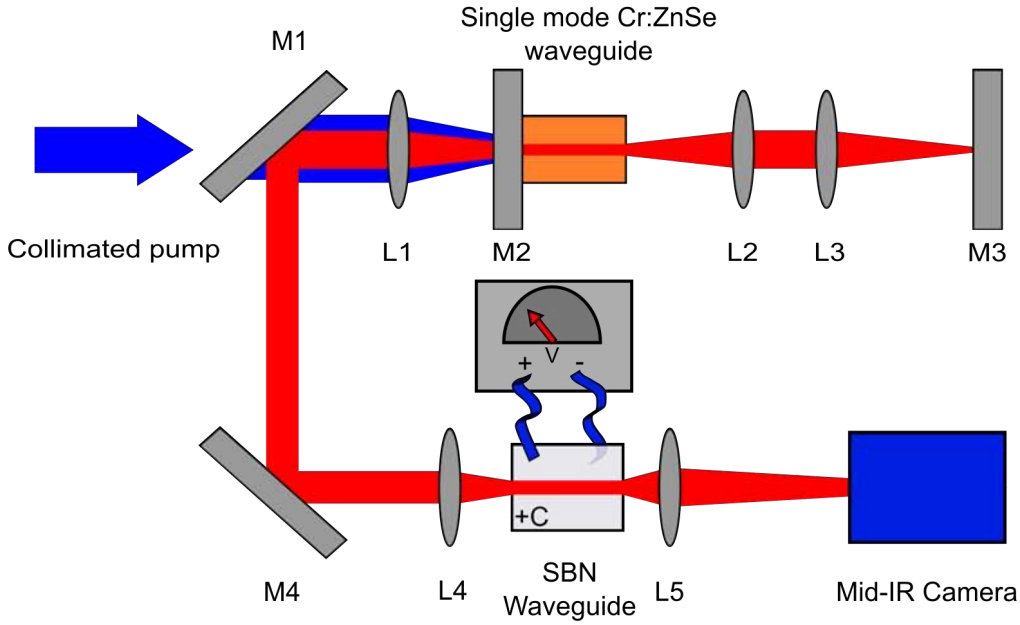

Figure 60: Schematic of experimental setup used to investigate the Mid-IR guiding properties of SBN waveguides with an applied electric field. L1-L4 are AR coated CaF_2 lenses with a focal length of 50 mm, L5 has a focal length of 20 mm. M1 is HR coated for the Tm:Fiber pump source and M3 is HR coated for the signal output of a Cr:ZnSe laser. M4 is a gold mirror. Note the SBN was coated on the top and bottom surfaces with silver paint to act as electrical contacts.

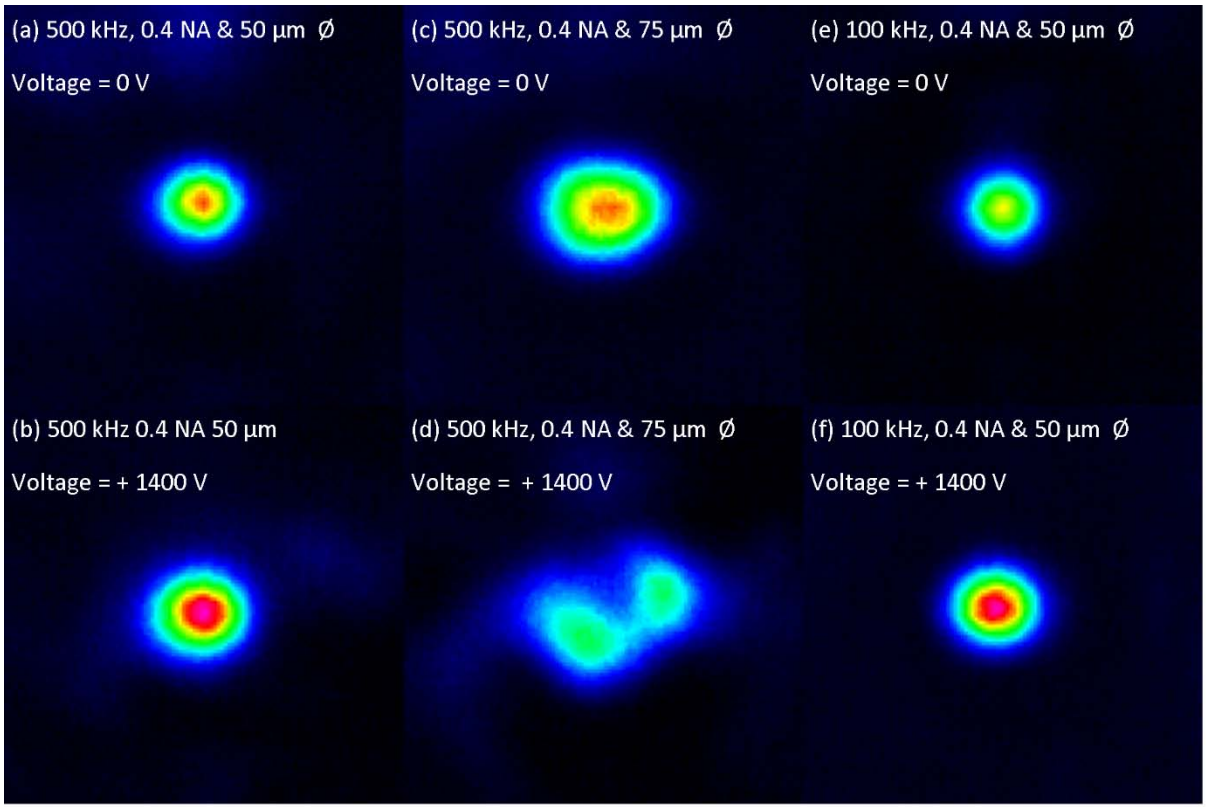

Figure 61: Electro-optic mode control at 2.4 µm of cladding waveguides inscribed in SBN:61. The electric field is applied along the c-axis of the crystal.

The cladding waveguides inscribed at 100 kHz with a 0.68 NA lens in SBN: 75 Mid-IR guiding properties were also investigated using the same methods as SBN:61. The waveguide did not propagated horizontally polarized light and only propagated vertical polarized light (in the direction of the c-axis). This agrees with what was observed at 1550 nm. The effect of applying an positive electric field to the positive c-axis face of the SBN:75 sample where found to be the same as SBN:61. Application of a negative field was also investigate, it was found that doing this reduce the NA of the waveguide and met that a multi-mode waveguide could be change to operate single mode, shown in Figure 62 with the 75 µm diameter waveguide. These results mean that the refractive index of the modified elements are not changing with applied electric field. When a positive electric field is applied the refractive index of the non-modified bulk SBN in the centre of the waveguide is increased. The opposite is true for an application of a negative electric field. Our first thought are applying a small electric field, that does not induce multimode operation, could be used to improve coupling efficacy. The implication for inserting a SBN devise, with ULI brag gratings inside the waveguide, into a Cr:ZnSe laser resonator is it is likely to have to operate in multimode operation to allow for reasonable wavelength tuning ranges. For application that require a single mode output, a MOPA system would be needed with a multimode wavelength tuneable oscillator and a single mode waveguide amplifier.

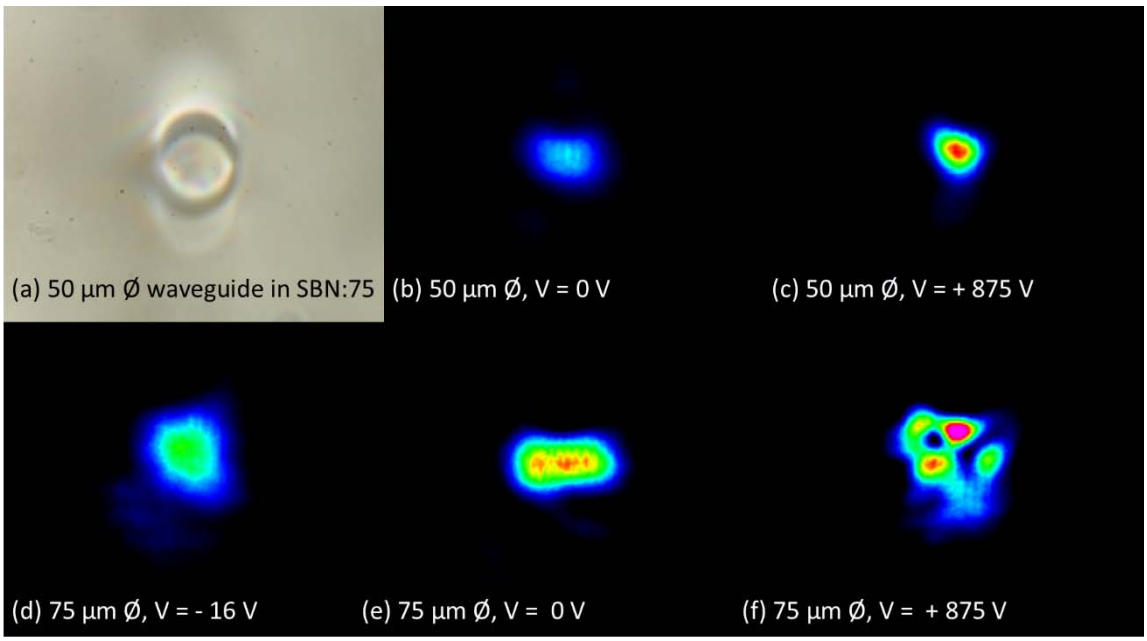

Figure 62: Electro-optic mode control at 2.4 µm of cladding waveguides inscribed in SBN:75.(a) microscope image of 50 µm diameter waveguide inscribed in SBN:75 with a PRF of 100 kHz, 0.68 NA lens and a pulse energy of 0.3 µW.

The ability to control the output mode of a waveguide could be very useful for many different application. Such as the ability to controllably couple light between a single mode waveguides and a cluster of single mode waveguides for phase-couple applications. It is also possible to extract information on the refractive index change induced in the SBN by the ULI by examining the point at which different waveguide

diameters change form single to multi-mode application. Measuring the refractive index change by ULI is often very difficult using other methods because of the small change induced typically of order 10^{-3}. Repeating these results over a number of wavelengths will allow the extraction of the dispersion characteristics of the cladding. Knowing this could allow for accurate desperation control in a modelocked Cr:ZnSe and Fe:ZnSe laser.

Summary

This results are a large step forward in the development of a no-free space component tuneable laser emitting in the atmospheric transition window. It has been found that fabrication of depressed cladding waveguides in SBN capable of guiding Mid-IR light is possible, something not demonstrate before by any other researchers. Initial measurements of propagation loss of SBN:75 cladding waveguides suggest the losses are much less than 1 dB/cm, which is suitable for inserting in to Cr:ZnSe or Fe:ZnSe laser resonators. The electro-optic properties of the bulk SBN is maintained after the inscription process making the material suitable for its intended applications. The waveguide dimeters and NA of the SBN depressed cladding waveguides are similar to that of ULI fabricated waveguides in Cr:ZnSe and Fe:ZnSe [35, 49]. This will facilitate efficient butt coupling between a ZnSe and SBN waveguides inside a laser resonator, allowing for the creation of a compact tuneable laser system. An example of what cavity might lock like is given in Figure 63.

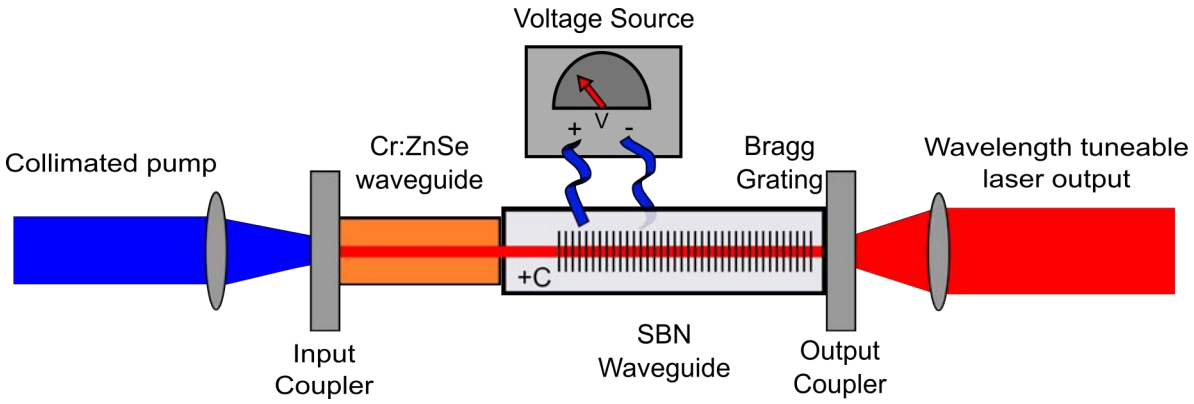

Figure 63: Schematic for Cr:ZnSe waveguide laser with SBN waveguide tuning element.

Publications and forthcoming publications

Title	Lead Author/Presenter and Description	Journal/Conference
Ultrafast Laser Inscription of Near Infrared Waveguides in Polycrystalline ZnSe.	**Dr. John R. Macdonald** Report of first channel waveguides in ZnSe.	Optics Letters 2010 Volume **35**(23) Pages 4036-4038.
Ultrafast Laser Inscription of Waveguide Structures in Cr2+:ZnSe.	**Dr. John R. Macdonald** Report of first channel waveguides in Cr^{2+}: ZnSe supporting guiding in the near infrared.	OSA Advances in Optical Materials Conference Proceedings February 2011. Paper AIFB5
Directly Written Mid-Infrared Waveguides in Zinc Selenide.	**Dr. John R. Macdonald** Report of first mid-infrared channel waveguides in ZnSe	OSA Advances in Optical Materials Conference Proceedings February 2012. Paper IF1A.3
Fabrication of Active Waveguides Using Femtosecond Lasers	**Prof. Ajoy K. Kar** Review of significant research conducted in Heriot-Watt NLO group	**Invited** OSA Advances in Optical Materials Conference Proceedings February 2012. Paper IF1A.1
Ultrafast laser inscription of photonic devices for integrated optical applications Stephen J. Beecher	**Dr. Stephen J. Beecher** An introduction to ultrafast laser inscription and a summary of recent technological advances	**Invited** A new paradigm of science driven by ultrafast lasers. Royal Society of Edinburgh Edinburgh, UK. February 2012
Ultrafast Laser Inscription – Science Today Technology Tomorrow	**Prof. Ajoy K. Kar** Update on recent progress in the field and expected impact on future technology	**Invited** ICOOPMA 2012, Nara, Japan June 2012 Paper 3B3-3, ID 1299
Light-Matter Interactions: Applications in Photonics and Biophotonics	**Prof. Ajoy K. Kar** Review of highly flexible nature of ultrafast laser inscription technology and its wide range of applications	**Invited** ICPEPA 2012, University of Rochester, USA August 2012 Paper TrC 14
Mid-infrared photonics enabled by 3D laser writing chalcogenide glass	**Prof. Ajoy K. Kar** Progress in mid-infrared photonic devices fabricated or enabled by ultrafast laser inscription	**Invited** SPIE Security + Defence, Emerging Technologies Edinburgh, UK. September 2012. Paper 8542-48
Compact mid-infrared Cr:ZnSe channel waveguide laser	**Dr. John R. Macdonald** First channel waveguide laser in Cr^{2+}:ZnSe	Applied Physics Letters 2013 Volume **102**(16) Page 161110
Efficient mid-infrared Cr:ZnSe channel waveguide laser operating at 2486 nm	**Dr. John R. Macdonald** High laser slope efficacy utilising depressed circular cladding waveguides	Optics Letters 2013 Volume **38** Page 2194
Laser-Inscribed Cr:ZnSe Channel Waveguide Lasers	**Dr. Patrick A. Berry** Progress on watt level output power waveguide lasers in Cr:ZnSe	OSA Advanced Solid-State Lasers Conference Proceedings Paris, France October 2013
Widely Tunable Cr:ZnSe Channel Waveguide Laser	**Dr. John R. Macdonald** First wavelength tubable channel waveguide laser in	OSA Advanced Solid-State Lasers Conference Proceedings

	Cr^{2+}:ZnSe	Paris, France October 2013
Optical Waveguides for Compact, High Power Mid-Infrared Lasers	**Prof. Ajoy K. Kar** Summary of current work with channel waveguides in Cr^{2+}:ZnSe and look at future devises.	**Invited** OSA Advances in Light Matter Interaction Conference Proceedings Mumbai, India November 2013
Ultrabroad Mid-Infrared Tunable Cr: ZnSe Channel Waveguide Laser	**Dr. John R. Macdonald** Demonstration of 700 nm of wavelength tuneablity in Cr^{2+}:ZnSe and a model of the system using Finite element analysis.	IEEE Journal of Selected Topics in Quantum Electronics 2015 Volume 21 Page 375-379
Gain-switched operation of ultrafast laser inscribed waveguides in Cr: ZnSe	**Mr Sean A. McDaniel** Demonstration of Cr:ZnSe waveguide laser operating gain-switched for reduced thermal load. The laser produced pulse energies of up to 12 µJ.	SPIE LASE Proceedings February 2015
Fe: ZnSe Channel Waveguide Laser Operating at 4122 nm	**Mr Adam Lancaster** First demonstration of a waveguide laser in Fe:ZnSe. With output powers of 76 mW	OSA CLEO Science and Innovations Proceedings May 2015
Mid-infrared laser emission from Fe: ZnSe cladding waveguides	**Mr Adam Lancaster** First journal article on Fe:ZnSe laser. Including detailed analysis of waveguide losses.	Applied Physics Letters 2015 Volume 107 (3) Page 031108

References

1. DeLoach, L.D., R.H. Page, and G.D. Wilke, *Transition metal-doped zinc chalcogenides: spectroscopy and laser demonstration of a new class of gain media.* IEEE Journal of Quantum Electronics, 1996. **32**: p. 885-895.
2. Page, R.H., et al., *Cr^{2+}-doped zinc chalcogenides as efficient, widely tunable mid-infrared lasers.* Quantum Electronics, IEEE Journal of, 1997. **33**(4): p. 609-619.
3. Sorokina, I.T., *Cr^{2+}-doped II–VI materials for lasers and nonlinear optics.* Optical Materials, 2004. **26**(4): p. 395-412.
4. McKay, J., K.L. Schepler, and G.C. Catella, *Efficient grating-tuned mid-infrared Cr^{2+}:CdSe laser.* Optics Letters, 1999. **24**(22): p. 1575-1577.
5. Moskalev, I.S., et al. *12-Watt CW Polycrystalline Cr2+:ZnSe Laser Pumped by Tm-Fiber Laser*. in *Advanced Solid-State Photonics*. 2009. Denver, Colorado: Optical Society of America.
6. Mirov, S.B., et al. *High Average Power Fe:ZnSe and Cr:ZnSe Mid-IR Solid State Lasers*. in *Advanced Solid State Lasers*. 2015. Berlin: Optical Society of America.
7. Sorokin, E., et al. *Ultrabroad Continuous-Wave Tuning of Ceramic Cr:ZnSe and Cr:ZnS Lasers*. in *Lasers, Sources and Related Photonic Devices*. 2010. San Diego, California: Optical Society of America.
8. Nilsson, J. and D.N. Payne, *High-power fiber lasers.* Science, 2011. **332**(6032): p. 921-2.
9. Baker, H., J. Lee, and D. Hall, *Self-imaging and high-beam-quality operation in multi-mode planar waveguide optical amplifiers.* Optics Express, 2002. **10**(6): p. 297-302.
10. McCarthy, J.E., et al., *Mid-infrared spectral broadening in an ultrafast laser inscribed gallium lanthanum sulphide waveguide.* Opt. Express, 2012. **20**(2): p. 1545-1551.
11. Beecher, S.J., et al., *Single Stage Ultrafast Laser Inscription of a Side-Polished Fiber-Like Waveguide Sensor.* Sensors Journal, IEEE, 2012. **12**(5): p. 1263-1266.
12. Ren, Y., et al., *Continuous wave channel waveguide lasers in Nd:$LuVO_4$ fabricated by direct femtosecond laser writing.* Opt. Express, 2012. **20**(3): p. 1969-1974.
13. Beecher, S.J., et al., *Strain field manipulation in ultrafast laser inscribed BiB_3O_6 optical waveguides for nonlinear applications.* Opt. Lett., 2011. **36**(23): p. 4548-4550.
14. Macdonald, J.R., et al., *Ultrafast laser inscription of near-infrared waveguides in polycrystalline ZnSe.* Optics Letters, 2010. **35**(23): p. 4036-4038.
15. Berry, P., et al. *Ultrafast Laser Inscription of Waveguide Structures in Cr^{2+}:ZnSe*. in *Advances in Optical Materials*. 2011. Istanbul, Turkey: Optical Society of America.
16. Thomson, R.R., et al., *Ultrafast laser inscription of an integrated photonic lantern.* Opt. Express, 2011. **19**(6): p. 5698-5705.
17. Thomson, R.R., et al., *Ultrafast laser inscription of a 121-waveguide fan-out for astrophotonics.* Opt. Lett., 2012. **37**(12): p. 2331-2333.
18. Mary, R., et al., *Compact, highly efficient ytterbium doped bismuthate glass waveguide laser.* Opt. Lett., 2012. **37**(10): p. 1691-1693.
19. Ren, Y., et al., *Mid-infrared waveguide lasers in rare-earth-doped YAG.* Opt. Lett., 2012. **37**(16): p. 3339-3341.

20. Choudhury, D., et al., *Quantum dot enabled thermal imaging of optofluidic devices.* Lab on a Chip, 2012. **12**(13): p. 2414-2420.
21. Choudhury, D., et al., *A 3D mammalian cell separator biochip.* Lab on a Chip, 2012. **12**(5): p. 948-953.
22. Brown, G., et al., *Ultrafast laser inscription of Bragg-grating waveguides using the multiscan technique.* Opt. Lett., 2012. **37**(4): p. 491-493.
23. Macdonald, J.R., et al., *Ultrafast laser inscription of near-infrared waveguides in polycrystalline ZnSe.* Opt. Lett., 2010. **35**(23): p. 4036-4038.
24. Psaila, N.D., et al., *Femtosecond laser inscription of optical waveguides in Bismuth ion doped glass.* Opt. Express, 2006. **14**(22): p. 10452-10459.
25. Nasu, Y., M. Kohtoku, and Y. Hibino, *Low-loss waveguides written with a femtosecond laser for flexible interconnection in a planar light-wave circuit.* Optics Letters, 2005. **30**(7): p. 723-725.
26. Macdonald, J.R., et al. *Directly Written Mid-Infrared Waveguides in Zinc Selenide*. in *Advances in Optical Materials*. 2012. San Diego, USA: Optical Society of America.
27. Macdonald, J.R., et al., *Compact mid-infrared Cr:ZnSe channel waveguide laser.* Applied Physics Letters, 2013. **102**(16): p. 161110-3.
28. Okhrimchuk, A., et al., *Low loss depressed cladding waveguide inscribed in YAG:Nd single crystal by femtosecond laser pulses.* Optics Express, 2012. **20**(4): p. 3832-3843.
29. Hu, J. and C.R. Menyuk, *Understanding leaky modes: slab waveguide revisited.* Adv. Opt. Photon., 2009. **1**(1): p. 58-106.
30. Snyder, A.W. and J. Love, *Ch. 24, Leaky Modes*, in *Optical Waveguide Theory*. 1983, Springer. p. 487 - 513.
31. Sorokina, I.T. and K.L. Vodopyanov, *Solid-State Mid-Infrared Laser Sources*. 2003: Springer.
32. Berry, P.A., et al., *Fabrication and power scaling of a 1.7 W Cr:ZnSe waveguide laser.* Optical Materials Express, 2013. **3**(9): p. 1250-1258.
33. Berry, P.A. and K.L. Schepler, *High-power, widely-tunable Cr^{2+}:ZnSe master oscillator power amplifier systems.* Optics Express, 2010. **18**(14): p. 15062-15072.
34. Sorokin, E., et al. *Ultrabroad continuous-wave tuning of ceramic Cr:ZnSe and Cr:ZnS lasers*. in *Advanced Solid-State Photonics*. 2010. San Diego, USA: Optical Society of America.
35. Macdonald, J.R., et al., *Efficient mid-infrared Cr:ZnSe channel waveguide laser operating at 2486 nm.* Optics Letters, 2013. **38**(13): p. 2194-2196.
36. Lagatsky, A.A., et al., *Fundamentally mode-locked, femtosecond waveguide oscillators with multi-gigahertz repetition frequencies up to 15 GHz.* Optics Express, 2013. **21**(17): p. 19608-19614.
37. Lancaster, A., et al. *1.94 GHz CW Modelocked Ytterbium-Doped Bismuthate Glass Waveguide Laser*. in *Advanced Solid State Lasers*. 2015. Berlin: Optical Society of America.
38. Mary, R., et al., *1.5 GHz picosecond pulse generation from a monolithic waveguide laser with a graphene-film saturable output coupler.* Opt. Express, 2013. **21**(7): p. 7943-7950.
39. Adams, J.J., et al., *4.0-4.5-μm lasing of Fe:ZnSe below 180 K, a new mid-infrared laser material.* Optics Letters, 1999. **24**(23): p. 1720-1722.

40. Mirov, S.B., et al., *Progress in Mid-IR Lasers Based on Cr and Fe-Doped II-VI Chalcogenides.* Selected Topics in Quantum Electronics, IEEE Journal of, 2015. **21**(1): p. 292-310.
41. Martyshkin, D.V., et al. *High Average Power (35 W) Pulsed Fe:ZnSe laser tunable over 3.8-4.2 μm*. in *CLEO: 2015*. 2015. San Jose, California: Optical Society of America.
42. Fedorov, V., et al. *Fe-doped II-VI Mid-Infrared Laser Materials for the 3 to 8 μm Region*. in *CLEO: 2013*. 2013. San Jose, California: Optical Society of America.
43. Firsov, K.N., et al., *Increasing the radiation energy of ZnSe : Fe 2+ laser at room temperature.* Laser Physics Letters, 2014. **11**(8): p. 085001.
44. Findlay, D. and R.A. Clay, *The measurement of internal losses in 4-level lasers.* Physics Letters, 1966. **20**(3): p. 277-278.
45. Okamura, Y., S. Yoshinaka, and S. Yamamoto, *Measuring mode propagation losses of integrated optical waveguides: a simple method.* Applied Optics, 1983. **22**(23): p. 3892-3894.
46. An, Q., et al., *Mid-infrared waveguides in zinc sulfide crystal.* Optical Materials Express, 2013. **3**(4): p. 466-471.
47. Gross, S., et al., *Low loss mid-infrared ZBLAN waveguides for future astronomical applications.* Optics Express, 2015. **23**(6): p. 7946-7956.
48. Lancaster, A., et al. *Fe:ZnSe Channel Waveguide Laser Operating at 4122 nm*. in *CLEO: 2015*. 2015. San Jose, California: Optical Society of America.
49. Lancaster, A., et al., *Mid-infrared laser emission from Fe:ZnSe cladding waveguides.* Applied Physics Letters, 2015. **107**(3): p. 031108.
50. Tolstik, N., E. Sorokin, and I.T. Sorokina, *Graphene mode-locked Cr:ZnS laser with 41 fs pulse duration.* Optics Express, 2014. **22**(5): p. 5564-5571.
51. Kuhl, J. and J. Heppner, *Compression of femtosecond optical pulses with dielectric multilayer interferometers.* Quantum Electronics, IEEE Journal of, 1986. **22**(1): p. 182-185.
52. Macdonald, J.R., et al., *Compact Cr:ZnS channel waveguide laser operating at 2333 nm.* Optics Express, 2014. **22**(6): p. 7052-7057.
53. Choudhury, D., J.R. Macdonald, and A.K. Kar, *Ultrafast laser inscription: perspectives on future integrated applications.* Laser & Photonics Reviews, 2014: p. n/a-n/a.
54. Ivleva, L.I., et al., *Growth of SBN single crystals by Stepanov technique for photorefractive applications.* Optical Materials, 1995. **4**(2–3): p. 168-173.
55. Mary, R., D. Choudhury, and A.K. Kar, *Applications of Fiber Lasers for the Development of Compact Photonic Devices.* Selected Topics in Quantum Electronics, IEEE Journal of, 2014. **PP**(99): p. 1-1.
56. Gunter, P. and J. Huignard, *Photorefractive Materials and Their Applications 1*. Photorefractive Materials and Their Applications, ed. P. Gunter and J. Huignard. Vol. 113. 2006, New York: Springer.